



UNIVERSITÀ
DEGLI STUDI
FIRENZE

PhD in
Chemical Sciences

CYCLE XXXVI

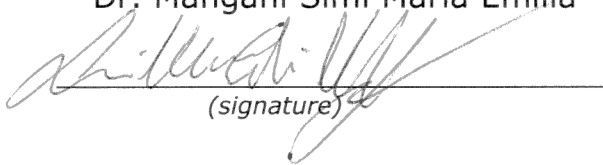
COORDINATOR Prof. Anna Maria Papini

Archaeometric study of Montelupo Maiolica

Academic Discipline (SSD) CHIM/12

Doctoral Candidate

Dr. Mangani Simi Maria Emilia


(signature)

Supervisor

Prof. Giuntini Lorenzo


(signature)

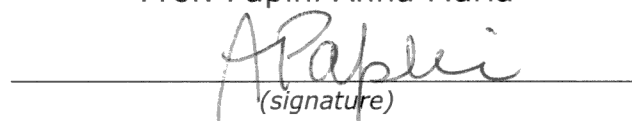
Co-Supervisor

Prof. Marilena Ricci


(signature)

Coordinator

Prof. Papini Anna Maria


(signature)

The consultation of the thesis is free. Unless a specific authorization is obtained from the author, the thesis can be, however, downloaded and printed only for strictly personal purposes related to study, research and teaching, with the explicit exclusion of any use that has – even indirectly – a commercial nature.

ABSTRACT

Ceramic materials are one of the most significant human technological achievements, and the Montelupine maiolica production, in the specific, represents an excellent example of this art in the Late Medieval-Renaissance period.

Focusing on this context, in order to valorise it, this project aims to define a multi analytical approach suitable for the study of the glazing coating of these maiolicas.

In fact, despite a vast diagnostic campaign carried out on the ceramic bodies of these artefacts, the complex stratigraphy of their glazes (white opaque glaze + intermediate chromophore-rich decorative layer + possible transparent superficial glaze) has never been exhaustively explored.

For this project, forty-two samples were selected thanks to the collaboration of the Museum of Ceramics of Montelupo and the Colorobbia Research Centre in order to cover the entire colour palette of Montelupo and the different production periods.

Preferring a non-invasive and non-destructive approach, more suitable for future application on well-preserved museum pieces, the objects were analysed with the following analytical strategy:

- The MA-XRF scanner was exploited to detect the different colours' characteristic elements by visualising their distribution in maps.
- The micro Raman spectrometer provided information on molecular bonding.
- The PIXE-PIGE analyses allow to obtain reliable quantitative data.

The information thus obtained was then compared with the SEM-EDS results (obtained by measuring the individual glaze layers of a selected set of samples) in order to evaluate the quality of the data acquired in the non-invasive approach.

In the case of the white areas (characterised by the sole presence of the white glaze and transparent coating), the chosen strategy allowed the identification of interesting trends in the concentrations of the main components. SnO₂ and PbO contents variations in time, in particular, seem to reflect not only the lower technological level of the archaic period but also the artistic (and evidently also technological) crisis that has affected Montelupo since the end of the 16th century. The highest contents of both these species (the first used as opacifier, the second as fluxes) are, indeed, recorded in the earliest and latest artefacts.

A good agreement is encountered between the non-invasive and the SEM-EDS results. However, a couple of critical issues emerged: the difficulty in identifying the tin-modified Naples Yellows and the impossibility of obtaining direct information on the presence/absence of the transparent glaze.

INDEX

Chapter 0. Introduction	1
Chapter 1. Reference Context	3
1.1 Historical Background	3
1.1.1 First Phases	4
1.1.1.1 <i>Archaic Maiolica and Archaic Blue Maiolica</i>	5
1.1.1.2 <i>Zaffera a Rilievo and Damaschino</i>	6
1.1.2 The Renaissance: Maiolica Golden Era	7
1.1.2.1 <i>The Cold Palette</i>	7
1.1.2.2 <i>The Warm Palette</i>	8
1.1.3 Last Phases	9
1.1.3.1 <i>Late 16th – Early 17th Century</i>	9
1.1.3.2 <i>18th century</i>	10
1.2 Materials Reference Context	11
1.2.1 Ceramic Body	12
1.2.2 Glazes	15
1.2.2.1 <i>Glass Generalities</i>	16
1.2.2.2 <i>Glass Formers</i>	16
1.2.2.3 <i>Glass Modifiers</i>	18
1.3 Production Processes	20
1.3.1 Preparation of Clay Mixture	22
1.3.2 Clay Shaping and Drying	23
1.3.3 Formulation of Coatings (Glazes)	23
1.3.4 First Firing	24
1.3.5 Application of Glazes and Decorations	25

Index

1.3.6	Second and Third Firing	25
1.3.7	Trade of the Finished Product	26
1.4	Bibliography	27
Chapter 2: Materials and Methods		30
2.1	Materials	31
2.2	Methods	37
2.2.1	X-Ray Fluorescence	38
2.2.1.1	<i>Theoretical Principles</i>	38
2.2.1.2	<i>The Equipment</i>	40
2.2.2	Raman Spectroscopy	41
2.2.2.1	<i>Theoretical Principles</i>	41
2.2.2.2	<i>The Equipment</i>	42
2.2.3	Ion Beam Analysis (IBA)	43
2.2.3.1	<i>Theoretical Principles</i>	44
2.2.3.2	<i>The Equipment</i>	45
2.2.4	Scanning Electron Microscope	46
2.2.4.1	<i>Theoretical Principles</i>	47
2.2.4.2	<i>The Equipment</i>	48
2.2.5	Bibliography	49
Chapter 3: Results and Discussion		52
3.1	White Areas	52
3.1.1	MA-XRF	52
3.1.2	IBA	55
3.1.3	Micro Raman	62
3.2	Decorations	67

Index

3.2.1	Green Decorations	68
3.2.2	Black/Brown Decorations	72
3.2.3	Blue Decorations	75
3.2.4	Yellow and Orange Decorations	81
3.2.5	Red Decorations	87
3.3	SEM-EDS	91
3.3.1	Transparent Glazes and White Glazes	92
3.3.2	Coloured Glazes	95
3.4	Bibliography	99
Chapter 4: Conclusions		105
Appendix A: The Samples		v
Appendix B: List of Publications		x

INTRODUCTION

Ceramic materials are certainly one of the most significant technological achievements in human history, as well as one of the oldest and most widespread.

The earliest evidence of fired clay dates back to 23,000 BCE, and since then, civilisations have produced countless ceramic objects for domestic, ritual, and artistic purposes.

Today, these materials constitute the majority of archaeological findings, making them valuable "guide fossils" for the most disparate geographical and temporal contexts.

Maiolica (porous ceramic body coated with a tin-rich glaze apparatus) stands out as one of the most refined products of Italian (and European) manufacturing from the late Middle Ages and Renaissance.

Conforming into a cultural climate aimed at the valorisation and rediscovery of small local contexts (often overshadowed by larger historical centres), this study focusses on the production reality of Montelupo Fiorentino.

The primary purpose of the project is to establish a comprehensive analytical methodology suitable for the study of complex (layered) artefacts such as maiolica to gain a deeper understanding of their glazing materials and evolution over time.

Due to the valuable historical-artistic values of these objects, it is preferable to adopt a non-invasive and non-destructive approach, with the potential for future application on well-preserved museum pieces.

Thanks to the collaboration of the Museum of Ceramics of Montelupo, a set of thirty-seven samples was selected in order to exhaustively cover the chromatic variability of the period of most significant interest (15th-16th century). Moreover, five further samples dating back to the earliest (14th century) and most recent (17th-18th century) production phases were provided by the Colorobbia Research Centre (Ce.Ri.Col), enabling a complete coverage of the production span.

Chapter 1 of this thesis provides a framework for the subsequent chapters. It, therefore, offers a preliminary overview of the maiolica's materials, with particular attention to the glazes that will be the focus of the experimental part. Moreover, a comprehensive view of the Montelupo context is depicted, covering both historical and political aspects, as well as production processes.

The details of the analysed samples are included in Chapter 2, together with the description of the chosen analytical approach and the specifications of the instruments exploited.

Introduction

A non-invasive and non-destructive analytical approach was chosen for the first phases of the research. Samples were observed at the optical microscope and then analysed through the X-ray Fluorescence (XRF) scanning system of the Labec-INFN (*Laboratorio di tecniche nucleari per l'Ambiente e i Beni Culturali-Istituto Nazionale di Fisica Nucleare*) laboratory and the micro Raman spectrometer from the Chemistry Department "Ugo Schiff" of the University of Florence. Semi-quantitative data were obtained due to the use of Particle Induced X-ray Emission (PIXE) and Particle Induced Gamma-ray Emission (PIGE) analyses.

With the consent of the Museum of Montelupo and the Superintendence of Florence, a small set of samples was selected to perform more specific (micro-invasive) analyses exploiting the Scanning Electron Microscope (SEM) of the MEMA (*Microscopia Elettronica e MicroAnalisi*) interdepartmental service centre. Based on the evidence collected a differential PIXE campaign was planned and conducted.

In Chapter 3, results from the archaeometric campaign are presented. To enhance clarity, the results are divided into two parts: the first part includes data obtained from white areas (opaque white glazes and transparent glazes), while the second part covers results from coloured areas.

Finally, Chapter 4 outlines the conclusions that are reached.

1 REFERENCE CONTEXT

1.1 HISTORICAL BACKGROUND

To gain a comprehensive understanding of the historical and artistic importance of Montelupo maiolica, it is necessary to broadly reconstruct the historical and geographical context of the Florentine Middle Valdarno.

The area presented evidence of human activity dating back to the Lower and Middle Palaeolithic; however, there are actual testimonies of stable settlements only by the end of the Bronze Age (11th-10th century BCE). From this period on, the area will no longer be abandoned:

- During the Etruscan Era, the left bank of the Arno, including Montelupo, was among the territories under Volterra.
- With the Roman colonisation (first half of the 1st century BCE) Valdarno became an important junction for the two major communication routes: the Arno (widely used since the 6th-5th century BCE), and the Roman military road (built under the consulate of Tito Quinzio Flaminio in 123 BCE and connecting Pisa to Florence).

When the Western Roman Empire collapsed, the region fell under the influence of the Carolingian Empire; first as Duchy-County of Lucca (entrusted by Charles the Great to the Bavarian Boniface) and after 846 CE becoming the March of Tuscany under Cadolingi's jurisdiction. It was a politically unstable period marked by frequent internal wars between local counts and marquises and by a progressive rise of ecclesiastical power at the local scale.

The definitive fall of the Cadolingi, in the first decades of the 11th century, resulted in increasing conflicts between local lordships and the Alberti family; during the temporary vacuum of power, the latter reached the power and took advantage of it to get Empoli and Montelupo out of the Pisotoian influence.

A rapid military expedition in 1174 CE established for the first time the interest of the Republic of Florence in the Valdarno area. The Florentines conquered the Monte Orlandi Castle (above Gangalandi) and one of the bridges that guaranteed the crossing of the Arno towards Pistoia. This action led to a conflict between Florence and Alberti Lordship (1184 CE), which the firsts eventually won.

Having definitively eliminated the presence of Alberti, the Republic of Florence undertook the grandiose reconstruction of the Montelupo Castle (1203-1206 CE) and, by the second half of the 13th century, Montelupo became the most crucial and faithful Florentine settlement in the Middle Valdarno.

Montelupo played a crucial role in defending the city against Pistoia and Pisa while serving as a vital economic and productive centre for Florence. Indeed, only under the Republic (then *Signoria* from 1250 CE) Montelupo did experience the political and economic stability that allowed the development of the flourishing ceramic production of our interest. Despite the difficulties faced through centuries¹, the Florentine funds² and, above all the strategic access towards national and international ports that the city guaranteed, played a fundamental role in the local economy (increasingly linked to that of Florence). (Berti, 2008a)

1.1.1 First Phases

Except for a few isolated manufactures probably operating with labour from the Islamic world (Savona, Brindisi, and Gela), the spread of Archaic Maiolica, the first glazed genre indigenous to Italy, is conventionally traced back to 1240 CE. It was clearly an initially slow process, starting from the coastal production centres most connected to the Islamic and Spanish world. However, even with these premises, Montelupo's delay of around forty years compared to the national context is surprising, especially considering Florence's wealth and influence.

The reasons behind this “underdevelopment” are complex and duly explored in (Berti, 2008a). For our purposes, we will limit to mentioning the two major factors.

Firstly, the constant conflict between the Medici family and the Visconti lords of Milan and Genoa, who exercised their power as far as the ports of Livorno and Pisa. This geopolitical situation, besides determining the imposition of duties for port access, also severely limited the circulation of exported and imported goods. Compared to potters from extra-Florentine areas, the Montelupine ones encountered the Moorish maiolica (trend of this period) later and more sporadically. As a result, they had fewer opportunities to deal with this technology.

Secondly, the lords of Florence initially did not encourage the development of the fire arts in the city. On one side, they tried to discourage the opening of kilns

¹Such as the famine of 1340 CE, the plague pandemic of 1348-1349 CE and the local occupation by a company of disbanded Spanish troops in 1538 CE (previously in the pay of Duke Cosimo of Medici).

²In support of the presence of Florence in the Montelupine territory, the possessions in the Montelupine curia of nobles' families of the *Gigliata* (i.e. Frescobaldi, Antinori, Spina) have to be cited, as well as the enormous construction site of the *Villa Medicea dell'Ambrogiana*. Commissioned by Cardinal Ferdinando between 1587 and 1591 CE, the site brought an influx of massive capital to Montelupo, making the fortune of several local families (including the Marmi). (Berti, 2001)

within the city walls for fire fear, on the other, they did neither promote any system that would benefit the ceramists of the *Contado* (i.e., Baccherento, Impruneta, Montelupo and Cancelli). In fact, between the 13th and 14th centuries, an indirect commission system was used, and all the trades passed through the *stovigliai*: retailers who were intermediaries between the private/public commission and the ceramists. Unfortunately, this system dispersed capital that otherwise would have gone directly to artisan and prevented potters from directly engaging with clients' preferences.(Cora, 1973)

1.1.1.1 Archaic Maiolica and Archaic Blue Maiolica



Figure 1 Example of Archaic maiolica:
"Boccale con Arpia" (1320-1340 CE)

The first developments of Montelupo archaic maiolica took place in this context following the dominant production methods of Tuscany and Central-Northern Italy. The most produced shape at this time was the *boccale* (jug) *con ansa a bastoncello* (Figure 1), with a clear minority production of open morphs (such as *catini*, *ciotole* and *rinfrescatoi* which were characterised by the particular flaring at "elephant's foot").

The reddish *bistugio* was obtained from iron-rich clays quarried from river accumulations and worked on a lathe (visible turning grooves). As little material as possible was used for the glazes (especially in 1280-1350 CE): open shapes were coated only in the visible parts, and the foot of the jugs were glazed with very thin layers. The same material-saving strategy was also applied to the decorations made solely with ramina

green and manganese black/brown. Solid colours were generally avoided in favour of phytomorphic "a graticcio" motif or, more rarely, pseudo-heraldic, geometric, and zoomorphic decorations.

Only the introduction of the new archaic blue maiolica genre in 1360 CE marked the first significant departure from Italian proto-maiolica production. The ceramic bodies evolved in the wake of the new Moorish aesthetic, and for the first time, the whitening of the *bistugio* was implemented according to the strategy illustrated in Paragraph 1.2.1. Furthermore, in these years, for the first time, decorative motifs imported directly from the Islamic world began to appear (such as the *albero della vita*), and they were rendered with the cobalt blue-like chromaticism recalling the maiolica of the Spanish area.(Berti, 1982)

1.1.1.2 Zaffera a Rilievo and Damaschino

However, it was only after 1380 CE that the first decorations created with the real, and expensive, cobalt blue were made in Montelupo: the so-called *zaffera a rilievo*.

With the *zaffera* and the tricolour *zaffera* (a very rare genre characterised by the simultaneous use of cobalt blue and green ramina-black manganese), Montelupo "painters" developed a more precise and characteristic language as well; language which was then applied to the tricolour archaic maiolica too (natural evolution of the archaic maiolica, with the introduction of the yellow/orange pigment in imitation of the Moorish lustre).

Politically, the defeat of the Visconti on October 9th, 1406 CE, finally allowed Florence (and Montelupo) to gain direct access to the Pisan port (and from there to Livorno). Ponte a Signa, therefore, became the main stopover between Pistoia and Pisa, and Montelupo found itself in a preferential location for trade towards the ancient Tyrrhenian route.³ Montelupo's position as a trade hub was further consolidated when the Florentines acquired the Livornese port in 1421.⁴ These events and the decline of that system of indirect commissions described above⁵ contributed to setting Montelupo maiolica as a most valid alternative to the Spanish one.



Figure 2 Example of Damaschino: "Bacile monocromo" (1440-60 CE)

The most innovative decorative genre of this moment was the *Damaschino* (Figure 2), inspired by Hispanic tradition but also strongly influenced by the thematic suggestions conveyed by the Anatolian-Syrian Islamic lustres. In the golden age of International Gothic, the concept of spaceless painting was established; each figure, totally deprived of natural three-dimensionality, was enclosed by continuous lines and isolated from the non-naturalistic background created by graphic signs and/or abstract elements (with merely symbolic value). This language, finally standardised, had such a

success in Tuscany, ultimately resulting in a true *horror vacui*.

³ The Tyrrhenian route was an ancient route that originated from the Spanish Levant, passed through Sicily, and extended to the Eastern Mediterranean.

⁴ The port was purchased from the Genoese for 100'000 *Fiorini*.

⁵ From what we know so far, the first documented direct commission was made by the Hospital of Santa Maria Nuova to the ceramist Tugio di Giunta in 1383 CE.

From a chromatic point of view, in its first phase between 1400 and 1440 CE, the *Damaschino* showed a strict blue monochrome created by using extremely diluted cobalt blue (in Montelupo as well as in the other main Italian maiolica centres Faenza and Pesaro). (Berti, 1997)

1.1.2 The Renaissance: Maiolica Golden Era

In the general context of the flourishing Renaissance, the Florentine's ferocious desire to economically depress their former enemy, Pisa, contributed to consolidating Montelupo as the most crucial centre of maiolica production in Tuscany. In 1440 CE, indeed, every Pisan maiolica manufacture was closed or converted to engobe production centre, effectively eliminating the competition in the region.⁶

1.1.2.1 The Cold Palette



Figure 3 Example of Cold-palette *Damaschino*: "Ciotola policroma" (1440-60 CE)

In this highly favourable climate, morphological and decorative genres multiplied, and ceramic bodies became whiter and thinner.

The cobalt blue palette, predominant between the end of the 15th and the beginning of the 16th century, was enriched from 1440 CE with the extensive addition of pale copper green, purple manganese and citrine yellow, resulting in the so-called "cold palette". During the same period, the decorative themes were finally aligned with the International Gothic repertoire: depictions of horses, falconers (Figure 3),

and symbols of virtue became the most common subjects.

However, it was a short-lived phase. Already from 1470 CE, there was a shift towards a figurative style, more aligned with Renaissance Art. The *Damaschino* crisis laid the groundwork for more realistic and hierarchically contextualised subjects. The central figure (typically human or a coat of arms) stood out on the visible face of the jugs or in the centre of the open shapes, and it was separated from the secondary decorations by a formal artifice. At this point, the influence of Moorish Spain was almost exclusively limited to the suggestion of specific

⁶ To be more precise, recent studies suggest that Pisan maiolica production continued until the end of the 15th century, albeit in limited. For more information: (Giorgio, 2010)

decorative motifs contextualised into the new purely Renaissance decorative syntax.

1.1.2.2 *The Warm Palette*

Between 1480 and 1510 CE, under the boost of Florentine mercantile capital, Montelupo reached the peak of maiolica production both from an aesthetic/artistic and technical point of view.

The maximum expression of the realist and polychrome Renaissance language was achieved thanks also to the adoption of a warmer palette (Figure 4): lighter blues and greens, warmer orange-yellows (the so-called *Giallone*) and, above all, the introduction of the Red of Montelupo were characteristic of this period.

The Red of Montelupo (Figure 5) was the highest achievement in the maiolica production even from the technical point of view. Indeed, it was an extremely rare and complex colour to obtain (probably



Figure 4 Example of warm palette: "Piatto a nastri con leone rampante" (1490-1510 CE)



Figure 5 The "Rosso Montelupo", Lorenzo di Piero Sartori (1509 CE).

made by third firing⁷), and there was no other known equivalent in any other Italian context. During the historical period in exam, the only similar pigment was the Anatolian Iznik Red.⁸ (Baratta, 2018). More information in Chapter 3.

At this point, the human figures and coats of arms already mentioned were joined by various decorative typologies:

- Between 1470 and 1480 CE, imitations of the characteristic Spanish metallic lustre motifs were commonplace ("parsley leaf"/"vine leaf").

⁷ For completeness's sake, starting from 1470 CE, a second type of third-fire decoration appeared in Montelupo, albeit somewhat limited: the Spanish-inspired metallic lustre.

⁸ It is worth noting that the discovery of archaeological evidence of a red pigment in Cafaggiuolo is consistent with the preview information. Cafaggiuolo's furnaces were indeed operated by Montelupine potters who, upon relocation, brought with them the technology for producing this colour.

- In 1490-1500 CE, decorative genres such as "floral", "peacock feather", and "Persian palm" became increasingly frequent (as well as in the other Italian centres).

However, it was probably between 1500 and 1520 CE that the Montelupine painters reached their highest point with the decorative family "in imitation of porcelain". At the urging of Florentine buyers, potters began to imitate the "blue poppy flowers", the "oriental knots", etc., from the Oriental/Chinese porcelains now available in Tuscany.(Berti, 1998)

1.1.3 Last Phases

1.1.3.1 Late 16th – Early 17th Century

Montelupo's golden era, however, suffered a first halt in the third decade of the 16th century CE. This was, indeed, a complex period for Tuscany.



Figure 6 Plate with "spiral arancio" decoration: late re-elaboration of "imitazione del lustro metallico" genre.

The last attempts to restore the Republic ended with the rise of Cosimo I de' Medici to the title of Duke, but not without consequences. In 1538 CE, a troop of Spanish mercenaries paid by Cosimo I, occupied the middle Valdarno. They sacked and destroyed Montelupo and other cities, as a sign of discontent for a payment received.

Moreover, beyond this traumatic event, the highly changed international context led to a general progressive redistribution of the Florentine funds, strongly contributing to the economic crisis of Montelupo (too much dependent on the Republic).

With the famine of 1590-1591 CE, the socio-economic situation in Mediterranean Europe deteriorated further.

Due to overpopulation during the 15th century, for the first time Egypt and Sicily were unable to meet the demand for cereals from Mediterranean Europe, which was forced to rely on Polish rye. Consequently, new and unexplored trade routes were opened. The Dutch (and English) ships, based in the new markets of Amsterdam or Lübeck, started transporting goods from Poland to Livorno (also Genoa, Lucca, Rome, and Naples), passing through the Strait of Gibraltar. The famine was followed by the economic crisis of 1618-1621 CE (more severe for Southern Europe) and various plague outbreaks in 1630–1632, 1655 and 1675 CE. These and other factors (i.e., the Thirty Years War and the Little Ice

Age) contributed to shifting international balances: the ancient Italian states gradually lost their position in European economic life and became marginalized.

In parallel to this socio-economic instability, there was also a profound creative crisis starting from 1530-1590 CE. Instead of producing new original decorations, the Montelupo artisans could only re-propose tired variations (Figure 6) of Early Renaissance native genres or "translations into the Tuscan language" of motifs created by other Italian centres. Despite the general crisis of this historical period, these new production centres emerged and imposed themselves thanks to new and original decorations: Urbino, Deruta, Venice, and above all, the always flourishing, Faenza.

It is worth noting that two Faentin potters (who moved to the contado in the 16th century) were responsible for introducing the Istoriated in Montelupo. This genre, albeit having some sort of originality and success, was, however, the last positive note in an otherwise dramatically descending trend.

In 1591, Montelupo's ceramists were compelled to seek aid from Grand Duke Ferdinand I. In response, he provided them with a donation in the form of a general commission: a direct, but sporadic, relationship between the court and manufactures was established for the first time. Some of the notable commissions that followed, included the production of maiolica floors for several European royal palaces (1611-1627 CE) and the creation of large maiolica jars (1620-end of 17th century). (Berti, 2008a)

Alongside the Grand Dukes' commissions, it is also worth mentioning:

- The vascular production for healthcare purposes for pharmacies and hospitals.⁹
- The creation of devotional ceramics in the wake of the Counter-Reformation.

Nonetheless, upon the conclusion of the plague pandemic in 1632 CE, Tuscany experienced a significant shift from being a leader exporter of maiolicas to a substantial importer (from Faenza, Albisola and Savona). (Berti, 1999)

1.1.3.2 18th Century

In the 18th century, only a few businesses were still operating in Tuscany, and even fewer were successful.¹⁰

According to "*Relazione sullo stato delle manifatture*" of 1768 CE, in Montelupo six manufacturers produced maiolica and ten earthenware.¹¹

⁹ The increase in morbidity prompted the Italian rulers, notably the Florentines, to establish a more efficient healthcare system.

¹⁰ i.e., The Chigi factory in San Quirico d'Orcia, the Ginori porcelains in Doccia and the Levantino company in Empoli.

¹¹ Only earthenware production remained competitive in Tuscany.

In general, in the 18th and 19th centuries, traditional workshops survived to satisfy only the low-cost market, while the wealthy classes turned towards Chinese porcelain, Dutch delftware or the new European porcelain from Meissen and Limoges. (Mangani et al., 2021)

As a result, the variety of morphologies produced was reduced drastically, and there was a solid technological regression.

- The ceramic bodies often returned to being reddish.
- The colour palette was highly restricted, with the almost exclusive use of ramina green, manganese brown (the two least expensive and most accessible colours) and, more rarely, orange.
- The white monochrome maiolica became the most popular, against an increasingly sporadic use of the cobalt blue.

With the foundation of the Kingdom of Etruria (1801-1807 CE) and the annexation to the French Empire (October 28th, 1807-1814 CE), Montelupo reached its lowest point, risking actual bankruptcy: based on the Imperial Statistics of 1811-1812 CE, only two furnaces were active in Montelupo and another two in Capriaia. (Berti, 2008a)

1.2 MATERIAL REFERENCE CONTEXT

The origin of the term "ceramic" can be traced back to the ancient Greek *keramos*, which in turn arising from the Sanskrit word meaning "to burn".

Ceramics are one of the most significant technological innovations in human history, as well as one of the oldest and most widespread. The earliest traces of fired clay, more than 10'000 fragments of statuettes found in 1920 near Dolní Vestonice (Moravia, Czech Republic), are dated back to 23'000 BCE. These artifacts, depicting mainly zoomorphic figures and women's bodies (the notorious "Venus of Vestonice", a 10 cm tall statue almost undamaged), are trailblazers for a very rich production: decorative potteries, art pieces, religion-related artifacts but also, perhaps above all, everyday-used objects (tableware, food/liquid vessels etc.) have been made by almost every ancient and modern civilisation.

The great success of this technology can be attributed to the abundance of needed raw materials (silicate minerals constitute the vast majority of the earth's crust) and the relative simplicity of the production processes, in the face of highly versatile final objects. Ceramics are, indeed, a remarkably diverse class

Montelupo products (from the kilns of Samminiato and Camaioni) were exported to Pisa, Lucca and the international market, often in parallel with the sheep farming context. Impruneta, instead, dominated the market of outdoor earthenware due to the better quality and durability of the pieces.

of materials, exhibiting a wide range of physical-mechanical (porosity, thermal conductivity, etc.) and aesthetic (e.g., colour) properties depending on materials and techniques employed. Clearly, as science has developed over the centuries, processes have become more refined and a greater number of usable precursors has become available, resulting in the development of high-performance products known as "advanced ceramics" (so-called in contrast with the "traditional ceramics" made from clay and silica).

This chapter will provide an overview of the "traditional ceramics" made by clay (called "potteries" or simply "ceramics", from now on), and their associated technologies. Nonetheless, only Maiolicas will be explored in depth, with a particular emphasis on those aspects relevant to better understand the analyses carried out in this thesis' work. Refer to (Barry Carter & Grant Norton, 2007) and (Kingery, 1976) for further information.

In anticipation of what will be discussed in the following paragraphs, maiolica is a specific kind of earthenware coated with a special tin-rich glazing apparatus (*smalto*), which has the double purpose of whitening the surfaces (typically reddish) and giving them liquid-resistant characteristics.

Assyrians in Mesopotamia (North Iraq) were probably the first to employ tin glazes to decorate bricks. However, over time this technology fell into disuse, until 9th century CE when it was re-discovered by the Islamic world. (Barry Carter & Grant Norton, 2007)

From there, passing through the Spanish Moorish Island of Majorca, maiolica was spread throughout Europe starting from the Mediterranean coasts. Pisa was, indeed, the first Tuscan centre to encounter these new artifacts and to attempt to imitate them, about 40 years earlier than the Florentine capital (of which Montelupo was the main kiln): the first archaeological evidence of maiolicas' circulation in the Florentine context appeared at the end of the 13th century, and only in the border areas with Pisa (Empoli). (Berti, 2008b)

Having specified the type of artefacts under exam, it is now necessary to make a brief mention of their constituent materials (production processes will be discussed in the next paragraph).

In the context of maiolica, two distinct parts can be identified in an artifact: the actual fired ceramic body (historically referred to as *bistugio*) and the glazed covering system (*smalti* and *vetrine* in historic bibliography), which will be the primary focus of this work.

1.2.1 Ceramic body

According to the generic definition provided by (Kingery, 1976), "A ceramic is nonmetallic, inorganic solid". Traditional ceramic, to be more specific, could be defined as synthetic, crystalline (or partially so), inorganic and non-metallic solid, obtained from the processing of natural raw materials (especially clays),

which are, first, mixed with water and shaped, and then irreversibly consolidated by heating (or sintering in more modern times).

Clay is the most important constituent of all the ceramic bodies. According to (Guggenheim et al., 1995), clays are all those materials, naturally occurring, primarily made by fine-grained minerals (<4 µm), typically plastic at appropriate water contents and able to harden when dried and/or fired.

This plasticity derives from the presence of clay minerals: hydrated aluminium phyllosilicates (sometimes partially replaced with Fe or Mg), which structure consists of alternating layers of $[\text{SiO}_4]^{4-}$ tetrahedra (T) combined with octahedrally coordinated aluminium ions (O). Four fundamental groups of clay minerals can be distinguished, based on how this repetition occurs: kaolinites, illite, vermiculites and smectites.

However, the inclusion in the final paste of non-clay materials/minerals is also crucial (whether naturally present in the clays or added by the potters). Silica sands¹², historically, were undoubtedly the most common temper agents: they moderate the plasticity of the clay paste reducing its shrinkage during the drying (and heating) processes.

It's valuable to underline that Sand's components (silica above all but also feldspars and other minerals) influence the reactions intercurrent in the firing cycle too (heating, firing, and cooling). Fluxes species such as carbonates or feldspars, in particular, are capable of lowering the melting point of the higher melting components in the mixture, promoting reactions in the firing cycle and the formation of amorphous phases in the final ceramic body. Extended vitreous phases are fundamental both as binders (of the final minerals/crystals), and to reduce the artifact's porosity.¹³

Low porosity, indeed, should enhance pottery's resistance to the effect of liquids contributing to its durability and resistance to alterations,¹⁴ but it was challenging to achieve in historic periods due to the high temperatures involved and the needed control in heating-firing-cooling processes in kilns. Often potters, not being able to operate in this condition, were used to cover the already fired potteries with one (or more) liquid-proof layers.

Based on the degree of vitrification reached in the firing process, ceramics can be divided into two macro groups:

¹² Often quarried with the same clay minerals.

¹³ Since ceramic bodies are not the focus of this thesis, no further details will be provided; for further information, refer to (Ferrer et al., 2015)

¹⁴ The intercurrent relation between porosity and the conservation status of a ceramic body is actually much more complex and should also take into account the position of the pores, their size distribution and interconnections. Since it cannot be treated exhaustively here, refer to the publications: (Reedy et al., 2017), (Santos et al., 2012), (Costa et al., 2017) to cite few.

- The vitreous stoneware and porcelain with low porosity (<5 %) (Campanella, 2007), deriving from high-temperature processes (1200 – 1300 °C), which favours the formation of amorphous fraction.

- The non-highly-vitreous earthenware typically characterised by higher porosity (> 10 %) (Campanella, 2007) obtained at working temperatures not high enough to develop a significant glassy phase (around 950 – 1050 °C). (Kingery, 1976) (Gracis et al., 2016)

Montelupo's production (and maiolica in general) undergoes this second category: based on the historical bibliography (i.e. the *Statuto* of 1389 and the *Atti Civili* of the 16th century), iron-rich clays quarried from the Arno's river deposits (near Montelupo) and the Montespertoli pit o Morzano¹⁵, were the main ingredients of the row mixture. (Berti, 2008b)

Finally, linking to the iron-rich clays above mentioned, it is necessary to mention the issue of the (possible) chromophores in earthenware, being Montelupo maiolicas recognised as aesthetically valuable assets.

Chromophore species can be present both in the starting clay paste (as impurities of clay minerals) and form during the firing phase (results of the complex reactions occurring in the more or less oxidizing reactor environment). For those reasons in past, it was common to obtain final artefacts, especially earthenware, with coloured ceramic bodies: typically, brownish (in the presence of α -Fe₂O₃ hematite) or black (spinel such as magnetite Fe₃O₄ or wüstite FeO). Although from an operative point of view, these compounds do not represent a real structural disadvantage (unlike the porosity that reduces the impermeability of the object to liquids), they were a significant aesthetic constraint for decorators.

This reason, reinforced by the spread in Europe of Chinese porcelain's fashion from the 14th century, drove ceramists to try to whiten the naturally coloured ceramic bodies exploiting several strategies (even combined).

Leaving apart the engobed production (more traditionally related to Pisa/Siena and developed in Montelupo only in the later moments), the earliest potters in the Florentine area were used to obtain this white background by applying a thick layer of the tin-rich glaze (*smalto*), derived from the Islamic tradition already discussed. This strategy, although aesthetically pleasing, had the great disadvantage of being pretty expensive. The Cassiterite (mineral source of SnO₂) was not available in the Tuscan area and had to be imported from overseas/foreign markets (more information in the next paragraph).

So, taking inspiration directly from the Spaniard competitor maiolica (increasingly imported into the Tuscany), the Montelupo's potters began to

¹⁵ The clay of Montespertoli, of the two, is the purest one as it is almost totally *nicchi*-free. Nicchis are fossils particularly difficult to remove by decantation and extremely dangerous during the firing cycle (they could cause a significant release of gas and the explosion of the artefact).

whiten the *bistugio* directly by adding calcium during the settling and maturation phases of the clay (probably as quick lime (CaO) or slaked lime Ca(OH)₂: *calce viva* or *grassello di calce* in reference bibliography).¹⁶ This technique was used, probably, for the first time around 1360 but it required long improvements until being perfectionated around 1440-1450 (however, it started to be widespread from the beginning of the 1400s). (Berti, 2003) More in-depth information about potteries' composition can be found in the second chapter of (Berti, 2003).

1.2.2 Glazes

In the previous paragraphs, it has been pointed out several times the necessity of coating systems able to confer liquid-resistant characteristics to the otherwise permeable earthenware.

Reducing the porosity of those kinds of artifacts is clearly the primary purpose of those coatings, but their aesthetic value should not be underestimated either.

For clarity, a couple of premises are necessary.

First of all, "coating" is actually a generic term used to indicate both the (more primitive) waterproofing lipidic or wax patinas and the more refined earthy or glaze coatings; but from now on the term will be used to indicate only glazes.

Secondly, it is worth noting that the English term "glaze" refers to any vitreous coating applied to a ceramic surface. In contrast, in Italian sources different terms are used.

Transparent glazes, both colourless and coloured, are usually referred to as *vetrine*, while the matte ones (white or coloured) are called *smalti*.

Finally, in the specific case of historical maiolica three types of glazes are generally distinguished:

- The white tin-rich opaque glaze applied directly on the *bistugio*, also called *smalto* in Italian, is the only layer always present in maiolicas, although not necessarily on all the surfaces (see paragraph 1.1.1.1).
- The coloured glazes used for the possible decorations.
- The transparent lead-rich final coating, named *coperta* or *coverta* in Italian. (Marmi & Berti, 2003a; Tite, 2009)

Since these glazes will be the focus of the experimental part of this thesis, they will be explored more thoroughly in Chapter 3.

For now, it is enough to keep in mind that from a chemical perspective, each type of glaze is primarily composed of glass.

¹⁶ Even with similar results, the Spanish strategy of *salatura* was actually quite different, using the NaCl as a whitener, not easily accessible in the Tuscan inland.

1.2.2.1 *Glass Generalities*

In literature is no easy to find a univocally recognized definition of this class of materials, citing (Shelby, 2005) it can be said that a glass is “an amorphous solid completely lacking in long range, periodic atomic structure, and exhibiting a region of glass transformation behaviour. Any material, inorganic, organic, or metallic, formed by any technique, which exhibits glass transformation behavior is a glass”.

Glasses can therefore present an enormous compositional variability. Operatively, although, all these possible batch materials can be divided in to two main categories: glass formers and glass modifiers.

1.2.2.2 *Glass Formers*

Glass formers, also known as network formers, are the most important components of the glass batch and often lend their name to the final product (such as silica glass or borosilicate glass).

Each glass is primarily made by one or more chemical species, which constitute the infinite three-dimensional random network that represents the actual structure of the glass itself.

Silica (SiO_2 , or more correctly $\text{SiO}_{4/2}$) is, traditionally, the most common glass former, but not the only one. Boric oxide (B_2O_3) and phosphoric oxide (P_2O_5) can efficiently form both single and multi-component oxide glasses. As well as many other compounds can perform as network formers under specific conditions (among all, aluminium oxide Al_2O_3 is pointed out).¹⁷

In the historical maiolica's glazes, silica is the primary glass former.

From the numerous diffraction experiments conducted so far ((Voyles & Abelson, 2003), (Vessal et al., 1996), (Warren & Bischoe, 1938) to cite few), it is clear that silica glass is actually formed by the same repetition unit of the corresponding crystals: the SiO_4 tetrahedra. The central tetra-coordinated silicon atom is bonded to the four oxygens with a high degree of internal order,

¹⁷ In this work will not be explored the reasons why some materials tend to form glass and others not (or at least not easily). In this regard, please refer to the structural theories (Zachariasen's above all), and to the kinetic theories of glass formation reported in (Shelby, 2005).

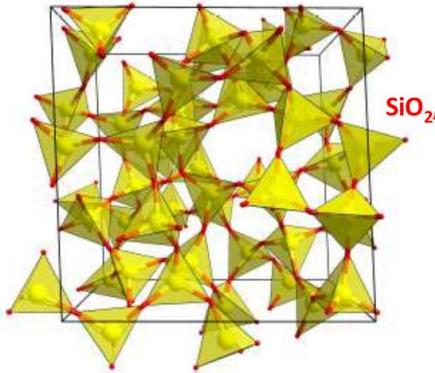


Figure 7 Disordered arrangement the tetrahedra in a silica glass.

which is consistent with the short-range order (≤ 0.25 nm) detected in experiments ($\text{Si}_1\text{-O}_1 \approx 0.162$ nm, $\text{O}_1\text{-O}_2 \approx 0.265$ nm, $\text{O}_1\text{-Si}_1\text{-O}_2$ angle = 109.5°).

Each tetrahedra, in turn, shares the corner-oxygens (defined in this case bridging-oxygens - BO) with four others neighbour tetrahedra, forming the continuous three-dimensional network mentioned above and shown in Figure 7: In pure silica glasses nearly 100% of the oxygens are bridging (except for some defect sites).

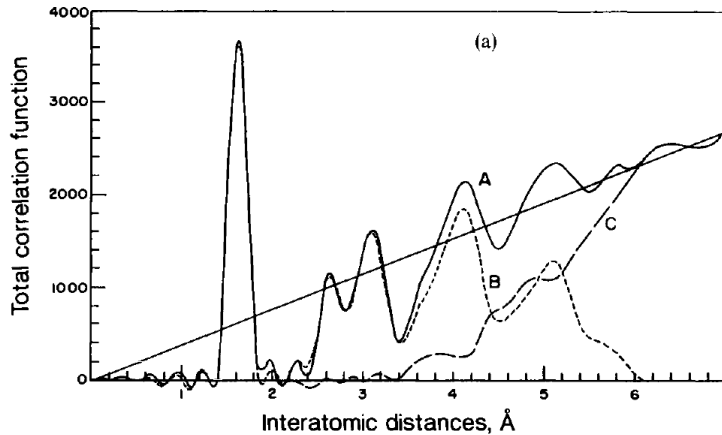


Figure 8 Total pair correlation function from X-ray diffraction experiment.

The disorder (i.e., broader distributions in lengths and angles) observable in the intermediate (≈ 0.3 nm) and long range (≥ 0.35 nm) (Figure 8) is, instead, explained by the variability in the $\text{Si}_1\text{-O}_4\text{-Si}_2$ angle (angle β between the tetrahedra) and admitting the rotations of adjacent tetrahedra, around:

- the corner-shared oxygen (angle α_1)
- the connecting line between shared oxygen and silicon atoms (angle α_2).

Pure silica glasses are the most refractory and resistant to acid corrosion; they also have low electrical conductivity, almost negligible coefficient of thermal expansion and good UV transparency. On the other hand, though, they need extremely high processing temperatures. Silica glass melting point (T_m) is around 1734°C , while even higher temperatures are necessary to obtain it from its precursors (above 2000°C).

1.2.2.3 Glass Modifiers

Although pure silica glasses possess interesting properties, they have the significant limitation of requiring very high processing temperatures.

As a result, dealing with multi-component oxide glasses is much more common, especially in historical times. The glass formers are so frequently added with the so-called modifiers: chemical species not directly participating in the glass network but able to modify it by creating (or stabilising) non-bridging-oxygens (NBO). The formation of NBOs reduces network connectivity, altering, consequently, the properties of the glass. Compared to silica glasses, a general decrease in viscosity and glass transition temperatures (T_g) is detected in the presence of NBO. On the other hand, all properties linked to ion mobility (i.e., diffusion, electrical conductivity, corrosion) and network “floppiness” (thermal expansion coefficient) increase. (Varshneya, 1994)

Some of these species, such as Na_2O , K_2O and PbO , have been employed since historical times as flux agents, added in the starting batch to significantly lower the processing temperatures.

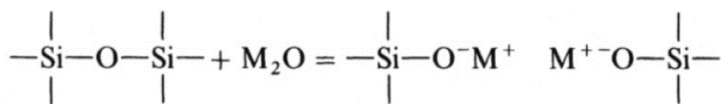


Figure 9 Neutralisation of M^+ positive unit charge by breaking an BO.

In alkali-silica glasses, alkalis enter the network as singly charged cations M^+ occupying interstitial sites. As the reaction in Figure 9 shows, the neutralisation of their positive unit charge is accomplished by breaking an oxygen bridge. Each NBO is associated with a nearby alkali ion to maintain local charge neutrality; consequently, the concentration of non-bridging oxygens increases proportionally to the alkali oxide content. (Shelby, 2005)

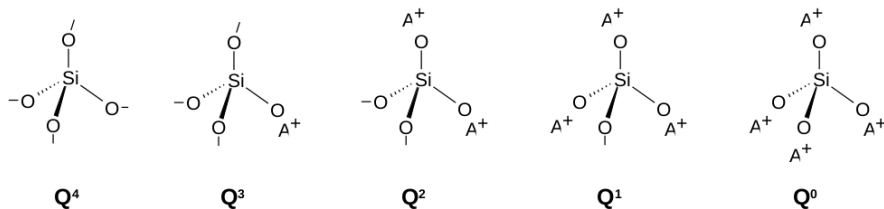


Figure 10 The Q^n species in equilibrium in the glass. A^+ : singly charged cation occupying interstitial sites

Exploiting the nomenclature system Q_n (Figure 10), in which a fully linked to the network tetrahedra (i.e., four BO) is referred to as Q_4 , while an isolated tetrahedra (i.e., four NBO) is a Q_0 unit, it is easily possible to calculate the effect of alkali oxide concentration on the relative theoretical concentrations of Q_n

units in alkali silicate glasses. Figure 11 show these distributions.⁷ (Karlsson & Froberg, 1987)

However, it is even more frequent to deal with three-component glasses: silica-alkali-alkaline earth glasses. The alkaline earth oxides, network modifiers as well, are characterised by a bivalent cation which creates two non-bridging-oxygens (every M^{2+} ion must have two neighbouring NBOs for neutralisation purposes). This structure provides stronger network linkages compared to the bicomponent silica-alkali glasses, since the M^{2+} ions are much more tightly bonded and behave as network stabilisers. The result is an overall higher chemical durability in the final glass. (Shelby, 2005)

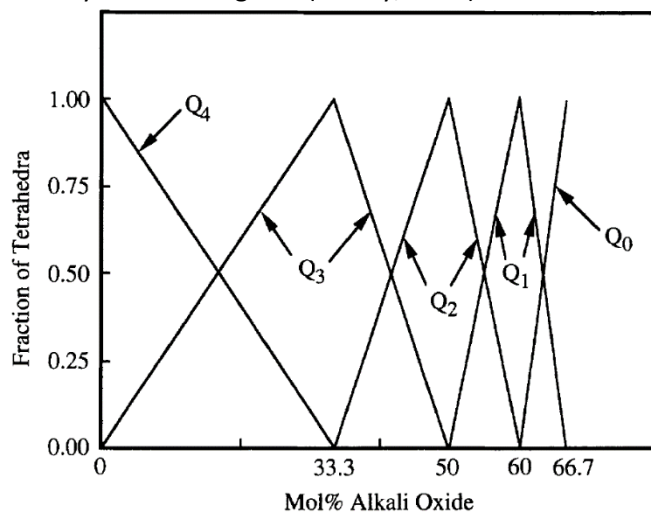


Figure 11 Relative (theoretical) concentrations of Q^n units in relation to the alkali oxide concentration in silicate glasses.

For summary's sake, so far, only network formers and modifiers have been discussed. However, referring to (Sun, 1947), it is important to point out the existence of intermediate cases. Based on single bond strength, Sun distinguishes, indeed, between glass formers (values > 80 kcal/mol) and glass modifiers (values < 60 kcal/mol), identifying, therefore, as "intermediate" those species having values between 60 and 80 kcal/mol. The paper mentioned above lists two of the most historically relevant species between the intermediates: Al_2O_3 and PbO .

Not wanting to delve into a discussion too broad to be analysed here: these species can behave both as glass modifiers and glass formers based on their concentration and glass composition.

In alkali aluminosilicate glasses, the aluminium structural configurations depend on the $[Al_2O_3/M_2O]$ molar ratio:

- for $[Al_2O_3/M_2O] < 1$, Al^{3+} ions behave as a network former (in tetrahedral coordination).

- at $[Al_2O_3/M_2O] = 1$, an absence of nonbridging oxygens in the structure is reached.

- for $[Al_2O_3/M_2O] > 1$, the Al^{3+} ions enter the network as a modifier in octahedral coordination.

Even more complex seems to be the behavior of PbO. Lead silicate glasses can contain up to 92 wt.% of PbO, which suggests that PbO may act as a network former, at least at higher concentrations (for so high PbO contents all SiO_2 tetrahedra would be isolated, i.e., not able to form the network). (Varshneya, 1994)

In their paper, (Verweij & Konijnendijk, 1976) reported relevant Raman results for the vitreous systems PbO- SiO_2 and K_2O -PbO- SiO_2 at different concentrations.

For the two-component glass, the Raman spectra collected for the 0.50PbO-0.50 SiO_2 and 0.45PbO-0.55 SiO_2 compositions seem to suggest a three-dimensional silica network with a short-range structure similar to the corresponding mineral alamosite⁸. The 0.30PbO-0.70 SiO_2 system exhibits slightly different structures, which are difficult to interpret but may suggest some kind of phase separations.

A structure similar to the first reported binary system is also found in the tri-component glasses K_2O -PbO- SiO_2 for SiO_2 contents < 65 mol%. The spectra acquired at compositions of approximately 55 mol% of SiO_2 , on the other hand, appear to be the sum of the contributions of the two different binary compositions (K_2O - SiO_2 , PbO- SiO_2), suggesting a trend towards phase separation. Finally, for concentrations above 65 mol% of SiO_2 , the tricomponent glass shows signals similar to those detected in the ternary compound K_2O -PbO-4 SiO_2 . Compared to the equivalent bicomponent glass, this might indicate a lower tendency to phase separation for higher SiO_2 contents.

However, for more in-depth information, please refer to the paper above and the exhaustive Ph.D. thesis work (Alderman, 2013).

1.3 PRODUCTION PROCESSES

A wide range of, historical and contemporary, documentation is available regarding Italian maiolica: from kiln inventories to *Atti Civili*, passing through tax documentation, actual treaties focused on production processes, and archaeometric studies.

For this thesis aims, however, reference will be made mainly to "*Li tre libri dell'arte del vasaio*"/"The Three Books of the Potter's Art" and to "*Segreti di Fornace*"/"The Ceramist's Secrets" (and to (Berti, 2008a), already mentioned numerous times in Paragraph 1.1).

The first one is a manuscript¹⁸ by the treatise writer, historian and ceramist Cipriano di Michele Piccolpasso (1524–November 21st, 1579 CE) of Castel Durante¹⁹, in which he reported several ceramists' techniques collected from different parts of Italy. (Piccolpasso, 2007a)

The second is a compendium that the merchant and potters Dionigi Marmi compiled (from 1636 CE to his death) to record recipes used in the art of fire in Montelupo. More specifically, in addition to his own techniques, Marmi also copied those described in the 15th-16th-century "Wellcome Code 479" (also known as the "Calabranzi Code")²⁰ and in the early 17th-century "Conradi Code"²¹. (Marmi & Berti, 2003b)

While Piccolpasso's testimony is riveting because it outlines a relatively complete glimpse of the Italian situation of the 16th century with fundamental indications on the origin of the raw materials, it is undoubtedly "*Segreti di Fornace*", in our case, that provides the most exhaustive and context-specific information of Montelupo.

Leaving aside momentarily the glazes recipes (they will be the focus of the following chapters), it is worth examining the complex Montelupine production processes, as revealed by the reference bibliography.

In Paragraph 1.1, the terms "furnaces" and "workshops" are reported several times as interchangeable synonyms without underlining the substantial difference between the two: the presence of the kiln.

The furnaces are typically "full cycle" manufacturers, with kilns and specialised spaces for clay processing and decoration. However, although there were several furnaces in Montelupo, even more common were workshops. These realities, specialised in only some phases of the process, were then forced to rely on others to obtain the finished object.

The bibliography regarding the "full cycle" furnaces identifies seven main phases: preparation of clay mixtures (Paragraph 1.3.1), clay shaping and drying (Paragraph 1.3.2), formulation of coatings (glazes) and colours (Paragraph 1.3.3), first firing (Paragraph 1.3.4), application of glazes and decorations

¹⁸ Currently located in the Victorian and Albert Museum of London.

¹⁹ The current city of Urbania in the province of Pesaro-Urbino, but historically under the domination of the Duchy of Urbino.

²⁰ The "Wellcome Codex 473" is a recipe book from the Calabranzi dynasty of Montelupian ceramists. The manuscript was probably compiled by various members of the family between 1456/1466 CE (with Francesco and Niccolò di Calabranzia) and the date of their transfer, perhaps, to Rome (certainly after 1544 CE: the date appears in reference to the *giallorino*). It was purchased by Marmi on December 8th, 1636 CE, probably in good conservation and without significant modifications/additions.

²¹ Although certainly attributed to the ceramists Ligurian Conradi family, the "Conradi Code" has a more uncertain dating: it is undoubtedly dated before 1639 CE, when Marmi purchased and copied it. The manuscript mainly contains recipes for ceramic colours, predominantly black and yellow.

(Paragraph 1.3.5), second and third firing (Paragraph 1.3.6), and trade of the finished product (Paragraph 1.3.7).²²

1.3.1 Preparation of clay mixtures

The clay purification and decantation processes were likely carried out using the so-called *trogoli*. Although they are not directly mentioned in any historical source, in Montelupo, at least four rectangular depressions (around 2.0 m deep and 3.5 - 2.5 m wide) probably used for this function have been unearthed. Additionally, a shallower pit (about 0.5 m) found near a well was likely used as a *pilla* for liquefying the clay.

The purification and decantation processes were so articulated:

- Liquefaction of the rough clay in the *pilla*.
- Transport of the liquefied product with a *borda* (a flat shovel) into a metal *crivello* (a sort of sieving machine with minute holes).
- Purification of the liquefied clay passing through the *crivello* holes and its deposition in the *trogolo* (while rougher inclusions remained trapped).
- Decantation in the *trogolo* by separating the solid portion from the water.
- Removal of water until full compaction of the deposited clay.
- Separation of clay from its heavier fraction accumulated in the lowest part of the *trogolo* (the last 20 - 30 cm contain mainly sand, mineral inclusions, etc.; this *reniccio* was reused for bricks).

All these processes were usually reiterated up to a maximum of four times depending on the purification degree required. Finally, the product was possibly added with lime (see paragraph 1.2.1) and transported via *barelle* into *terrai* or *conserve* (special covered tanks).

At this point, a second phase began to remove the gases.

Small portions of clay (approximately the size of a fist) were taken and flattened until thin, circular disks (*pagliacci*) were obtained. They were placed vertically on a rough wall (in the shade) until they dried entirely and fell off. The clay was then collected, re-watered before being softened and subjected to two preliminary manipulations: a bare-feet compression followed by manual kneading.

In this last phase, extra sand, minerals, *bistugio's* powders etc., might be added if necessary.

²² Clearly this is a logical-abstract sequence extrapolated from the entire context of Montelupo. In reality, especially within a pre-industrial context, every single furnace rarely followed this process.

1.3.2 Clay shaping and drying

Referring to the sources, artisans could use several strategies to shape the pottery, which also diversified based on the product type. The *terracottai* (i.e. earthenware makers) mainly used the "*a colombino*" technique, while the *stovigliai* (i.e., maiolica makers) preferred the use of the lathe mentioned above. However, other techniques, such as the casting and the leaking, were known and used.

Consequent to the shaping, both from a logical/procedural and logistical point of view, there was the drying step. The fresh product (called "raw" or "green") was placed in a specific storage, not too cold or humid, where it remained until completely dry.

1.3.3 Formulation of coatings (glazes)

Many local court documents report information about exchanges/trades of raw materials between the Montelupo manufacturers. This might indicate that only some furnaces had the necessary facilities for creating coating/glaze precursors. In contrast, all the others were forced to buy them as already formed *marzacotto*.

The *marzacotto* was the base for the recipe of each glaze, and citing Piccolpasso, it was made through the: "*accordo fatto con la rena e con la feccia*".²³ (Piccolpasso, 2007b)

Artisans usually created a mixture of finely ground silica sand and lees, which was fired. Thanks to the presence of (potassic) fluxes, the siliceous portions could melt and subsequently vitrify (by sufficiently rapid cooling). The glass thus created was then collected (by breaking the container) and grounded to obtain a powder that could serve as a base for the glazes.

It is worth noting that the *marzacotto* (with the *coverte*) is also the focus of Marmi's first book of "*Segreti di fornace*". Here, twenty-two different recipes are reported, two of them added by Marmi himself in 1636 (the numbers 12 and 13).

Consistently with Piccolpasso, Marmi reported the use of silica sands (i.e., *pietra pesta* or *rena*) and lees (i.e., *feccia chotta* or *alume di feccia*) as main components of the row batch as well, but he often mentioned the addition of salt too.

However, other strategies were probably used in Montelupo: glass/glaze scraps and/or glasses purchased directly from glassmakers could also be exploited as well.

²³ The winery lees, indeed, contain significant amounts of Potassium bitartrate ($KC_4H_5O_6$).

In any case, once obtained, the *marzacotto* was then *accordato* (i.e., added) with lead oxide, tin oxide and possibly colours in a *fornello a riverbero*²⁴ at temperatures, not typically high, but such as to allow the fusion of the above-mentioned metals.

Finally, the *marzacotto* (enriched in PbO, SnO₂ and colours) was grounded according to various strategies.

1.3.4 First firing

The shaped and completely dried artefact underwent a first firing cycle to obtain the already mentioned *bistugio*.

Probably every production structure equipped with a kiln had a system composed of three different chambers:

- The bottom chamber for the fuel (probably small-sized wood).
- The intermediate chamber for the second firing which will be deepened in the following paragraph.

- The top chamber, called *fornaciotto*, for firing the raw-dried artefact. *Fornaciotto's* location at the top of the kiln and its smaller dimensions (especially in high) allowed it to reach the highest temperature possible (around 980 °C).

Although no archaeological evidence of the upper chambers has been found yet, archaeologists consider this type of structure the most reasonable. Constructions extending vertically upward would be consistent with the relatively small size of ground-level findings and their positioning along the hill ridges. Additionally, a system that allowed the simultaneous firing of glazes/decorations and ceramic bodies at the price of the same quantity of wood would also be the most economically advantageous option.

In Montelupo, the presence of specialised figures known as *fornaciai* is testified by historical sources.

They were responsible for checking kiln's integrity before each firing cycle, positioning the artefacts²⁵ and, above all, controlling the operative times and the thermal curve.

The latter two factors were the most complex to control, especially in a pre-industrial context.

The kiln had to progressively heat up to T_{max} , stabilise at this temperature for a certain amount of time (enough to soften the glazes and subsequently melt them), and finally cool down to ambient temperature. These processes were long (between twenty-four and thirty-six hours) and subject to enormous

²⁴ The *fornello a riverbero* is a specific small kiln with an indirect heating system typically used in the metallurgical "industry".

²⁵ The objects needed not to interfere with the flame draft.

variability (size of the kiln, fuel size, degree of dehydration of the clay) and had to be controlled based only on empirical observation.²⁶

1.3.5 Application of glazes and decorations

All the coatings and decorations were typically applied on the bistugio as water dispersion of the marzacotto, preserved in earthenware basins placed in a specific furnace area called *la pila dei colori*.

Firstly, the ceramic body was dipped inside the basin containing the dispersion of marzacotto-SnO₂ (in water) to apply the opaque white *smalto* layer. The different glaze thicknesses between exposed and non-exposed faces discussed in Paragraph 1.1.2 can be explained by assuming the presence of different containers with varying concentrations of marzacotto in water. The artefacts were then placed on shelves (the *incavigliati*) to dry before being decorated.

For this second step, several objects were placed on a turning plate (the *tondo*) or a lathe. The artist drew the subject (or part of it) with a brush (or similar tools) on the first artefact, and by turning the table, he repeated it on the following one, and so on, according to a "serial production" model.

After further drying, the ceramics were finally covered with the lead-rich transparent *coverta* on the visible parts to make the surface shinier.

1.3.6 Second and third firing

The second firing occurred in the kiln's intermediate chamber, at lower temperature compared to those involved in the first firing, even if sufficiently high to soften (and melt) the various enriched marzacotto layers applied to the bistugio.

In this phase, even more than in the first, the correct placements of the artefacts were fundamental: they had to be narrow enough to optimize the space but not too close to risk the fusing of glazes of different objects.

To prevent this, in some cases, the semi-finished products were protected by special containers (*cassette* or *caselle*), which also acted as a barrier against naked flames and ashes transported by convective motion.

A separate discussion must be made for the third firing hypothesised for the Red of Montelupo.

The traces, albeit very rare, of native metallic lustre maiolica found in Montelupo (attributable to the 1570s) suggest the local use of the so-called

²⁶ The *fornaciai* observed mainly the colour of the kiln's internal earthenware walls and the state of cooking of the so-called *provicelle* (i.e., small ceramic objects inserted in the kiln as a reference and connected to retractable iron rods).

muffola: a special furnace commonly used in Moorish Spain and characterised by a small firing chamber isolated from the open flame. Even though these structures reached relatively low temperatures (around 620-630 °C), they had the great advantage of firing the artefacts in a controlled atmosphere (a reducing one in the case of lustres).

However, it is difficult to establish whether these kilns were also used for the third firing of Rosso Montelupo, which instead would require an oxidising environment (this point will be explored in greater detail in Chapter 4).

1.3.7 Trade of the finished product

Finished products were traded by either land or river/sea.

In the first case, the *fattorini* carried out the deliveries operationally. They took responsibility for the products' integrity (maiolica are fragile artefacts, easily breakable during transport on unpaved roads) and for the money required to pay customs taxes. Due to these responsibilities, they were often owner's relatives.

In the second case, all the responsibilities were assumed by the *navicellai*.²⁷ Generally, the fluvial route was the most convenient, especially after the Pisa's conquest and the abolition of the customs tax needed to reach the port. This route allowed large loads to be moved with less effort and risks, while offering easier international access.

Montelupo leaned on three types of trade:

- Direct commissions from public institutions (pharmacies, hospitals etc.) and private entities (although rarer).
- The local Tuscan market, accessible through land and river routes.
- The international market, reached thanks to the Florentine commercial network (Montelupo maiolica has been found all around the Mediterranean basin and along the Atlantic routes of England and Holland).

²⁷ *Navicellai* were the boat owners. They were independent figures in the ceramic "industry" and responded directly to the *Tribunale della Mercanzia*. Due to the significant amount of money involved, the latter ensured that the goods were not destroyed/lost culpable (and was responsible for punishments, too).

1.4 Bibliography

- Alderman, O. L. G. (2013). *The Structure of Vitreous Binary Oxides: Silicate, Germanate and Plumbite Networks* [Doctor of Philosophy, University of Warwick].
<http://go.warwick.ac.uk/wraphttp://go.warwick.ac.uk/wrap/58185>
- Baratta, I. (2018, March 29). *Il Rosso di Montelupo, capolavoro di una secolare tradizione della ceramica*. Finestra Sull'Arte.
- Barry Carter, C., & Grant Norton, M. (2007). *Ceramic Materials. Science and Engineering*. Springer Science+Business Media .
- Berti, F. (1982). Note sulla maiolica arcaica di Montelupo Fiorentino. *Archeologia Medievale*, 9, 175–192.
- Berti, F. (1997). *Storia della ceramica di Montelupo. Uomini e fornaci in un centro di produzione dal XIV al XVIII secolo. Volume primo: Le ceramiche da mensa dalle origini alla fine del XV secolo*. (Editoriale Tosca srl, Ed.; Vol. 1). Aedo srl.
- Berti, F. (1998). *Storia della ceramica di Montelupo. Uomini e fornaci in un centro di produzione dal XIV al XVIII secolo. Volume secondo: La ceramica da mensa dal 1480 alla fine del XVIII secolo*. (Editoriale Toscana srl, Ed.; Vol. 2). Aedo srl.
- Berti, F. (1999). *Storia della ceramica di Montelupo. Uomini e fornaci in un centro di produzione dal XIV al XVIII secolo. Volume terzo: Ceramiche da farmacia, pavimenti maiolicati e produzioni "minori".: Vol. Terzo* (Editoriale Tosca srl, Ed.). Aedo srl.
- Berti, F. (2001). *Storia della ceramica di Montelupo. Uomini e fornaci in un centro di produzione dal XIV al XVIII secolo. Volume quarto: Una storia di uomini, le famiglie dei vasai.: Vol. Quarto* (LCD, Ed.). Aedo srl.
- Berti, F. (2003). *Storia della ceramica di Montelupo. Uomini e fornaci in un centro di produzione dal XIV al XVIII secolo. Volume quinto: Le botteghe: tecnologia, produzione, committenze. Indici.: Vol. Quinto* (LCD, Ed.). Aedo srl.
- Berti, Fausto. (2008a). *Il Museo della ceramica di Montelupo : storia, tecnologia, collezioni = The Ceramics Museum of Montelupo : history, technology, collections*. Polistampa.
- Berti, Fausto. (2008b). *Il Museo della ceramica di Montelupo : storia, tecnologia, collezioni = The Ceramics Museum of Montelupo : history, technology, collections*. Polistampa.
- Campanella, L. (2007). *Chimica per l'arte*. Zanichelli.
- Cora, G. (1973). *Storia della maiolica di Firenze e del contado Secoli XIV e XV* (Casa editrice Sansoni, Ed.; Vol. 1).

- Costa, D., Leal, A. S., Mimoso, J. M., & Pereira, S. R. M. (2017). Consolidation treatments applied to ceramic tiles: Are they homogeneous? *Materiales de Construcción*, 67(325). <https://doi.org/10.3989/mc.2017.09015>
- Ferrer, S., Mezquita, ; A, Gomez-Tena, ; M P, Machi, ; C, & Monfort, E. (2015). Estimation of the Heat of Reaction in Traditional Ceramic Compositions. *Applied Clay Science*, 108, 28–39. <https://doi.org/10.1016/j.clay.2015.02.019>
- Giorgio, M. (2010). L'ultima maiolica pisana: novità e aggiornamenti sulla produzione di maiolica arcaica a Pisa nel XV secolo. In Centro Ligure per la Storia della Ceramica (Ed.), *Atti XLIII Convegno Internazionale della Ceramica*. All'Insegna del Giglio.
- Gracis, S., Thompson, V., Ferencz, J., Silva, N., & Bonfante, E. (2016). A New Classification System for All-Ceramic and Ceramic-like Restorative Materials. *The International Journal of Prosthodontics*, 28(3), 227–235. <https://doi.org/10.11607/ijp.4244>
- Guggenheim, S., Martin, R. T., Alietti, A., Drits, V. A., Formoso, M. L. L., Galán, E., Köster, H. M., Morgan, D. J., Paquet, H., Watanabe, T., Bain, D. C., Ferrell, R. E., Bish, D. L., Fanning, D. S., Guggenheim, S., Kodama, H., & Wicks, F. J. (1995). Definition of clay and clay mineral: Joint report of the AIPEA nomenclature and CMS nomenclature committees. In *Clays and Clay Minerals* (Vol. 43, Issue 2, pp. 255–256). Clay Minerals Society. <https://doi.org/10.1346/CCMN.1995.0430213>
- Karlsson, K. H., & Froberg, K. (1987). Structural Units in Silica Glasses. *Chemical Geology*, 62, 1–5. [https://doi.org/https://doi.org/10.1016/0009-2541\(87\)90051-9](https://doi.org/https://doi.org/10.1016/0009-2541(87)90051-9)
- Kingery, W. D. B. H. K. , U. D. R. (1976). *Introduction to Ceramics* (2nd Edition). Wiley.
- Mangani, S. M. E., Mazzinghi, A., Mandò, P. A., Legnaioli, S., & Chiari, M. (2021). Characterisation of decoration and glazing materials of late 19th-early 20th century French porcelain and fine earthenware enamels: a preliminary non-invasive study. *European Physical Journal Plus*, 136(10). <https://doi.org/10.1140/epjp/s13360-021-02055-x>
- Marmi, D., & Berti, F. (2003a). *Segreti di fornace*. Aedo.
- Marmi, D., & Berti, F. (2003b). *Segreti di fornace*. Aedo.
- Piccolpasso, C. (2007a). *The Three Books of the Potter's Art - Li tre libri dell'arte del vasaio: Vol. single* (A. Fay Halle, A. Bos, T. B. Keeper, & M. Beck Coppola, Eds.; Second). Scholar Press.
- Piccolpasso, C. (2007b). *The Three Books of the Potter's Art - Li tre libri dell'arte del vasaio: Vol. single* (A. Fay Halle, A. Bos, T. B. Keeper, & M. Beck Coppola, Eds.; Second). Scholar Press.
- Reedy, C. L., Anderson, J., & Reedy, T. J. (2017). Quantitative Porosity Studies of Archaeological Ceramics by Petrographic Image Analysis. *MRS Proceedings*, 1656, 337–353. <https://doi.org/10.1557/opl.2014.711>

- Santos, T. P., Fátima Vaz, M., Pinto, M. L., & Carvalho, A. P. (2012). Porosity characterization of old Portuguese ceramic tiles. *Construction and Building Materials*, 28(1), 104–110. <https://doi.org/10.1016/j.conbuildmat.2011.08.004>
- Shelby, J. E. (2005). *Introduction to Glass Science and Technology* (Second Edition). The Royal Society of Chemistry.
- Sun, K.-H. (1947). Fundamental Condition of Glass Formation. *Journal of the American Ceramic Society*, 30(9), 277–281. <https://doi.org/https://doi.org/10.1111/j.1151-2916.1947.tb19654.x>
- Tite, M. S. (2009). The production technology of Italian maiolica: a reassessment. In *Journal of Archaeological Science* (Vol. 36, Issue 10, pp. 2065–2080). Academic Press. <https://doi.org/10.1016/j.jas.2009.07.006>
- Varshneya, A. K. (1994). *Fundamentals of inorganic glasses*. Academic Press.
- Verweij, H., & Konijnendijk, W. L. (1976). Structural Units in K₂O-PbO-SiO₂ Glasses by Raman Spectroscopy. *Journal of the American Ceramic Society*, 517–521. <https://doi.org/https://doi.org/10.1111/j.1151-2916.1976.tb09422.x>
- Vessal, B., Wright, A. C., Hannon', A. C., & Thomson, J. J. (1996). Alkali silicate glasses: interpreting neutron diffraction results using the molecular dynamics simulation technique. In *Journal of Non-Crystalline Solids* (Vol. 196).
- Voyles, P. M., & Abelson, J. R. (2003). Medium-range order in amorphous silicon measured by fluctuation electron microscopy. *Solar Energy Materials and Solar Cells*, 78(1–4), 85–113. [https://doi.org/10.1016/S0927-0248\(02\)00434-8](https://doi.org/10.1016/S0927-0248(02)00434-8)
- Warren, B. E., & Bischof, J. (1938). The Structure of Silica Glass by X-Ray Diffraction Studies. *Journal of the American Ceramic Society*, 49–54. <https://doi.org/https://doi.org/10.1111/j.1151-2916.1938.tb15742.x>

2 MATERIALS AND METHODS

The extensive use of ceramics throughout history makes them common and well-researched archaeological finds. Numerous archaeometric investigations have been conducted so far to gain further insight into different production centres, exploiting different analytical approaches for different purposes: (Antonelli et al., 2014), (Manca et al., 2023), (Tite, 2009) just to name a few. As outlined in Paragraph 1.1, Montelupo is an exciting context from various points of view but still relatively little studied (especially in comparison to other realities, such as Faenza).

It is worth noting, in this regard, that although Montelupo's productive peak was relatively short (during the Florentine Renaissance), it remained for centuries a vital economic hub for the Middle Valdarno, which still maintains a solid connection to the ceramic industry today.

By inserting itself into a broader cultural climate of valorisation and rediscovery of local contexts often overshadowed by larger historical centres, this research seeks to expand and complete the cognitive framework of Montelupo by filling those gaps that have persisted until now.

Indeed, if more systematic studies are available for Montelupine ceramic bodies (Berti, 2003), knowledge about the glazes and decorations is mainly inferred from historical sources (Marmi & Berti, 2003), (Piccolpasso, 2007). A few papers have been published but are often fragmentary and decontextualised: (Ferrer et al., 2012), (Manca et al., 2023) (Matin, 2019).

The present research precisely aims to define a multi-analytical approach capable of providing a satisfactory and contextualised characterisation of these complex ceramic samples, also recognised as Cultural Heritage assets. In this regard, preserving the state of conservation of maiolicas is of utmost importance.

This last factor plays a crucial role in choosing the analytical strategy. Since the goal is to select a set of analytical methods that can be effectively applied on both musealised artefacts and sherds, therefore a non-invasive and non-destructive approach must be preferred.

2.1 MATERIALS

Firstly, the Museum of Ceramics of Montelupo Fiorentino¹ has been involved thanks to the willingness of Dr Alessandro Mandolesi (former Scientific Director of the Montelupo Museum System), Dr Lorenza Camin (current Scientific Director of the Montelupo Museum System) and Dr Alessio Ferrari (Conservator of the Museum of Montelupo).

Through close collaboration with Dr Ferrari, in particular, a set of samples sufficiently compliant with the needs of this project was identified in the Museum's deposits.

In mutual agreement with the Museum, the choice was oriented towards small sherds rather than well-preserved artefacts, mainly for safety and practicality reasons linked to the transport of the samples to the University of Florence (Unifi) and the National Institute of Nuclear Physics (*Istituto Nazionale di Fisica Nucleare*, INFN) laboratories.² Then again, the fact that the analyses are carried out on fragments does not affect either the reproducibility of the chosen approach nor the results achieved.

Due to Dr Ferrari's expertise, it was possible to select a set that not only met the requirements for statistical significance but displayed a wide range of morphological features and decorative styles.

Morphological variability facilitates the measurements. Having samples equivalent in all aspects except for geometry would partially solve the issues linked to "geometrical interferences" between the sample and the instrument's mechanical parts. This is a common problem working with objects with very concave/irregular shapes, which can prevent the correct positioning of the measuring heads/detector systems etc.

Regarding the decorative styles, the ideal would have been to acquire samples spanning the entire production (from the temporal point of view) featuring all available colours. If the second requirement was easily fulfilled, more difficulties were encountered for the first one.

Specifically, in the Museum's deposits a vast and varied assortment of late Medieval and Renaissance artefacts (corresponding to the period of historical development and peak) is available, while later samples are scarcer (limited to samples C22 and C06), and archaic examples are virtually non-existent.

Thanks to the invaluable assistance of Dr Giovanni Baldi, the Scientific Director of the Colorobbia Research Centre (CE.RI.COL)³, it has been possible to fill this gap. The Research Centre, located in the Middle Valdarno and specialised in the production and distribution of raw and semi-finished materials for the ceramic









¹ <https://www.museomontelupo.it/>





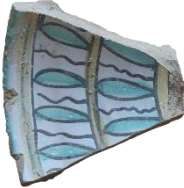



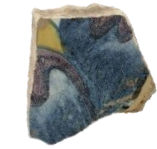
² <https://home.infn.it/>

³ <http://www.colorobbiaconsulting.it/ce.ri.col.html>










and glass industry, has kindly provided samples from the initial production phases (CR1 and CR2) and the latest (CR3, CR4 and CR5).

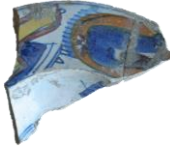









Table 1 displays the samples' specifications, while in Appendix A are visible the photos at higher magnification with relative code and metric reference.

Sample code	Date	Phase	Photo	Other info	Colours
CR1	1280-1320	Archaic maiolica		CE.RI.COL; Puntazza scavo; MTL 169	Bk/Br, Gr
CR2	1380-1400	Early production		CE.RI.COL; Lares. Via XX Settembre; MTL 172	Bk/Br, Gr
A01	1420-1440			MCM; BET1; BET1 164	Bk/Br, Gr
A05	1420-1440			CMC; BET1; BET1 276	Bk/Br, Gr
A08	1440-1460			MCM; BET1; BET1 32	Bk/Br, Gr, Y
A09	1440-1460	Early Renaissance		MCM; BET1; BET1 31	Bk/Br, Gr, Y
C17	1440-1470			MCM; Tridente	Bl, Bk/Br
C18	1440-1470			MCM; Baccio 2	Bl, Bk/Br

A13	1460-1480	Early Renaissance		MCM; Tridente	Bl, Bk/Br
A14	1460-1480			MCM; Tridente	Bl, Bk/Br
A15	1460-1480			MCM; Tridente	Bl, Bk/Br
A16	1460-1480			MCM; Scavo Tolmino	Bl, Bk/Br
C23	1460-1480			MCM; Tolmino Bellucci	Bl, Y
C09	1470-1490			MCM; Bet Corridoio	Bl, Bk/Br, Y
A10	1480-1490	Renaissance Golden era		MCM; Orto scart.	Bl, Bk/Br, Y
A12	1480-1490			MCM; Orto scart.	Bk/Br, Gr, Bl, Y
A17	1480-1490			MCM; Scavo Tolmino	Bk/Br, Bl, Y

Chapter 2: Materials and Methods

A20	1480-1490			MCM; Bellucci	dkBl
A21	1480-1490	Renaissance Golden era		MCM; Bellucci	Bl
A26	1480-1490			MCM; Buca Borsellini	Bk/Br, Gr, Bl, dkBl, Y
A27	1480-1490			MCM; Buca Borsellini	dkBl, Y
C11	1480-1490			MCM; Fossa Borsellini	Gr, Bl, lgBl, Y
C13	1480-1490			MCM; Baccio 2	Bk/Br, Bl, O
C19	1480-1490			MCM; Pozzo Lavatoi RC	Bl, Pr
C01	1490-1500			MCM; Fossa Spagni	Bl, O, R
C03	1490-1500			MCM; SCT 88	Gr, Bl, lgBl, O, R

C14	1490-1510	Renaissance Golden era		MCM; Orto Scartagli	Bl, Y, O, R
C05	1500-1510			MCM; Orto Scartagli	Gr, Bl, Y, R
C08	1500-1510			MCM; Baccio 2	Gr, Bl, O, R
C10	1500-1510			MCM; Baccio 2	Gr, Bl, O, R
C12	1500-1510			MCM; Fossa Borsellini	Bl, O
C15	1500-1510			MCM; Orto Scartagli	Bl, Y, R
C07	1505-1515			MCM; Pozzo Lavatoi V	Bl, Y, O, R
C02	1510-1520			MCM; Orto Scartagli	Bl, Y
C04	1510-1520			MCM; Orto Scartagli	Gr, B, Y, R
C16	1510-1520			MCM; Orto Scartagli	Bl, Y, O, R








C21	1520-1530			MCM; Fossa Spagni	Bl, Y, O
C20	1530-1550	Late Renaissance		MCM; Fossa Spagni	Bl, O
C22	1600-1630	17 th century		MCM; Casa Baccio	Bk/Br, Gr, Bl, Y, O
CR3	17 th c.			CE.RI.COL.; MTL 156	dkBl, Y
C06	1750-1780	18 th century		MCM; Gilio II	Bk/Pr, Gr, lgBl, O
CR4	18 th c.			CE.RI.COL.; MTL 132	Gr
CR5	18 th c.			CE.RI.COL.; MTL 133	Gr

Table 1 List of samples and their specifications. In other information: supplier (MCM: Museum of Ceramic of Montelupo; CE.RI.COL: Colorobbia Research Centre); archaeological excavation (if known) and other codes. Colours: Gr: green; Bk/Br: black/brown; Pr: purple; Bl: blue; lgBl: light blue; dkBl: dark blue; Y: yellow; O: orange; R red.

2.2 METHODS

As stated at the beginning of this chapter, the primary purpose of the present work is to define a multi-analytical approach suitable for studying historical maiolicas.

More specifically, with the aim to prioritise the conservative state of these artefacts, it was explored the possibility of providing their satisfactory characterisation (at least of the glazes and decorations) by resorting to a predominantly non-invasive and non-destructive approach (Cheung et al., 2017). The most important thing to clarify is that the analytical campaign concentrates solely on the coating and decoration apparatus.

Even if the sherds' exposed ceramic body is accessible, it is also true that most of the selected techniques cannot probe the *bistugio* in a well-preserved sample. Consequently, it was decided to act as if the samples were intact.

Outlined the overall approach, the actual analytical strategy was developed considering the most commonly used techniques in archaeometry and the facilities available at both the University of Florence and the *Laboratorio di tecniche nucleari per l'Ambiente e i Beni Culturali* (LABEC) of the INFN.

The preliminary observations made with LABEC's Dino-Lite Digital Microscope AM4113T⁴ served as a valuable guideline for the extensive elemental and molecular analyses carried out using the X-Ray Fluorescence scanner of the LABEC Laboratory (MA-XRF) and the micro-Raman spectrometer of the *Dipartimento di Chimica "Ugo Schiff"* (DICUS). The complementarity of these two techniques, not surprisingly among the most used in archaeometry, ensured a good characterisation of the surfaces under examination.

Following these results, Ion Beam Analyses (IBA) were strategically planned and conducted at the LABEC-INFN laboratory to acquire reliable semi-quantitative data.

However, even with all the valuable results obtained, some limitations in the chosen approach emerged, mainly due to the (complex and variable) stratigraphy of the maiolicas: so, the possibility of sampling from a small group of artefacts (seven in total, appropriately selected) was explored with the Museum of Ceramics o Montelupo.

With permission granted by the Cultural Heritage Superintendence, seven polished sections from samples C01, C04, C06, C14, C21, C22 and C23 were made at the *Laboratorio Materiali lapidei e geologia applicata, dell'ambiente e del paesaggio, Dipartimento di Scienze della Terra, (LAM-DST)*.⁵

⁴ <https://www.dino-lite.eu/it/prodotti/microscopen/universal/am4113t>

⁵ <https://www.dst.unifi.it/vp-190-materiali-lapidei-e-geologia-applicata-dell-ambiente-e-del-paesaggio.html>

The Scanning Electron Microscope (SEM) analyses carried out on these polished sections at *Centro di Servizi di Microscopia Elettronica e Microanalisi* (MEMA)⁶ proved useful in dispelling doubts and provided a solid base to explore the possibility of obtaining comparable information about the layering of maiolica in a non-invasive manner: using differential Particle Induced X-ray Emission (differential PIXE).

2.2.1 X-Ray Fluorescence

XRF is one of the most used analytical techniques in Cultural Heritage diagnosis as it identifies a wide range of chemical elements (with atomic number $Z > 11$) constituting the sample in a totally non-invasive and non-destructive way, and without requiring any sample preparation. (Seccaroni & Moiola, 2004)

The INFN-CHNet MA-XRF scanner was selected as the first used instrument mainly for its relative ease and speed of execution and for the possibility of working by maps.

The scanning system not only detects the characteristic elements of the different colours but also offers a defined picture of their relative distributions, better clarifying the chemical nature of the involved materials and highlighting any inhomogeneities. Providing elemental distribution maps, XRF also bypasses the poor representativeness of the single-point analyses compared to the whole sample. (Sottili et al., 2022)

2.2.1.1 Theoretical Principles

XRF is performed by detecting the characteristic X-rays emitted from the target after its interaction with a primary X-ray beam.⁷

Following the Lambert-Beer law ($I = I_0 e^{-(\mu\rho x)}$), the primary X-ray is more likely to interact with the target, being either absorbed (Photoelectric effect) or scattered (Compton or Rayleigh scattering), the greater the surface density (ρx)⁸ of the material and the total cross-section of interactions (μ)⁹ are.¹⁰

⁶ <https://www.mema.unifi.it/>

⁷ In the case of X-ray tube sources (typically used in CH) the primary radiation is an X-ray beam with a continuous spectrum and energy up to a few tens of keV (depending on the potential difference applied to the ends of the tube).

⁸ With ρ : material volume density, x : material thickness.

⁹ $\mu = k (\sigma_{\text{Ph}} + \sigma_{\text{C}} + \sigma_{\text{R}})$; k : proportionality constant, σ_{Ph} : Photoelectric effect cross section, σ_{C} : Compton scattering cross section and σ_{R} : Rayleigh scattering cross section.

¹⁰ It is worth noting that the sample's characteristic X-rays undergo the same effects; this aspect is fundamental to consider during the signal detection/processing phases.

In the case of a photoelectric effect (the most probable one, at the XRF's operative energies), the Primary X-ray photon interacts with a target's atom in which it is absorbed. Following this absorption, the incident photon energy is transferred to an atomic electron (photoelectron), which is then ejected. As a result, a photoelectron is expelled, and an inner-shell vacancy is created. This unstable atomic configuration is followed by a rapid de-excitation (order of 10^{-15} s) through the transition of one of the outer-shell electrons to fill the internal gap.

The rearrangement is (usually) accompanied by the emission of an X-ray photon with energy characteristic of the atomic species examined (since the energy is equal to the difference in the electrons' binding energy in the two shells between which the transition occurred). The energy of the X photon depends on the generating atom, according to Moseley's law: atoms with higher Z generate higher energy characteristic X-rays, and vice versa.

The probability of the photoelectric effect increases for higher Z of the material and lower energy of the photon inducing it, roughly following the relationship reported in Equation 1.

$$\sigma_{Ph} \propto Z^5 / E_X^{3.5}$$

Equation 1 σ_{Ph} : Photoelectric effect cross section, Z: average atomic number of the material and E_X : energy of the incident photon.

The total number of emitted photons (at that specific energy) provides an indication that can be traced back to the concentration of that specific atom in the sample.

When it comes to XRF analysis, high Z atoms in the target generate more intense and energetic characteristic X-rays, while low Z atoms generate less intense and less energetic characteristic X-rays. The latter are also easily self-absorbed within the target due to their lower energy (having higher probabilities to react for photoelectric effect), making them harder to detect.

As a result, the technique is less sensitive to light elements than heavy ones. Indeed, to efficiently detect low energy X-rays (such as those of elements lighter than Si) it is necessary to use an He flow in front of the detector and of the primary X-ray beam.

The information is then displayed as an X-ray spectrum,¹¹ in which all the detectable characteristic X-ray lines of the target's atoms are present.¹²

¹¹ According to Siegbahn's notation, the characteristic X-ray lines are indicated with a series of letters (K, L, M, etc.), referring to the shell in which the primary ionization occurs, and by an alphanumeric subscript (α_1 , α_2 ..., β_1 , β_2 ... etc.) which indicates, instead, the shell of origin of the electron that fills the gap. (Van Grieken & Markowicz, 2001)

¹² A few "masking" effects of the characteristic lines may occur: escape peaks, pile-ups and phenomena of partial (or complete) overlap of the emission lines of different elements.

2.2.1.2 The Equipment

All measurements were carried out with an updated XRF Scanner (Figure 1) developed by CHnet-INFN (Cultural Heritage network of the National Institute of Nuclear Physics). As is made clear by the numerous published works, it is a tool specifically designed and optimised for the analysis of Cultural Heritage (even non-movable ones, given the extreme compactness of the instrumentation). (Taccetti et al., 2023)

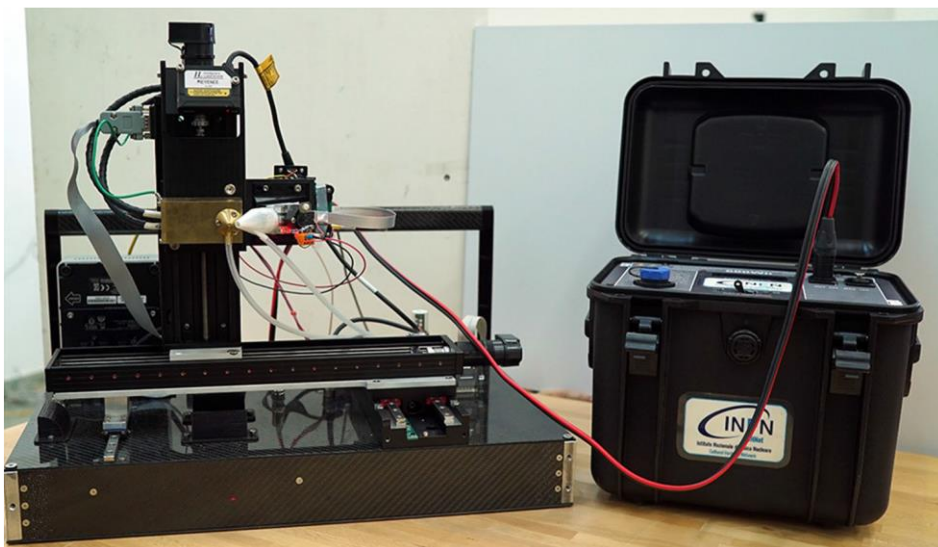


Figure 1 MA-XRF scanning system developed by CHnet-INFN.

The measuring head consists of:

- A Moxtek MAGNUM® X-ray tube (overall size 30 x 30 x 60 mm³, exit window = 127 μm in Be, $V_{\max} = 40$ kV, anode $I_{\max} = 100$ μA) and its alimentionation.
- The acquisition system consists of a detector SDD Amptek XR100 (active area = 70 mm² collimated at 50 mm², thickness = 500 μm, weight = 130 g, possibility of He fluxing) and compact digitalizer (DT5780 of CAEN).

The measuring head is coupled to a highly-light linear motor system in the three X-Y-Z dimensions. The prototype used for this thesis work mounts the following Physik Instrument motor models: VT-80 - 300 (from 300 mm) for the X direction; VT 80-150 (from 150 mm) for the Y direction; M404.2PD (50 mm) for the Z direction. The X and Y slides are used for movements parallel to the surface to be analysed, while Z determines the correct distance between the latter and the measuring head. A telemeter automatically adjusts the Z movement during the measurement, to keep the distance constant even when the surface of the

scanned area is not flat and/or parallel to the scanning plane, as often happens in case of maiolica.

Movement is managed by the Mercury TM/C-862 DC PI system controlled directly by computer via USB cable.

Thanks to the movement of the X-Y motors, the measuring head moves along the scanning area with a raster scan. The software, developed in house, control motion, data acquisition and elaboration, producing distribution maps of the elements of interest.

2.2.2 Raman Spectroscopy

Raman, similarly to XRF, is a spectroscopic method that allows gathering data on the sample's composition without any preliminary preparation and damage. Micro Raman spectroscopy, in particular, not only integrated the exclusively elemental information obtained with MA-XRF (clarifying some doubts relating to pigments) but also enabled the examination of particles/crystals present on sample surfaces at a high spatial resolution.

2.2.2.1 Theoretical principles

In this case, the used probe is a laser beam with radiation's wavelength (UV, Visible or IR) carefully selected based on the analysed sample and, therefore, capable of interacting with the vibrational motion of its molecules without being absorbed.

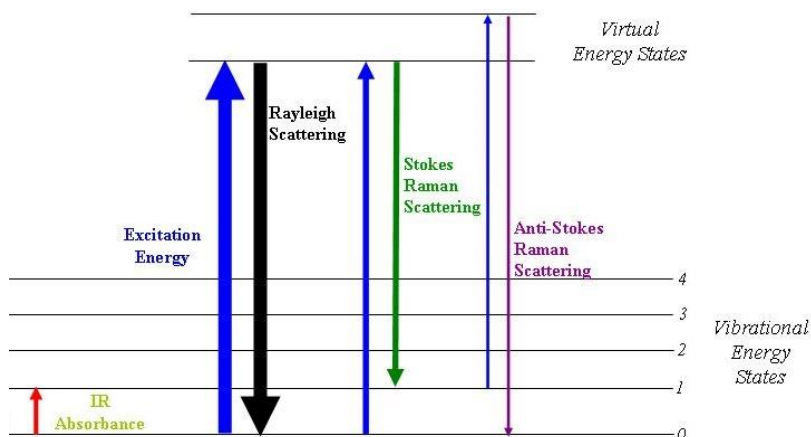


Figure 2 Scheme of the possible scattering phenomena following the molecule absorption of the IR radiation.

In the target, the molecule's bonding electrons form a charged cloud around the nucleus; under the effect of the radiation's electric field (E), this cloud is polarised, determining the transition of the molecule from the fundamental vibrational state (the one with the lowest energy) to the short-live virtual state. This virtual state is unstable, and the way de-excitation takes place determines the type of scattering that occurs.

The incident laser beam (wavelength = λ_o) can interact with the molecule of interest via elastic (Rayleigh scattering, $\lambda_d = \lambda_o$) or inelastic scattering. In the second case, it is referred to as Raman Stokes when $\lambda_f > \lambda_o$ and anti-Stokes Raman if $\lambda_f < \lambda_o$ (Figure 2).

Both Raman Stokes and Raman anti-Stokes scatterings are rare phenomena (around one photon every 10^6 to 10^8 incident photons), but the first one is usually more probable.

The Raman effects are due to the modulation of the laser radiation by the molecules' normal modes of vibration. Since each molecule has peculiar vibration energies (polarizability depends on how tightly the electrons are bound to the nuclei), the vibration spectra obtained at the end of the measurement can be considered fingerprints of the molecules.

They are relatively complex spectra in which three main parameters characterise each individual spectral band/peak:

- The vibrational shift which is influenced by the vibration modes (and so by bond strength).
- The intensity which depends on the molecular polarizability during the vibration.
- The band shape, which is determined by the surroundings.

2.2.2.2 The Equipment

The micro-Raman spectra were acquired in the laboratories of the *Dipartimento di Chimica "Ugo Schiff"*, using the Renishaw RM2000 Raman inVia instrument, consisting of a single grating monochromator (1200 lines/mm, about 4 cm^{-1} spectral resolution) and a cooled CCD detector.

The spectrometer was coupled with a Leica DM2700 optical microscope (20x and 50x optics exploited) and notch filters were employed to decouple Rayleigh and Raman scattering. (Calandra et al., 2022) (Ricci et al., 2023)

All samples were analysed with the Argon laser at 514 nm, acquiring (mainly) in the $120\text{-}1200 \text{ cm}^{-1}$ spectral range.

Laser power, exposure time and accumulations were instead varied based on the colour and type of sample analysed.

All the spectra were processed with OriginPro® software.

2.2.3 Ion Beam Analysis (IBA)

Ion Beam Analysis (IBA) includes a wide range of analytical techniques, yet for this particular study, only Particle Induced X-ray Emission (PIXE) and Particle Induced Gamma-ray Emission (PIGE) analyses were used.

Similar to MA-XRF, PIXE and PIGE provide a multi-elementary characterisation of the samples without any preparation and are non-invasive and not deliberately destructive.¹³

However, their use in the Cultural Heritage field is limited due to the need for costly, scarcely accessible, and non-mobile equipment such as particle accelerators (although technological advancements are rapidly evolving) (Taccetti et al., 2023).

Despite this, they were still included in this work because of their complementarity with XRF.

Notably, PIXE offers higher sensitivity for light elements (low Z) compared to XRF, while the PIGE even identifies the presence of some elements with $Z < 11$ (totally not-detectable to XRF).

Furthermore, the combined use of PIXE and PIGE provides reliable (semi) quantitative data of elemental concentrations, which is instead not possible with XRF. In comparison to XRF, the higher reliability of PIXE and PIGE quantitative analysis is mainly due to the use of a monochromatic proton beam with known energy on the sample (energy straggling effects), but also to the smaller probed thicknesses in PIXE than in XRF.

Typically, at 3 MeV energy the proton beam probes a few tens of μm thickness, while an XRF Primary X-ray beam can reach depths of several tens of μm . For stratified samples, such as maiolicas, the lower penetration of the protons enables to obtain, with good approximation, quantitative information of the glazes alone (excluding the contributions from the ceramic body, present instead in XRF).

The energy of the incident beam can be varied to probe different sample thicknesses, exploiting the differential PIXE technique. (Grassi, 2009) (Grassi et al., 2005)

¹³ Regarding this last point, it is essential to underline the absolute safety in maiolica's application: please refer to papers (Absil et al., 2002) (Beck et al., 2013) and especially (Zucchiatti & Agulló-Lopez, 2012) for further information.

2.2.3.1 Theoretical Principles

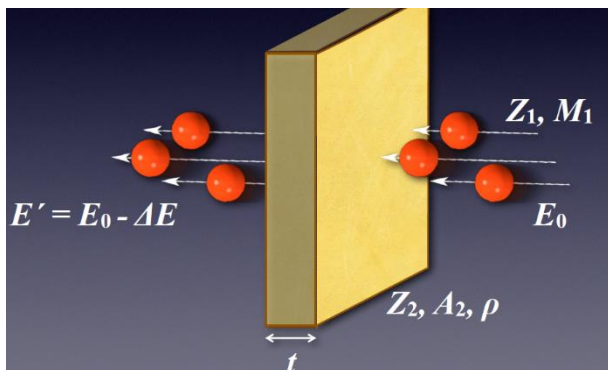


Figure 3 Scheme of interaction of the charged particle beam - target.

PIXE and PIGE are multi-analytical techniques that rely on detecting the characteristic radiations (X-rays and Gamma-rays, respectively) emitted by the target when probed with a charged particle beam (typically protons or α particles) with energy around a few MeV.

The ions of the incident beam (initial energy = E_0) interacting with the target

atoms mainly through Coulomb-type interactions, gradually decelerate to a certain $E' < E_0$ (the intensity of the beam remains constant): Figure 3.

The final energy loss depends on the Z_2 of the material, its thickness and E_0 ; in particular, a target is defined as "infinitely thick" if all the particles of the beam stop within its thickness ($E' = 0$).

Stopping Power (S) is the macroscopic and measurable quantity that describes the average interaction of the ion beam with the material. It considers both the ion interactions with the nucleus (S_n) and electrons (S_e) of the target's atoms (Figure 4).

At typical IBA energies, the most likely reaction is the ionization of the atom due to the expulsion of an inner-shell electron.

As already discussed for the XRF technique, this instability is followed by a de-excitation through electronic readjustment, accompanied by a release of energy that

can trigger two competitive processes: the emission of an X photon (X fluorescence) or the expulsion of an outer-shell electron (Auger effect). In PIXE

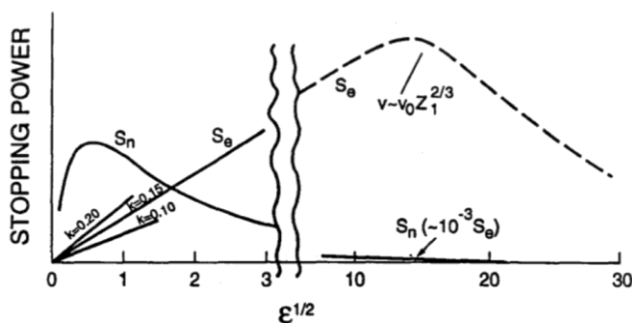


Figure 4 Trends of nuclear stopping power (S_n) and electronic stopping power (S_e) as a function of the energy of the incident beam (ϵ is the reduced term of E)

analysis, as well as in XRF, these characteristic X-rays are detected,¹⁴ and the signal is processed until obtaining an $I(E_x)$ spectrum.

However, the ion beam can also interact with the nuclei of the target's atoms, exciting them: the γ -rays, detected in PIGE analysis, are indeed the product of the de-excitation of aforementioned nuclei.

It is worth noting that, the same probe (in this case, protons) at the same energy (i.e., 3 MeV) has notably lower γ -rays production cross sections (σ_γ) than that of X-ray production.¹⁵

As a result, PIGE generally has lower sensitivity compared to PIXE. However, this drawback is somewhat compensated by the fact that γ -rays are not affected by self-absorption phenomena in the target due to their high energies.¹⁶

2.2.3.2 The Equipment

The IBA analyses were carried out at the INFN LABEC laboratory using the Cultural Heritage extracted-beamline of the High Voltage Engineering Europe's 3MV Tandatron electrostatic accelerator: Figure 5.

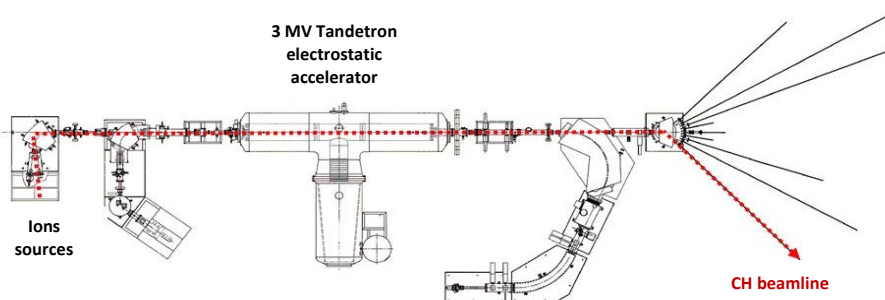


Figure 5 Scheme of the High Voltage Engineering Europe's Tandatron accelerator at LABEC-INFN laboratory.

Total IBA configuration was used to simultaneously perform PIXE and PIGE analyses. The samples' characteristic emissions (both X-rays and Gamma-rays) are collected by several detectors: two SDDs (Silicon Drift Detector), referred to as "Small" and "Big" and one hyperpure Germanium detector.

The detector "Small" (SDD Ketek, active thickness = 300 μm , active surface = 10 mm^2 , 10 μm Be entrance window), coupled with a He fluxing system saturating

¹⁴ It is worth noting that, also in this case, the characteristic X-rays undergo those self-absorption phenomena mentioned for the XRF.

¹⁵ Cross sections (σ_γ) for γ -ray production are also extremely dependent on the energy of the incident beam (resonance-type trends).

¹⁶ Operatively, the use in PIGE of detectors that subtend solid angles greater than those used for x-ray detection in PIXE also contribute to minimising the lack of sensitivity of the first technique.

the detector-sample distance (~ 45 mm), is optimised for counting X-ray photons of the lightest elements (roughly up to Ca).

The detector "Big" (SDD Ketek, active thickness = 450 μm , active surface = 150 mm^2 , 25 μm Be entrance window, distance from the target = 2 cm), thanks to a greater solid angle of detection (which guarantees sufficient counting statistics even for the high-energy X-rays) and a Mylar absorber of 425 μm thickness is exploited for the detection of the most energetic characteristic X-rays.

Finally, a hyperpure Germanium detector from Ortec[®] (20% relative efficiency, distance of approximately 6 cm from the sample) for γ -rays detection, allowed the identification and quantification of elements with $Z \leq 11$. In Maiolica, it was fundamental to have a more accurate quantification of Na (but also to exclude the presence of Li and B, characteristic elements of restoration and modern glazes).

To obtain the semi-quantitative analyses, all the samples were placed approximately 10 mm from the extraction window (a Si_3N_4 membrane of 500 nm thickness) and probed using a 3 MeV proton beam (2970 keV effective on target) with currents in the order of 100 pA and measuring time $t = 300$ s.

For the differential PIXE measurements, the same conditions were maintained by varying only the energy of the incident beam. Each point was probed with proton beams at 2 MeV (1910 keV on target), 3 MeV (2935 keV on target), 4 MeV (3950 keV on target) and 5 MeV (4955 keV on target).

All the acquired spectra were processed with Gupix.win[©] software.

2.2.4 Scanning Electron Microscope (SEM)

The SEM-EDS spectroscopy (Scanning Electron Microscope - Energy Dispersion Spectroscopy), compared to the analyses discussed so far, has the significant disadvantage of being invasive.¹⁷ For this reason, only a small set of maiolicas underwent the necessary sampling and preparation procedures to perform this technique. In the specific case of insulating materials, indeed, a preliminary preparation involving (graphite) metallization is also required.

Nonetheless, the use of SEM-EDS proved to be fundamental in obtaining direct information on the stratigraphy of the samples' glazes: number of layers, their thickness and morphology, composition, identification of crystals, etc.

It is also important to underline that despite being invasive, these analyses are not destructive: the polished sections created for this study are perfectly preserved and can be studied in the future for any further analysis.

¹⁷ At least in this case, where sampling is necessary to obtain information about the glazes' stratigraphic cross-sections.

2.2.4.1 *Theoretical Principles*

The scanning electron microscope consists of a vacuum column which includes all the fundamental parts of the instrument: the source of the primary electrons, the two magnetic lenses for focusing the beam on the sample, the so-called scanning coils (which give the electron beam the necessary movement for the scans) and the detectors.

Like MA-XRF, SEM-EDS provides both punctual information (useful for higher counting statistics and investigating small-scale inhomogeneity) and compositional maps, with also the possibility to obtain high-resolution images (typically image resolution in the range of 1-10 nm).

When the primary electronic probe interacts with the sample, it triggers several processes that produce different signals: secondary electrons, back-scattered electrons, and characteristic X-rays, which are used respectively for morphological images, compositional images, and compositional analysis.

Secondary Electrons (SEs) are generated through inelastic collisions between primary electrons and the atoms of the target. This can alter the trajectory of the electrons and cause a loss of energy, which is transferred to the target atom. Typically, SEs have low energy (< 100-50 eV), and since the inelastic scattering probability decreases with the kinetic energy, the average distance that an SE travels in the target is quite small (around 10 nm).

While SEs cannot provide compositional information, they do offer insight into the surface or near-surface regions of a sample.

Inelastic scattering, indeed, is the most commonly occurring mechanism at the SEM-EDS measurement conditions, so the Secondary Electrons are the most intense and used signal to obtain high-resolution surfaces' morphological images.

On the other hand, Back-Scattered Electrons (BSE) occur as a result of elastic collisions between the primary electrons and the target's atoms. In this case, only the electrons' trajectory changes while their high energy is conserved: BSEs, indeed, provide information from the first few μm of the samples.

Moreover, the production probability of the Back-Scattered Electrons varies directly with the atomic number of the chemical elements present in the target, so they bring compositional information. This information is usually converted in a grayscale compositional image where the darker areas (i.e., fewer BSEs detected) correspond to lighter elements and the lighter ones to elements with higher atomic weight (which return more signal).

Finally, the primary electrons of the incident beam can also interact with an inner-shell electron of a target's atom, expelling it. As in XRF and PIXE, the unstable ionised atom's configuration rapidly re-adjusts, filling the inner-shell vacancy with an outer-shell electron and emitting a characteristic X-ray. The characteristic X-rays come from the first 2-5 μm of the sample and are

fundamental for the sample's qualitative and semi-quantitative compositional analysis.

2.2.4.2 The Equipment



Figure 6 SEM-EDS equipment at MEMA laboratory.

The SEM-EDS analyses were performed at the *Centro di Servizi di Microscopia Elettronica e Microanalisi* (MEMA) of the University of Florence, exploiting the ZEISS EVO MA15 scanning electron microscope reported in Figure 6.

Primary Electron source: tungsten filament, 20 kV potential difference and 700 pA currents; with the Oxford Instruments plc's INCA EDS detector. INCAEnergy 250

software and a Co standard were used for data elaboration and semi-quantitative analyses. The Quorum Q150R ES was employed to metallise the samples' surfaces with graphite. (Cantisani et al., 2021) (Gurrieri et al., 2021)

2.3 BIBLIOGRAPHY

- Absil, J., Garnir, H.-P., Strivay, D., Oger, C., & Weber, G. (2002). Study of color centers induced by PIXE irradiation. *Nuclear Instruments and Methods in Physics, Research B*(198), 90–97. [https://doi.org/https://doi.org/10.1016/S0168-583X\(02\)01522-7](https://doi.org/https://doi.org/10.1016/S0168-583X(02)01522-7)
- Antonelli, F., Ermeti, A. L., Lazzarini, L., Verità, M., & Raffaelli, G. (2014). An archaeometric contribution to the characterization of renaissance maiolica from urbino and a comparison with coeval maiolica from pesaro (The Marches, central Italy). *Archaeometry*, 56(5), 784–804. <https://doi.org/10.1111/arcm.12045>
- Beck, L., Gutiérrez, P. C., Miserque, F., & Thomé, L. (2013). Proton beam modification of lead white pigments. *Nuclear Instruments and Methods in Physics Research, Section B: Beam Interactions with Materials and Atoms*, 307, 20–24. <https://doi.org/10.1016/j.nimb.2012.12.073>
- Berti, F. (2003). *Storia della ceramica di Montelupo. Uomini e fornaci in un centro di produzione dal XIV al XVIII secolo. Volume quinto: Le botteghe: tecnologia, produzione, committenze. Indici.: Vol. Quinto* (LCD, Ed.). Aedo srl.
- Calandra, S., Cantisani, E., Vettori, S., Ricci, M., Agostini, B., & Garzonio, C. A. (2022). The San Giovanni Baptistery in Florence (Italy): Assessment of the State of Conservation of Surfaces and Characterization of Stone Materials. *Applied Sciences (Switzerland)*, 12(8). <https://doi.org/10.3390/app12084050>
- Cantisani, E., Calandra, S., Barone, S., Caciagli, S., Fedi, M., Garzonio, C. A., Liccioli, L., Salvadori, B., Salvatici, T., & Vettori, S. (2021). The mortars of Giotto's Bell Tower (Florence, Italy): raw materials and technologies. *Construction and Building Materials*, 267. <https://doi.org/10.1016/j.conbuildmat.2020.120801>
- Cheung, C. S., Liang, H., Maev, R. G., Gavrillov, D., Thickett, D., Cheung, C. S., Liang, H., Twyde, J., Maev, G., & Gavrillov, D. (2017). Using non-invasive non-destructive techniques to monitor cultural heritage objects. *Insight* •, 59(5). <https://doi.org/10.1784/insi.2017.59.1.XXX>
- Ferrer, P., Ruiz-Moreno, S., López-Gil, A., Chillón, M. C., & Sandalinas, C. (2012). New results in the characterization by Raman spectroscopy of yellow pigments used in ceramic artworks of the 16th and 17th centuries. *Journal of Raman Spectroscopy*, 43(11), 1805–1810. <https://doi.org/10.1002/jrs.4160>

- Grassi, N. (2009). Differential and scanning-mode external PIXE for the analysis of the painting “Ritratto Trivulzio” by Antonello da Messina. *Nuclear Instruments and Methods in Physics Research, Section B: Beam Interactions with Materials and Atoms*, 267(5), 825–831. <https://doi.org/10.1016/j.nimb.2008.12.018>
- Grassi, N., Migliori, A., Mandò, P. A., & Calvo Del Castillo, H. (2005). Differential PIXE measurements for the stratigraphic analysis of the painting Madonna dei fusi by Leonardo da Vinci. *X-Ray Spectrometry*, 34(4), 306–309. <https://doi.org/10.1002/xrs.821>
- Gurrieri, S., Liuzzo, M., Giuffrida, G., & Boudoire, G. (2021). The first observations of CO₂ and CO₂/SO₂ degassing variations recorded at Mt. Etna during the 2018 eruptions followed by three strong earthquakes. *Italian Journal of Geosciences*, 140(1), 1–12. <https://doi.org/10.3301/IJG.2020.25>
- Manca, R., Chiarantini, L., Tartaglia, E., Soldovieri, F., Miliani, C., & Catapano, I. (2023). Non-Invasive Characterization of Maiolica Layer Structure by Terahertz Time-Domain Imaging. *Coatings*, 13(7). <https://doi.org/10.3390/coatings13071268>
- Marmi, D., & Berti, F. (2003). *Segreti di fornace*. Aedo.
- Matin, M. (2019). Tin-based opacifiers in archaeological glass and ceramic glazes: a review and new perspectives. In *Archaeological and Anthropological Sciences* (Vol. 11, Issue 4, pp. 1155–1167). Springer Verlag. <https://doi.org/10.1007/s12520-018-0735-2>
- Piccolpasso, C. (2007). *The Three Books of the Potter's Art - Li tre libri dell'arte del vasaio: Vol. single* (A. Fay Halle, A. Bos, T. B. Keeper, & M. Beck Coppola, Eds.; Second). Scolar Press.
- Ricci, M., Sebastiani, F., Becucci, M., Rogozny, M., & Parfenov, V. (2023). A Spectroscopy-Based Multi-Analytical Approach for Studies in Conservation: Decorations in the Alexander Palace (Tsarskoye Selo). *Spectroscopy Journal*, 1(3), 121–136. <https://doi.org/10.3390/spectroscj1030011>
- Seccaroni, C., & Moiola, P. (2004). *Fluorescenza X. Prontuario per l'analisi XRF portatile applicata a superfici policrome* (Seconda). Nardini Editore.
- Sottili, L., Giuntini, L., Mazzinghi, A., Massi, M., Carraresi, L., Castelli, L., Czelusniak, C., Giambi, F., Mandò, P. A., Manetti, M., Ruberto, C., Guidorzi, L., Re, A., Lo Giudice, A., Torres, R., Arneodo, F., Mangani, S. M. E., Calusi, S., & Taccetti, F. (2022). The Role of PIXE and XRF in Heritage Science: The INFN-CHNet LABEC Experience. In *Applied Sciences (Switzerland)* (Vol. 12, Issue 13). MDPI. <https://doi.org/10.3390/app12136585>
- Taccetti, F., Castelli, L., Chiari, M., Czelusniak, C., Falciano, S., Fedi, M., Giambi, F., Mandò, P. A., Manetti, M., Massi, M., Mazzinghi, A., Ruberto, C., Ronzino, P., Bini, I., Frati, S., Benetti, F., Cestelli Guidi, M., Ciatti, M., Frosinini, C., ... Giuntini, L. (2023). MACHINA, the Movable Accelerator for

- Cultural Heritage In-situ Non-destructive Analysis: project overview. *Rendiconti Lincei*, 34(2), 427–445. <https://doi.org/10.1007/s12210-022-01120-6>
- Taccetti, F., Castelli, L., Czelusniak, C., Giambi, F., Manetti, M., Massi, M., Mazzinghi, A., Ruberto, C., Arneodo, F., Torres, R., Castellá, F., Gheco, L., Mastrangelo, N., Gallegos, D., Morales, A., Tascon, M., Marte, F., & Giuntini, L. (2023). Novel implementation of the INFN-CHNet X-ray fluorescence scanner for the study of ancient photographs, archaeological pottery, and rock art. *Rendiconti Lincei*, 34(2), 515–522. <https://doi.org/10.1007/s12210-023-01143-7>
- Tite, M. S. (2009). The production technology of Italian maiolica: a reassessment. In *Journal of Archaeological Science* (Vol. 36, Issue 10, pp. 2065–2080). Academic Press. <https://doi.org/10.1016/j.jas.2009.07.006>
- Van Grieken, R., & Markowicz, A. (Eds.). (2001). *Handbook of X-Ray Spectrometry* (second). CRC Press. <https://doi.org/10.1201/9780203908709>
- Zucchiatti, A., & Agulló-Lopez, F. (2012). Potential consequences of ion beam analysis on objects from our cultural heritage: An appraisal. *Nuclear Instruments and Methods in Physics Research, Section B: Beam Interactions with Materials and Atoms*, 278, 106–114. <https://doi.org/10.1016/j.nimb.2012.02.016>

3 RESULTS and DISCUSSION

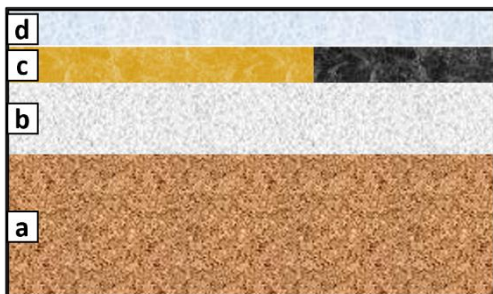


Figure 1 Reconstruction of maiolica's stratigraphy as reported in (Piccolpasso, 2007): a-Earthenware (Bistugio); b-White matt Glaze (Smalto); c-Coloured Layer; d-Transparent Glaze (Coverta).

In this chapter, the results will be presented in three distinct sections: the first and the second paragraphs will focus on the non-invasive campaign conducted on the white and coloured areas, respectively, providing a clear understanding of each. The final paragraph will delve into the SEM-EDS analysis in order to contextualise them and highlight their contributions.

Before discussing the analyses, it

is essential to underline that the results in Paragraphs 3.1 and 3.2 will be reported by "chromatic area" and not by single glaze/layer.

Referring to what is reported in Paragraph 1.3, it is well known that maiolica is characterised by a layered coating/decoration system (reported in Figure 1). Nonetheless, the non-invasive approach chosen does not allow the discrimination of the composition of each individual layer (directly). Instead, all the exploited techniques provide information that is averaged over the entire probed thickness.

3.1 WHITE AREAS

3.1.1 MA-XRF

Firstly, the samples were analysed with the MA-XRF scanner. The maps¹ thus obtained (from areas including also coloured decorations) provide a general idea of the glazes' main characteristic elements and their distribution on the surface of the different samples without, however, highlighting significant variations over the centuries.

¹ In the maps, the detected intensity of each element characteristic X-rays is converted in a chromatic scale in which the red (or the white) corresponds to the higher and the dark green (or black) to the lower intensity.

In Figure 2, the elemental distribution map of sample A05 is reported as example.

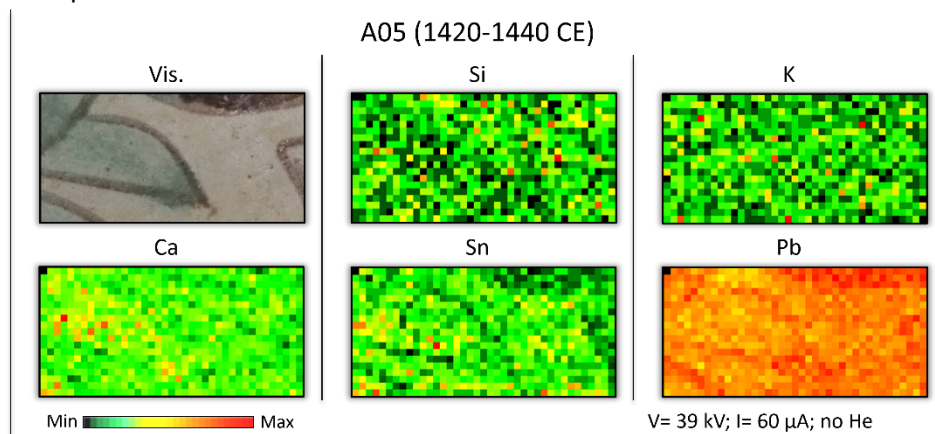


Figure 2 Si, K, Ca, Sn and Pb elemental distribution maps in the early Renaissance maiolica A05. $v=5$ mm/s, $stepX=stepY=1$ mm; collimator diameter= $800\ \mu\text{m}$

In the white areas, MA-XRF detects the characteristic elements of both the white glaze (*smalto*) and the eventually transparent superficial glaze (*coverta*). It is not possible to discriminate whether a specific element comes from one or the other.

However, observing the variations across the surface of the signal related to a specific element, can lead to interesting considerations.

The uniformity in X-rays intensity detected in the case of Si, K and Ca for the white areas is consistent with the historical recipes already discussed in Chapter 1. These elements are attributable to the basic recipe of all the glazes, and they should be present in both the white *smalto* and the *coverta* (and also in the decorative layers). The unexpected presence of Ca, not intentionally added by the artisans according to the recipes, is likely due to impurities of the raw materials. (Othman et al., 2023) (Rasmussen, 2019)

Interestingly, inhomogeneities are instead visible in the Sn distribution maps. The significantly less intense signals detected in correspondence with some chromatic areas could indicate the absorption of the Sn's characteristic X-rays² by the more superficial colourants. This interpretation would be aligned with the documented use of cassiterite as an opacifier in the opaque white glazes. The interpretation of the Pb maps requires a more in-depth discussion.

² This absorption is even more evident since the maps are created using the Sn L characteristic lines. At the used voltages (39 kV), the quantity of primary X photons possessing sufficient energy to cause ionisation in the K shell of Sn is insufficient to generate a characteristic X signal of adequate intensity for detection.

In superficial transparent glazes' historical recipes, the use of significant amounts of *ghetta* (PbO) to enrich the starting *marzacotto* is referenced. (Marmi & Berti, 2003)

Based on this information, it would be reasonable to assume a certain degree of homogeneity in Pb distribution maps throughout all the samples' surfaces, as in the case of sample A05 in Figure 2 and in other studies: (Mangani et al., 2021)³.

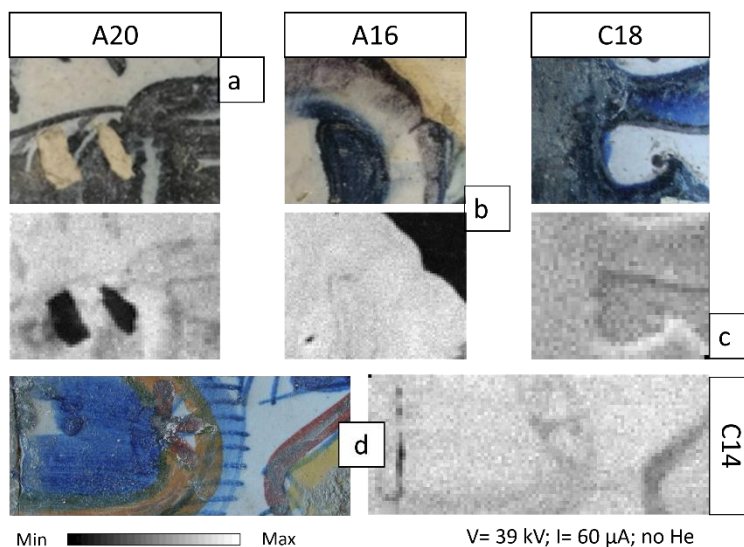


Figure 3 Pb distribution maps in samples: A20 (1480-1490), A16 (1460-1480), C18 (1440-1470) and C14 (1490-1510).

Nevertheless, this pattern is present only in a few samples A05, A10, A17, C05, C20, C22 and A16 reported in Figure 3-b.

More often, samples show an uneven distribution in Pb signals: sometimes milder (Figure 3-d), others more marked (Figure 3-a, Figure 4-c).

Following what is reported in (Tite, 2009a), this might suggest the presence of very thin coatings or their complete absence. In these cases, the majority of lead's Characteristic X-rays detected would originate from the *smalto* and the lower Pb signals collected in the decorations would be consistent with the smaller concentrations of this element in the colourants-enriched *marzacotto* used for these areas. Finally, there are some samples where the higher Pb signals are detected from the coloured areas (mainly yellows); these will be explored in the following paragraph.

It is important to note that Na, Mg and Al presence in surfaces have yet to be discussed so far, not because they are not present but due to the intrinsic

³ In fact, Pb tends to generate very intense X-ray emissions (for the reasons addressed in Paragraph 2.2.1.1), which usually saturate the detected signal working with this type of Lead-rich transparent glaze.

limitation of XRF towards lighter elements. Although it is technically possible to detect Na (and consequently Mg and Al) working in a He atmosphere (and with concentrations > 1 wt%), it was preferred to rely on PIXE (which has significantly higher sensitivity for low-Z elements) and PIGE (for the quantification of Na, in particular) for these elements.

3.1.2 IBA

Using the MA-XRF maps as a guide, a selected set of samples was investigated with IBAs to obtain reliable semi-quantitative information.

The concentrations of all the elements were taken from PIXE, except for Na obtained from PIGE (by comparison with known standards). Using GUPIXWin© software, the oxides' concentrations were calculated from the detected elements, setting a priori the formula of the most probable oxide of each element. The results of the most significant compounds are shown in Table 1.

In addition to the main components reported, further species are detected in concentrations < 0.1 wt%: Cr₂O₃, TiO₂, NiO, CuO, ZnO, Rb₂O, SrO, and Bi₂O₃ traces can be attributed to raw material impurities. (Cherniak & Watson, 2020) (Ollila et al., 2014)

The IBAs confirm the data obtained through MA-XRF and also detect Na, Mg and Al with good signal statistics.

Leaving aside the Mg (present in all the samples in not particularly interesting concentrations) and the already expected Al, the presence of Na₂O is significant as it aligns with Marmi's report on adding salt to the initial *marzacotto* mixture.

Overall, K₂O is always the main fluxing agent (Na₂O concentrations are always lower than that of K₂O), but significant amounts of Na₂O are recorded in the oldest and most recent samples (peaking at around 3 wt% in samples C17 and C18).

In general, the major oxides concentrations, i.e., SiO₂ (45-70 wt%), PbO (20-40 wt%), K₂O (4-5 wt%), and Al₂O₃ (3-5 wt%), are consistent with the high-Lead-content glazes typical of the Italian maiolica during the reference period. (Tite, 2009b)

However, the traces of P₂O₅ detected in some samples deserve to be discussed with more attention.

According to what is reported by Marmi, in Montelupo *marzacotto* was made using *rena* (sand), *feccia* (lees) and *sale* (salt): the K₂O in the final glaze is primarily derived from the potassium bitartrate (KC₄H₅O₆) found in the winey lees (and from k-feldspars of the alumina-siliceous sand).

From this perspective, therefore, the P₂O₅ does not seem to be related to raw materials, but two possible explanations might be explored:

In "*Segreti di Fornace*", Marmi (Marmi & Berti, 2003) reports his interpretation of the two codes already discussed (Paragraph 1.3) in a historical period of commercial and technological crisis for the maiolica. Therefore, it should not be surprising that he considered the winey lees as the only other flux beside ghetta, ignoring, on the other hand, the use, commonly widespread until the 17th century, of the potassic ashes (richer in P) in marzacotto's mixtures. Admitting the use of these potassic ashes in Montelupo, in replacement or conjunction with the winey lees, could explain the traces of P₂O₅ detected.

On the other hand, high P contents are also commonly detected in the corrosion crusts deriving from degraded glazes, together with higher Pb and Ca concentrations in the crusts' surface (Kolářová et al., 2023).

The phosphorous detection in only a few samples (which, it should be underlined, do not show visible crusts), might be more consistent with the second hypothesis but more in delve analyses are necessary.

Table 1 PIXE-PIGE semi-quantitative results on samples' white areas. "-" indicated no detected oxide.

	CR1	CR2	C17	C18	C23	C09	C11
	conc ± err (wt %)	conc ± err (wt %)	conc ± err (wt %)	conc ± err (wt %)	conc ± err (wt %)	conc ± err (wt %)	conc ± err (wt %)
Na ₂ O	1.7 ± 0.2	1.4 ± 0.2	3.7 ± 0.9	3.1 ± 0.7	1.0 ± 0.2	1.7 ± 0.3	0.8 ± 0.1
MgO	1.4 ± 0.2	0.5 ± 0.1	0.7 ± 0.2	0.7 ± 0.2	0.5 ± 0.2	0.5 ± 0.2	0.5 ± 0.2
Al ₂ O ₃	3.1 ± 0.2	4.2 ± 0.1	3.6 ± 0.2	5.1 ± 0.2	2.9 ± 0.2	3.2 ± 0.2	2.3 ± 0.2
SiO ₂	43.7 ± 0.5	64.2 ± 0.3	55.6 ± 0.6	63.5 ± 0.6	60.2 ± 0.5	64.3 ± 0.6	58.5 ± 0.4
P ₂ O ₅	-	-	6.8 ± 0.2	-	-	-	-
K ₂ O	1.9 ± 0.1	3.81 ± 0.07	3.7 ± 0.1	5.0 ± 0.1	1.7 ± 0.1	3.9 ± 0.1	4.0 ± 0.1
CaO	3.6 ± 0.2	2.2 ± 0.1	5.8 ± 0.1	2.5 ± 0.1	1.0 ± 0.1	2.1 ± 0.1	1.8 ± 0.1
MnO	0.32 ± 0.03	< 0.1	< 0.1	0.27 ± 0.03	< 0.1	< 0.1	< 0.1
Fe ₂ O ₃	1.1 ± 0.1	0.23 ± 0.02	0.31 ± 0.03	0.31 ± 0.03	0.26 ± 0.04	0.29 ± 0.04	0.31 ± 0.04
SnO ₂	16.8 ± 1.6	8.2 ± 0.8	10.3 ± 1.2	10.7 ± 1.2	5.0 ± 0.9	9.1 ± 1.5	8.5 ± 1.1
PbO	43.0 ± 3.9	17.5 ± 1.6	19.6 ± 2.1	17.4 ± 1.9	20.0 ± 3.4	30.3 ± 4.4	39.0 ± 4.8
	C13	C19	C01	C03	C14	C05	C08
	conc ± err (wt %)	conc ± err (wt %)	conc ± err (wt %)	conc ± err (wt %)	conc ± err (wt %)	conc ± err (wt %)	conc ± err (wt %)
Na ₂ O	0.6 ± 0.1	0.7 ± 0.1	0.68 ± 0.08	0.9 ± 0.1	1.2 ± 0.2	1.6 ± 0.3	1.3 ± 0.2
MgO	0.4 ± 0.2	0.5 ± 0.2	0.6 ± 0.2	-	-	-	0.2 ± 0.1
Al ₂ O ₃	3.6 ± 0.2	2.6 ± 0.2	3.4 ± 0.2	3.6 ± 0.1	4.1 ± 0.2	5.4 ± 0.2	3.4 ± 0.2
SiO ₂	62.1 ± 0.5	64.9 ± 0.5	60.9 ± 0.4	64.4 ± 0.4	61.2 ± 0.4	69.7 ± 0.4	61.9 ± 0.4
P ₂ O ₅	1.0 ± 0.2	-	-	-	-	-	-
K ₂ O	5.2 ± 0.1	4.4 ± 0.1	5.5 ± 0.1	5.5 ± 0.1	5.2 ± 0.1	4.6 ± 0.1	5.2 ± 0.1
CaO	2.2 ± 0.1	0.7 ± 0.1	2.0 ± 0.1	1.26 ± 0.06	1.7 ± 0.1	2.07 ± 0.06	1.8 ± 0.1
MnO	< 0.1	< 0.1	< 0.1	< 0.1	< 0.1	< 0.1	< 0.1
Fe ₂ O ₃	0.49 ± 0.05	0.19 ± 0.03	0.50 ± 0.05	0.20 ± 0.02	0.25 ± 0.03	0.24 ± 0.02	0.23 ± 0.03
SnO ₂	0.7 ± 0.2	5.7 ± 1.1	1.4 ± 0.6	0.6 ± 0.1	2.5 ± 0.4	0.5 ± 0.1	0.7 ± 0.2
PbO	31.4 ± 3.1	21.8 ± 3.9	36.4 ± 3.7	19.5 ± 2.1	26.8 ± 3.4	21.5 ± 2.2	24.9 ± 3.3

	C10	C12	C15	C07	C02	C04	C16
	conc ± err (wt %)	conc ± err (wt %)	conc ± err (wt %)	conc ± err (wt %)	conc ± err (wt %)	conc ± err (wt %)	conc ± err (wt %)
Na ₂ O	1.3 ± 0.2	0.46 ± 0.06	1.1 ± 0.2	1.1 ± 0.2	0.9 ± 0.1	1.1 ± 0.1	1.1 ± 0.2
MgO	-	0.3 ± 0.2	-	0.4 ± 0.2	-	-	0.3 ± 0.1
Al ₂ O ₃	3.8 ± 0.2	4.4 ± 0.2	3.2 ± 0.2	3.4 ± 0.2	3.4 ± 0.2	3.2 ± 0.2	4.8 ± 0.2
SiO ₂	58.8 ± 0.5	67.5 ± 0.5	58.1 ± 0.4	66.3 ± 0.5	65.7 ± 0.4	68.8 ± 0.4	62.3 ± 0.4
P ₂ O ₅	-	0.3 ± 0.2	-	0.3 ± 0.2	-	-	-
K ₂ O	5.1 ± 0.1	4.7 ± 0.1	5.4 ± 0.1	5.6 ± 0.1	5.3 ± 0.1	5.7 ± 0.1	5.1 ± 0.1
CaO	2.6 ± 0.1	2.2 ± 0.1	2.7 ± 0.1	1.32 ± 0.07	1.17 ± 0.07	1.09 ± 0.07	1.03 ± 0.07
MnO	< 0.1	< 0.1	< 0.1	< 0.1	< 0.1	< 0.1	< 0.1
Fe ₂ O ₃	0.25 ± 0.04	0.26 ± 0.04	0.42 ± 0.04	0.45 ± 0.04	0.26 ± 0.03	0.32 ± 0.04	0.30 ± 0.03
SnO ₂	0.4 ± 0.2	2.2 ± 0.5	0.6 ± 0.2	1.0 ± 0.2	1.6 ± 0.3	0.6 ± 0.2	2.1 ± 0.3
PbO	30.9 ± 4.8	23.4 ± 3.7	34.4 ± 3.6	26.6 ± 2.6	26.5 ± 3.5	19.8 ± 2.2	23.1 ± 2.7

	C21	C20	C22	CR3	C06	CR4	CR5
	conc ± err (wt %)	conc ± err (wt %)	conc ± err (wt %)	conc ± err (wt %)	conc ± err (wt %)	conc ± err (wt %)	conc ± err (wt %)
Na ₂ O	0.57 ± 0.07	1.1 ± 0.2	1.0 ± 0.2	1.2 ± 0.2	1.3 ± 0.2	0.8 ± 0.2	1.3 ± 0.2
MgO	0.5 ± 0.2	0.4 ± 0.2	-	0.6 ± 0.1	-	0.3 ± 0.2	-
Al ₂ O ₃	2.7 ± 0.2	4.1 ± 0.2	3.6 ± 0.2	5.0 ± 0.2	4. ± 0.2	3.7 ± 0.2	4.0 ± 0.2
SiO ₂	69.8 ± 0.5	69.7 ± 0.4	59.6 ± 0.5	63.5 ± 0.4	49.3 ± 0.4	44.1 ± 0.4	50.2 ± 0.4
P ₂ O ₅	-	-	-	-	-	-	-
K ₂ O	4.4 ± 0.1	5.4 ± 0.1	2.4 ± 0.1	4.8 ± 0.1	1.4 ± 0.1	1.2 ± 0.1	1.2 ± 0.1
CaO	1.6 ± 0.1	1.10 ± 0.07	0.38 ± 0.08	2.2 ± 0.1	0.5 ± 0.1	1.4 ± 0.1	0.30 ± 0.07
MnO	< 0.1	< 0.1	< 0.1	0.43 ± 0.04	< 0.1	< 0.1	< 0.1
Fe ₂ O ₃	0.38 ± 0.05	0.35 ± 0.04	0.29 ± 0.04	0.56 ± 0.05	0.22 ± 0.03	0.30 ± 0.04	0.14 ± 0.03
SnO ₂	2.1 ± 0.4	1.0 ± 0.2	1.7 ± 0.4	1.1 ± 0.2	3.3 ± 0.5	3.8 ± 0.7	2.5 ± 0.7
PbO	20.0 ± 2.7	19.1 ± 1.9	37.6 ± 5.7	24.9 ± 2.3	41.4 ± 5.8	60.0 ± 8.6	39.8 ± 4.8

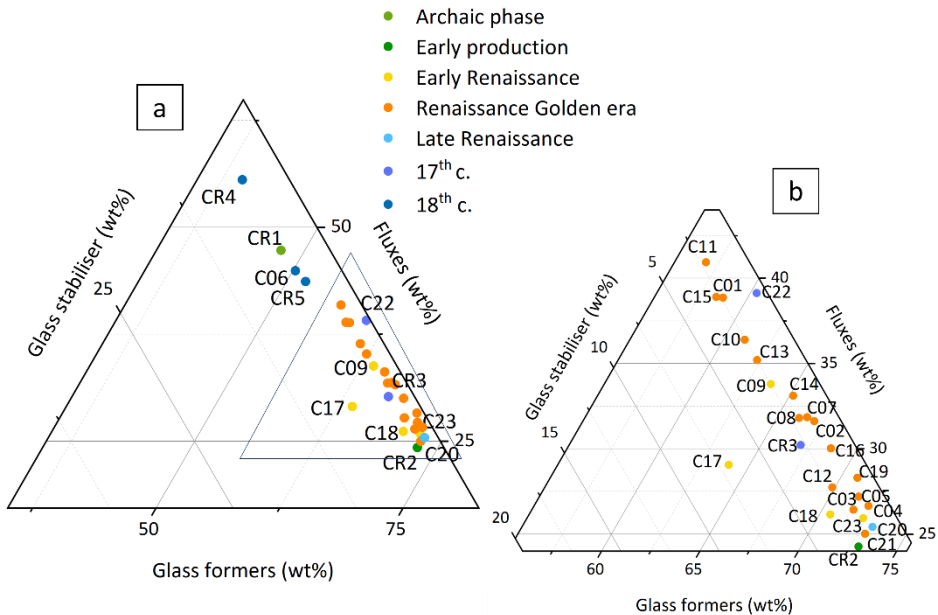
Interesting information is obtained by monitoring the variations of the main oxides over time. Graphic 1 reports the ternary diagram of the glazes' main components so calculated:

- Glass former(s): SiO_2
- Fluxes: PbO wt% + K_2O wt% + Na_2O wt%.
- Glass stabilisers: MgO wt% + CaO wt%.

Al_2O_3 is considered a network former (and therefore added to SiO_2) for ratios $[\text{Al}_2\text{O}_3/\text{M}_2\text{O}] < 1$, or a glass stabiliser for $[\text{Al}_2\text{O}_3/\text{M}_2\text{O}] > 1$ (and so added to MgO wt% + CaO wt%). See Paragraph 1.2.2.3.

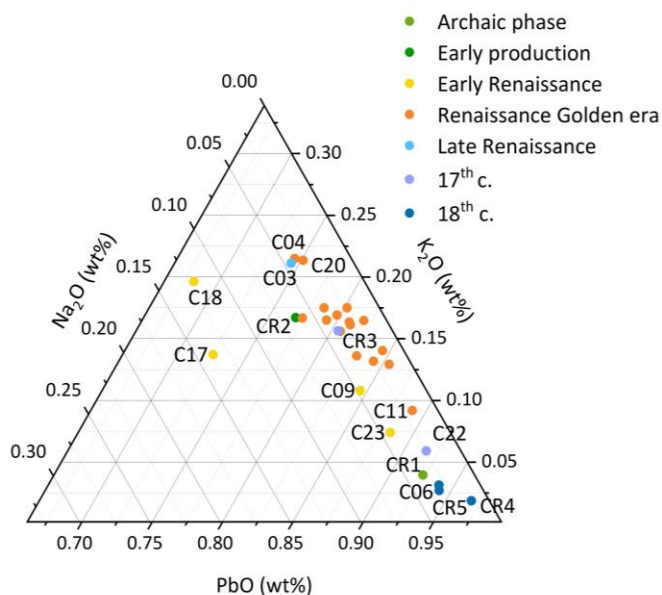
Interestingly, among the samples analysed, only the eighteenth-century samples C06, CR4 and CR5 show $[\text{Al}_2\text{O}_3/\text{M}_2\text{O}] > 1$.

The samples generally present an evident dispersion deriving mainly from the fluctuations in fluxing agents' concentrations. These compositional variations are consistent for pre-industrial artefacts, especially since (based on MA-XRF evidence) not all samples probably have the same stratigraphy. Even starting from the same production technology, samples coated with the transparent glaze will be richer in lead oxide.



Graphic 1 Ternary diagrams of Glass formers (SiO_2 or $\text{SiO}_2+\text{Al}_2\text{O}_3$, if $\text{Al}_2\text{O}_3/\text{M}^+<1$), Fluxes ($\text{PbO}+\text{K}_2\text{O}+\text{Na}_2\text{O}$), and Glass stabilisers ($\text{MgO}+\text{CaO}$ or $\text{MgO}+\text{CaO}+\text{Al}_2\text{O}_3$, if $\text{Al}_2\text{O}_3/\text{M}^+>1$). a: all the samples analysed. b: focus on Renaissance samples.

Moreover, the Graphic 1 shows a clear compositional difference between the maiolicas from the 18th and the 13th centuries and the rest of the set: samples CR1 (1280-1320 CE), CR4 (18th c.), CR5 (18th c.) and C06 (1750-1780 CE) exhibit considerably higher concentrations of fluxes agents.



Graphic 2 Ternary diagrams of glazes' main fluxes: PbO, K₂O and Na₂O. Some labels are removed for clarity (a few samples from the Renaissance Golden era).

C06 and CR1), but also with C22 (1600-1630 CE): these, more modern, maiolicas are much richer in PbO and poorer in K₂O.

The Early Renaissance samples C23 (1460-1480 CE) and C09 (1470-1490 CE), as well as the Golden Era sample C11 (1480-1490),⁴ fall somewhere in between the two extremes mentioned above.

At significantly lower PbO concentrations, two other clusters are highlighted:

- The first formed by the three samples C03 (1490-1500 CE), C04 (1510-1520 CE) and C20 (1530-1550 CE).
- The second formed by the two Early Renaissance samples, C17 and C18 (1440-1470), which, as anticipated, have the highest Na₂O contents among those analysed.

Finally, regarding SnO₂ concentrations, a trend is evident (Table 1).

The highest values are found in the oldest samples (with a peak of 16.8 wt% in CR1) and gradually decrease to the Renaissance Golden Era samples (after 1490 CE). From this time on, the detected SnO₂ stabilises around 1-2 wt%, consistent with the improving of the *bistugio*'s whitening technique with quicklime. Towards the last stages of production (18th century samples), a

The ternary diagram (Graphic 2) that relates the three primary fluxes (PbO, K₂O, and Na₂O) highlight a slight difference.

In fact, in this case, there is a significant uniformity in composition among most of the Renaissance Golden era samples (except for C11, C04, and C03).

Greater differences emerge between the latter and, not only the already pointed out 18th-13th century samples (CR4, CR5,

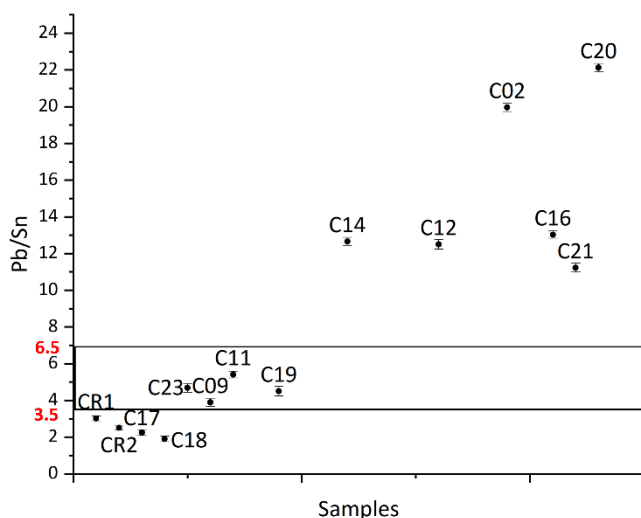
⁴ It is important to point out that the samples, although formally from different production periods, are practically contemporary.

slight increase in SnO₂ concentrations is recorded, however, without exceeding 4% wt.

Moreover, according to the findings presented in the paper (Martin, 2019), an investigation into the potential use of the Pb/Sn ratio to detect the presence/absence of the transparent glaze is conducted. Martin's study delves into the chemical reactions resulting in the cassiterite's formation within maiolica glazes and provides valuable data on Italian and Tuscan maiolica (contemporary to our interest).

The information presented in the paper clearly pertains solely to the white glazes, and they should not be directly comparable to those reported in the Table 1 which, instead, mediate the SnO₂-PbO concentrations for the *smalto + coverta* (if present) system.

However, in principle, the presence of the transparent glaze (not containing SnO₂) should affect the Pb/Sn ratio by raising it. Therefore, by monitoring the discrepancy between the ratio calculated in the present study and the data reported in the paper, an insight into the presence of the *coverta* should be gained.



Graphic 3 Graph of the Pb/Sn ratio calculated for Montelupo's maiolicas (the samples not shown have higher, out of scale, values).

The results are summarised in Graphic 3.

The Pb/Sn ratio calculated for samples CR1, CR2, C17 and C18 is perfectly in line with the values (Pb/Sn < 3.5) found in the case of Archaic maiolicas, as well as samples C23, C09, C11 and C19 fall within the variability (3.5-6.8) of the white glazes described by Martin.

All the other samples, however, present Pb/Sn ratios totally out of line compared to the range proposed in the paper. Albeit the possible absence of the *coverta* could be hypothesised at least for samples CR1, CR2, C17, C18, C23, C09, C11 and C19, more evidence is needed: of the samples reported by Martin, only five are Tuscan (of which only one is from Montelupo) and dated between the 14th and 15th centuries.

3.1.3 Micro Raman

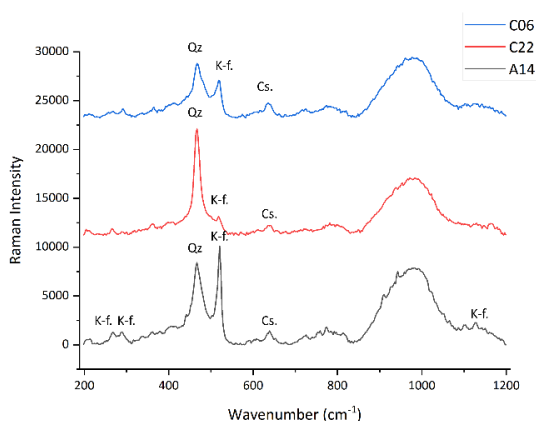


Figure 4 Raman spectra of samples C06, C22 and A14. Quartz peak: 468 cm^{-1} ; K-feldspar peaks: 155 cm^{-1} , 288 cm^{-1} , 515 cm^{-1} and 1120 cm^{-1} ; Cassiterite peak: 635 cm^{-1} .

With a clearer idea of the samples' composition, the micro Raman campaign was strategically planned. This technique proved to be invaluable as it provided us with information on both the crystalline phases and the amorphous aluminosilica network of the glazes in a completely non-invasive and non-destructive manner.

Conducting spectroscopic analyses for the white areas was quite

challenging: strong fluorescence phenomena were often observed, and, in general, a saturation of the signal was often reached even for relatively low incident laser intensities. Consequently, it was not possible for all samples to acquire spectra with a satisfactory signal/noise ratio. (Nardecchia et al., 2021) This, added to the complexity of the already intricate spectra, makes interpretation difficult.

For all the samples, the acquired spectra⁵ exhibit both narrow peaks (relating to the crystalline phases) and broad bands (due to the amorphous part of the glaze).

Focussing on the peaks, basically all the samples reveal signals attributable to Quartz (468 cm^{-1}), K-feldspars (155 cm^{-1} , 288 cm^{-1} , 515 cm^{-1} and 1120 cm^{-1}), and Cassiterite (635 cm^{-1}) which is therefore confirmed to be the opacifier used in Montelupo. Figure 4

Only in the samples C16, C21, C22, CR1 and CR4, a shift of the peak at 515 cm^{-1} towards lower wave numbers is recorded, probably indicating the presence of plagioclase (510 cm^{-1}); while, in samples C12, C14, A17, and CR01 the line at 1085 cm^{-1} typical of CaCO_3 is observed. Figure 5

⁵ Between three and five spectra acquired for each sample, in different point of the white areas.

A whole series of sporadic peaks of difficult interpretation are also found in a few spectra. Referring to the paper (Verweij & Konijnendijk, 1976), some could derive from crystalline silicate phases newly formed during the glaze's firing or residues of the raw materials. Verweij & Konijnendijk lead back to the crystalline phases: $K_2O \cdot SiO_2$ the peak at 590 cm^{-1} (visible in samples C14, CR1); $K_2O \cdot 2SiO_2$ the peak at 1100

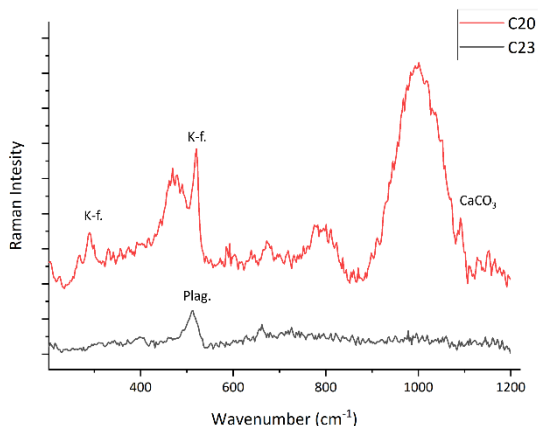


Figure 5 Raman spectra of samples C20 and C23. Plagioclase peak: 510 cm^{-1} ; $CaCO_3$ peak: 1085 cm^{-1} .

cm^{-1} (samples C23, C22, 17, C14); $PbO \cdot SiO_2$ peaks at 950 and 980 cm^{-1} (samples CR4, A15, A14, A06); $K_2O \cdot 2PbO \cdot 2SiO_2$ the peak at 400 cm^{-1} (samples C06, C10, A03, A23); $K_2O \cdot 4PbO \cdot 8SiO_2$ peaks at 380 and 1170 cm^{-1} (samples A03, A05).⁶

As reported in Paragraph 1.2.2 a pure silica glass is a three-dimensional network of $SiO_{4/2}$ corner-sharing tetrahedra. In a pure silica glass, all the corner oxygens are BO and are shared with neighbour tetrahedra: the density of Si-O bonds is at its maximum and the melting temperature (T_m) is at its highest. This unit is a covalent entity with a well-defined vibrational signature characterised mainly by a clearly visible band around 500 cm^{-1} , corresponding to the ν_2 banding mode of the SiO_4 tetrahedron.

More often, however, especially for historical glazes, the need to carry out the firing process at lower temperatures led to modifying the covalent network of pure silica by adding fluxing agents to the raw batch. These compounds have the consequence of inserting, into the network, non-covalently bonded atoms capable of interacting with the repeating unit and creating NBO (and therefore lowering the processing temperatures).

Glasses with this composition (glass former + fluxes + glass modifiers) are characterised by the increase in intensity of the band at 1000 cm^{-1} relating to the ν_1 and ν_3 stretching modes of Si-O. (Prinsloo et al., 2011)

In particular, this band becomes much more intense (compared to that at 500 cm^{-1}) as the number of NBO increases: silica-rich glasses will be characterised by intense bands around 500 cm^{-1} , while the 1000 cm^{-1} band will dominate the

⁶ It is worth noting that these peaks are often visible in only one of the spectra acquired on the surface of the specific sample, unlike the cassiterite, quartz and k-feldspar signals, which are found in (almost) all the points analysed.

spectra of glasses richer in fluxes. Hence, it is possible to obtain information relating to the composition of the glass and its processing temperature from a Raman spectrum.

Based on numerous studies ((Colomban, 2004), (Cesaratto et al., 2010), (Ricciardi et al., 2007) and (Colomban et al., 2006) to cite a few), an attempt to calculate the polymerisation index of Montelupo glazes was made in order to verify the firing temperatures reported in the historical bibliography.

The polymerisation index is defined as the ratio of the areas under the bands at 500 cm⁻¹ and 1000 cm⁻¹ respectively (Equation 1). (Cesaratto et al., 2010)

$$I_p = \frac{A_{500}}{A_{1000}}$$

Equation 1

In the paper (Colomban et al., 2006), six different families of glasses are distinguished based on numerous evidence:

- First family, identified by $I_p < 0.3 - 0.5$, mainly includes lead-rich silicate glazes processed at low temperatures (< 700°C).
- Second family, $0.5 < I_p < 0.8$, made up of lead-rich silicate glazes processed at intermediate temperatures (approximately 800°C).
- Third family, $0.8 < I_p < 1.1$, corresponding to the oldest alkaline glasses and enamels.
- Fourth ($1.1 < I_p < 1.3$) and Fifth families ($1.3 < I_p < 2.5$), related to Ca-based glassy silicate.
- Sixth family ($2.5 < I_p$), includes K-based glazes.

The spectra characterised by the best signal/noise ratio and the least number of peaks derived by crystalline phases⁷ were selected among all the acquired.

Sample	CR2	C17	C23	C11	A21	A17	A27	C14	C05
Date	1380-1400	1440-1470	1460-1480	1480-1490	1480-1490	1480-1490	1480-1490	1490-1510	1500-1510
I_p	0.48	0.21	0.27	0.19	0.26	0.38	0.2	0.25	0.39
± err	±0.02	±0.08	±0.09	±0.06	±0.02	±0.13	±0.03	±0.06	±0.08

Sample	C10	C15	C04	C21	C20	C22	CR4	C06
Date	1500-1510	1500-1510	1510-1520	1510-1520	1530-1550	1600-1630	18 th c.	1750-1780
I_p	0.23	0.23	0.23	0.39	0.23	0.22	0.24	0.17
± err	±0.06	±0.07	±0.06	±0.09	±0.07	±0.07	±0.05	±0.02

Table 2 Polymerisation Index: $I_p = A_{500}/A_{1000}$ calculated from several maiolicas of different datings.

⁷ the greater cross-section of the crystalline phases compared to the amorphous ones tends, in our case, to make the band at 500 cm⁻¹ difficult to see being often masked by the quartz and k-feldspars peaks.

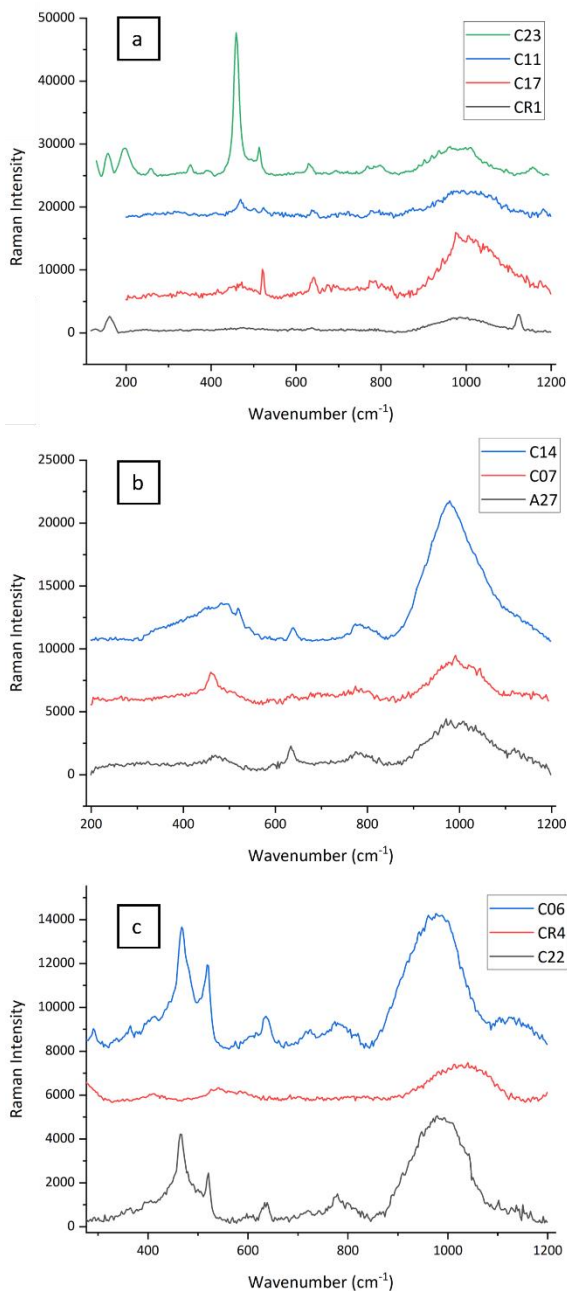


Figure 6 Raman spectra obtained from: a-Archaic and early maiolicas. b-Renaissance Golden era maiolicas. c-Late productions (17th - 18th c.).

Exploiting Fityk software⁸ the baseline was subtracted from the spectra and the areas under the bands around 500 cm^{-1} and 1000 cm^{-1} calculated⁹. In the specific case of Montelupo samples, A_{1000} was calculated taking into account the spectrum region between approximately 700 and 1200 cm^{-1} , for reasons that will be discussed later.

The results obtained are summarised in Table 2. Unfortunately, not all samples were suitable for this type of analysis, but the calculated data seem to confirm firing temperatures lower than 700 °C (First family defined by Colomban). Focusing on the band around 1000 cm^{-1} (the most diagnostic in the case of Pb-rich glazes), an attempt at more refined analysis was also made, trying to identify the wavenumbers of the different tetrahedral arrangements.

By theory, the 1000 cm^{-1} band can be deconvoluted into the Q^n components discussed in the Paragraph 1.2.2.2, and their wavenumber and intensity are proved to be characteristic of glaze's

⁸ <https://fityk.nieto.pl/>

⁹ The Gaussian function was used to approximate each band while for the peaks (excluded so as not to overestimate the areas) a Lorentzian function was exploited.

compositions and firing temperatures.

The paper (Ricci et al., 2007), reports similar analyses conducted on maiolicas of comparable composition to those of Montelupo.

Although notable similarities are visible between Montelupo spectra (Figure 6) and those reported in the study (such as the presence of the band centred at 788 cm^{-1} characteristics of the stretching of Q^0 isolated tetrahedra: Figure 7), further investigations will be necessary.

	Q^0	Q^1	$Pb^{+2}(SiO_3)$	Q^2	Q^3	Q^4
Unfired	–	–	992m	1049s	1094s	1162w
300 °C	–	–	985m	1050s	1094s	1126m
450 °C	778w	905m	984m	1043s	1089s	1141w
600 °C	788m	918m	980s	1024w	1064s	1153m
750 °C	785m	915m	975s	1048s	–	1149m
850 °C	787m	923m	978s	1049s	–	1152m
920 °C	793m	917w	980s	1049s	–	1155w
990 °C	789m	917m	972s	1040vs	–	1151m

Figure 7 Spectral position (cm-1) and relative intensity of the stretching modes (Ricci et al., 2007)

3.2 DECORATIONS

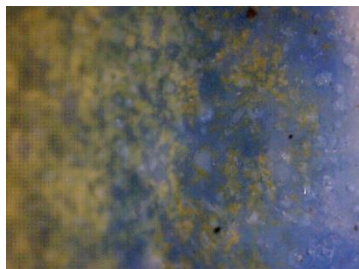


Figure 8 Yellow fine particles in blue uniforme glaze in sample C20. Optical microscope in reflected light, 180x.

Before delving into each individual colour, two premises are necessary.

First, it is important to reaffirm once again what was already said about white areas, especially in relation to the semi-quantitative IBA data reported below.

The oxides' concentrations are calculated from the characteristic X-rays (and γ -rays) of the entire probed thickness. They, therefore, provide an average indication of the entire glaze apparatus and not of the single coloured layer. In fact, the data reported for the

coloured areas throughout the present paragraph will be used to observe the variations of individual oxides compared to the white areas of the same sample.

Second, through the preliminary observations under the reflected light optical microscope, the presence of two distinct types of colours became evident (Figure 8).

The yellows, oranges, reds, and browns/blacks/purples seem to be made by matt glazes with dispersed particles (crystals or powders) within the amorphous matrix.

In contrast, blues and greens appear as uniformly transparent coloured glazes. In these second cases, based on preview studies (Calas et al., 2020; Tite, 2009a), the presence of colourants made by transition metal ions dissolved within the aluminosilicate network is assumed.

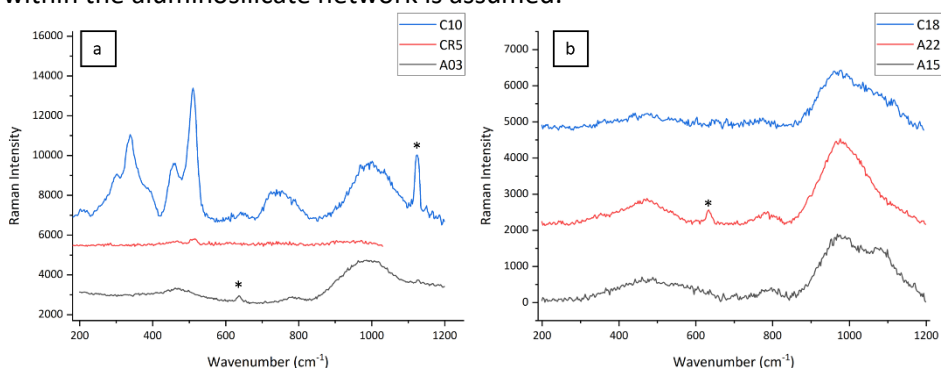


Figure 9 Raman spectra acquired on: a- Green decorations in samples C10 (1500-1510), CR5 (18th c.) and A03 (1420-1440). b- Blue decorations in samples C18 (1440-1470), A22 (1480-1490) and A15 (1460-1480). *Cassiterite peak =633 cm⁻¹; K-feldspar peak=1120 cm⁻¹.

The Raman analyses carried out on all the blues and on CR1, CR2, A01, A05, A08, A09, C23 greens (Figure 9) appear to support this hypothesis: these spectra, indeed, reveal only the distinctive bands of the amorphous silica glaze and the quartz, K-feldspars and cassiterite peaks already discussed. However, in the Renaissance Golden era samples, greens display also definite peaks linked to one (or more) crystalline phases. This point will be further explored in the subsequent paragraph.

Regardless, all colours underwent a similar approach to that previously employed for the white areas.

3.2.1 Green Decorations

From a preliminary visual analysis, the presence of two shades of green within the reference set is evident.

A bluish-green hue characterises the oldest and the more modern samples (pre-1490 CE and 18th century), while a green more yellow tending distinguishes the Renaissance Golden era ones (post-1490 CE).

The surfaces of the samples were first analysed with the MA-XRF scanner to identify the main elements and their distributions in the samples' surfaces.

The elemental distribution maps of the A09 and C04 samples are visible in Figure 11 and Figure 10, respectively, showcasing the two shades of green: a clear correlation between the green areas and the element copper is highlighted for all samples.

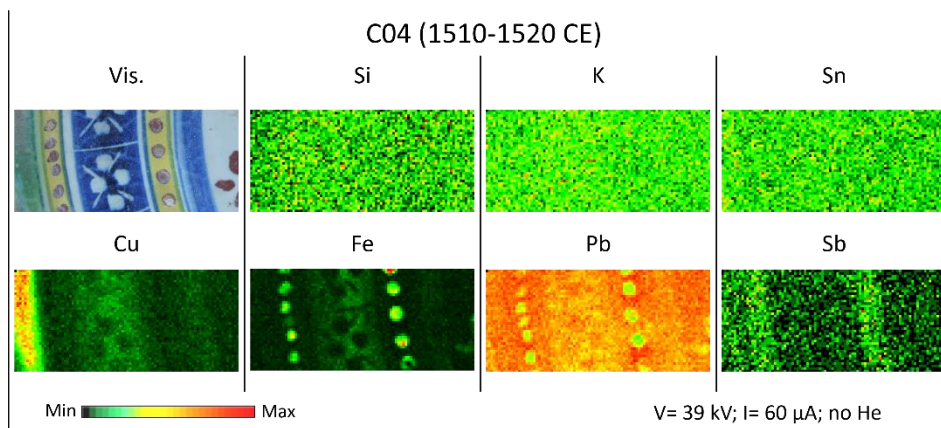


Figure 10 Elemental distribution maps for sample C04; chosen in representative for all the green-yellowish hue.

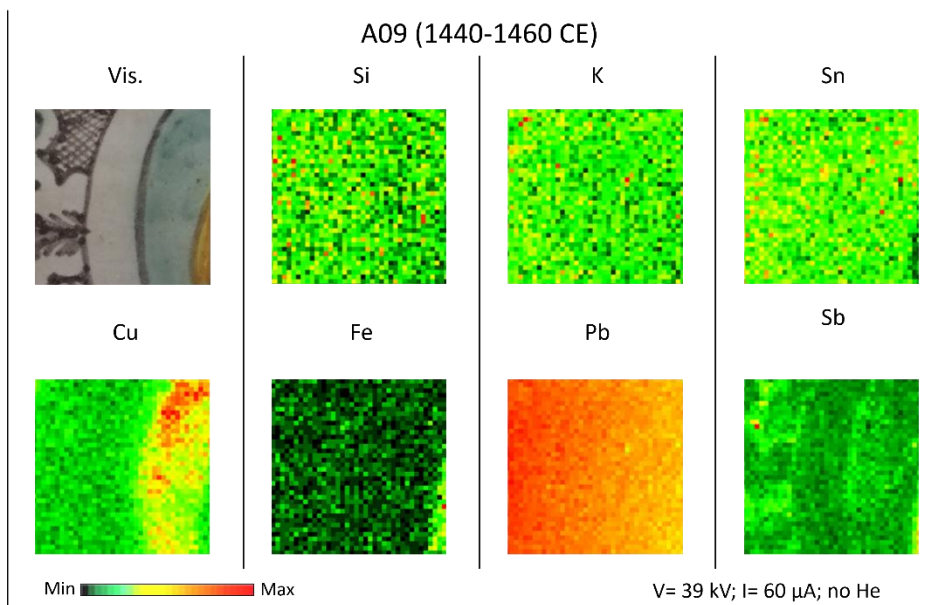


Figure 11 Elemental distribution maps for sample A09; chosen in representative for all the green-blueish hue.

The use of a copper-based colourant would be consistent with historical recipes (referring to the always-mentioned (Marmi & Berti, 2003)) and archaeometric studies conducted in other contexts contemporary to Montelupo. (Crupi et al., 2010), (Odelli et al., 2022). Research have shown that the Cu^{2+} ions in octahedral coordination, when dissolved into a particularly lead-rich glaze, can create this shade of green, tending towards blue. The final colour may vary based on factors such as the thickness of the decorative layer, the firing temperatures, and the concentration of the chromophore. (Peng et al., 2022), (Wang et al., 2022)

A vague distribution of the Sb signals in the green areas also appears in some maps of the Renaissance samples. Nonetheless, the absorption effect on the characteristic X-rays of this element¹⁰ prevents its unambiguous detection in all samples.

The semi-quantitative analyses obtained with IBA provide greater clarity in this regard: Table 3.

The comparison of concentrations emerging in the green areas with those deriving from the white ones of each sample, confirmed the role of Cu^{2+} as the primary chromophore. In samples C03, C10, C04 and C22, the Sb_2O_5 traces are also revealed, probably deriving from a Naples Yellow pigment mixed with the green glaze to make it brighter and less blueish. The Raman spectra acquired in the same greens seem to confirm this hypothesis.

¹⁰ The characteristic L lines of Sb overlap with the K_α lines of Ca and K.

Chapter 3: Results and Discussion

Table 3 Semi-quantitative IBA analyses on white (Wt.) and green (Gr.) areas. "-" no detected oxide. In addition to the reported oxides, the following were also detected: Cr₂O₃, MnO, NiO, ZnO, Rb₂O, SrO, BaO in concentrations <0.1 wt% and almost constant for each measurement point.

		CR01		CR2		C23		C11	
	wt%	Wt.	Gr.	Wt.	Gr.	Wt.	Gr.	Wt.	Gr.
Na ₂ O	c.	1.7	1.5	1.4	2.2	1.0	1.0	0.8	0.8
	± err	0.2	0.2	0.2	0.3	0.2	0.2	0.1	0.1
Al ₂ O ₃	c.	3.1	4.4	4.2	6.1	2.9	5.1	2.3	2.7
	± err	0.2	0.2	0.1	0.2	0.2	0.2	0.2	0.2
SiO ₂	c.	43.7	36.4	64.2	55.6	60.2	54.9	58.5	49.5
	± err	0.5	0.5	0.3	0.5	0.5	0.5	0.4	0.5
K ₂ O	c.	1.8	1.5	3.8	5.0	1.7	1.6	4.0	4.9
	± err	0.1	0.1	0.1	0.1	0.1	0.1	0.1	0.2
CaO	c.	3.6	4.4	2.2	3.5	1.0	1.9	1.8	2.8
	± err	0.2	0.2	0.1	0.1	0.1	0.1	0.1	0.1
Fe ₂ O ₃	c.	1.0	1.5	0.23	0.54	0.26	0.52	0.31	0.38
	± err	0.1	0.1	0.02	0.06	0.04	0.05	0.04	0.06
CuO	c.	0.27	2.1	< 0.1	1.4	< 0.1	1.3	< 0.1	2.0
	± err	0.02	0.2		0.1		0.1		0.3
SnO ₂	c.	16.8	14.5	8.2	8.7	5.0	3.3	8.5	4.6
	± err	1.6	1.3	0.8	1.1	0.9	0.4	1.1	1.0
PbO	c.	43.0	42.1	17.5	21.3	20.0	23.4	39.0	30.0
	± err	3.9	3.3	1.7	2.1	3.4	2.5	4.8	4.8

Chapter 3: Results and Discussion

		C03		C10		C04		C22	
wt%		Wt.	Gr.	Wt.	Gr.	Wt.	Gr.	Wt.	Gr.
Na ₂ O	c.	0.9	1.2	1.3	1.8	1.1	1.9	1.0	1.6
	± err	0.1	0.2	0.2	0.3	0.1	0.3	0.1	0.3
Al ₂ O ₃	c.	3.6	3.5	3.8	5.8	3.2	6.8	3.6	3.9
	± err	0.1	0.2	0.2	0.2	0.2	0.2	0.2	0.2
SiO ₂	c.	64.4	59.5	58.8	57.4	68.8	62.9	59.6	45.9
	± err	0.4	0.4	0.5	0.5	0.4	0.5	0.5	0.5
K ₂ O	c.	5.5	4.9	5.1	4.8	5.7	5.7	2.4	2.5
	± err	0.1	0.1	0.1	0.1	0.1	0.1	0.1	0.1
CaO	c.	1.3	1.0	2.6	2.4	1.1	1.6	0.38	0.94
	± err	0.1	0.1	0.1	0.1	0.1	0.1	0.08	0.09
Fe ₂ O ₃	c.	0.20	0.39	0.25	0.48	0.32	0.37	0.29	2.4
	± err	0.02	0.04	0.04	0.05	0.04	0.05	0.04	0.1
CuO	c.	< 0.1	1.1	< 0.1	1.4	< 0.1	1.9	0.32	2.7
	± err		0.1		0.1		0.2	0.05	0.1
SnO ₂	c.	0.6	1.5	0.4	0.3	0.6	0.5	1.7	1.6
	± err	0.1	0.3	0.2	0.1	0.1	0.2	0.4	0.3
Sb ₂ O ₅	c.	-	1.4	-	0.4	-	0.3	-	0.5
	± err		0.3		0.2		0.2		0.2
PbO	c.	19.5	31.8	30.9	25.2	19.8	20.3	37.6	39.2
	± err	2.1	3.2	4.8	2.5	2.2	2.6	5.7	2.0

		C06		CR4		CR5	
wt%		Wt.	Gr.	Wt.	Gr.	Wt.	Gr.
Na ₂ O	c.	1.3	1.4	0.8	0.8	1.3	1.0
	± err	0.2	0.2	0.2	0.2	0.2	0.2
Al ₂ O ₃	c.	4.0	3.2	3.7	3.5	4.0	4.1
	± err	0.2	0.2	0.2	0.2	0.2	0.2
SiO ₂	c.	49.3	42.2	44.1	33.0	50.2	35.9
	± err	0.4	0.4	0.4	0.4	0.4	0.4
K ₂ O	c.	1.4	1.2	1.2	0.6	1.1	0.6
	± err	0.1	0.1	0.1	0.1	0.1	0.1
CaO	c.	0.5	0.7	1.4	1.0	0.3	0.8
	± err	0.1	0.1	0.1	0.1	0.1	0.1
Fe ₂ O ₃	c.	0.22	0.50	0.30	0.32	0.14	0.40
	± err	0.03	0.05	0.04	0.05	0.03	0.05
CuO	c.	< 0.1	3.4	0.18	4.2	0.19	3.1
	± err		0.3	0.02	0.7	0.05	0.4
SnO ₂	c.	3.3	3.6	3.8	5.1	2.5	3.0
	± err	0.5	0.5	0.7	0.9	0.7	0.5
PbO	c.	41.4	39.1	60.0	68.3	39.8	49.9
	± err	5.8	4.0	8.6	10.6	9.8	6.7

3.2.2 Black/Brown Decorations



Figure 12 Black's fine grain in sample C18. Optical microscope in reflected light, 180x.

Black is the other characteristic colour of the Montelupo early phases, and it was mainly used as outline of the coloured areas or as a decorative filling.

Unlike green, it is found almost exclusively in early samples and in the late ones, while it is almost entirely replaced with dark blue during the Renaissance's peak.

As mentioned, at the optical microscope (Figure 12) black appears as a pigment, sometimes having brown or purple hue, dispersed within a transparent glaze.

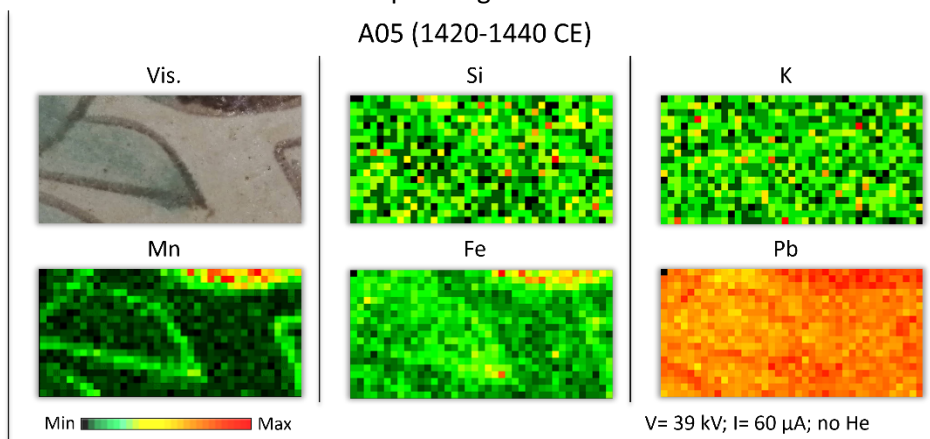


Figure 13 Elemental distribution maps for sample A05.

The XRF scanner's elemental distribution maps (Figure 13) highlight a composition of this colour that is practically constant over time. This colour is undoubtedly characterised by the presence of manganese and, in some cases, by the presence of iron traces.

The semi-quantitative PIXE-PIGE (Table 4) analyses confirm what already emerged by MA-XRF, allowing a clear assessment of the Fe contribution: compared to the reference white areas, an increase in Fe_3O_4 concentrations is systematically detected in all the samples, with the exception of C22.

The different quantities of Fe_3O_4 , in relation to MnO , do not appear to have a specific trend over time nor to be linked to a particular shade of colour. Also noteworthy are the very slight increases in CuO recorded in the case of the oldest samples.

Chapter 3: Results and Discussion

Table 4 Semi-quantitative IBA analyses on white (Wt.) and black (Bk.) areas. In addition, MgO, Cr₂O₃, NiO, ZnO, Rb₂O, SrO, BaO are also detected in constant conc. <0.1 wt%.

		CR01		CR02		C17		C23	
	wt%	Wt.	Bk.	Wt.	Bk.	Wt.	Bk.	Wt.	Bk.
Na ₂ O	c.	1.7	1.6	1.4	1.7	3.7	1.7	1.0	1.1
	± err	0.2	0.2	0.1	0.1	0.1	0.2	0.2	0.2
Al ₂ O ₃	c.	3.1	3.7	4.2	4.9	3.6	3.2	2.9	6.3
	± err	0.2	0.3	0.1	0.2	0.2	0.2	0.2	0.2
SiO ₂	c.	43.7	33.9	64.2	59.8	55.6	33.5	60.2	42.7
	± err	0.5	0.5	0.3	0.4	0.6	0.4	0.5	0.4
K ₂ O	c.	1.8	1.2	3.8	4.6	3.7	2.6	1.7	1.7
	± err	0.1	0.1	0.1	0.1	0.1	0.1	0.1	0.1
CaO	c.	3.6	4.1	2.2	2.9	5.8	3.7	1.0	1.9
	± err	0.2	0.2	0.1	0.1	0.1	0.2	0.1	0.1
MnO	c.	0.32	1.6	< 0.1	1.1	< 0.1	3.4	< 0.1	13.7
	± err	0.03	0.1		0.1		0.1		0.4
Fe ₃ O ₄	c.	1.1	2.4	0.23	0.74	0.31	5.8	0.30	2.1
	± err	0.1	0.2	0.02	0.06	0.03	0.2	0.02	0.1
CuO	c.	0.27	0.17	< 0.1	0.27	< 0.1	0.12	< 0.1	0.11
	± err	0.02	0.01		0.02		0.01		0.01
SnO ₂	c.	16.8	13.5	8.2	11.2	10.3	6.0	5.0	3.7
	± err	1.6	1.1	0.8	1.0	1.2	0.4	0.9	0.4
PbO	c.	43.0	47.0	17.5	16.8	19.6	27.5	20.0	26.7
	± err	3.9	3.2	1.7	1.3	2.1	0.8	3.4	0.8
		C13		C22		C06			
	wt%	Wt.	Bk.	Wt.	Bk.	Wt.	Bk.		
Na ₂ O	c.	0.6	1.0	1.0	1.4	1.3	1.3		
	± err	0.2	0.2	0.2	0.3	0.2	0.2		
Al ₂ O ₃	c.	3.6	4.2	3.6	3.5	4.0	3.0		
	± err	0.2	0.2	0.2	0.3	0.2	0.2		
SiO ₂	c.	62.1	54.9	59.6	50.5	49.3	40.8		
	± err	0.5	0.5	0.5	0.5	0.4	0.4		
K ₂ O	c.	5.2	4.6	2.4	3.0	1.4	1.0		
	± err	0.1	0.1	0.1	0.1	0.1	0.1		
CaO	c.	2.2	3.7	0.4	0.5	0.5	0.6		
	± err	0.1	0.1	0.1	0.1	0.1	0.1		
MnO	c.	< 0.1	2.6	< 0.1	1.4	< 0.1	1.3		
	± err		0.3		0.1		0.1		
Fe ₃ O ₄	c.	0.49	0.56	0.29	1.0	0.22	2.0		
	± err	0.05	0.07	0.04	0.1	0.03	0.1		
CuO	c.	< 0.1	< 0.1	0.32	< 0.1	< 0.1	< 0.1		
	± err			0.05					
SnO ₂	c.	0.7	2.1	1.7	1.9	3.3	2.8		
	± err	0.2	0.4	0.4	0.3	0.5	0.3		
PbO	c.	31.4	28.0	37.6	33.3	41.4	51.0		
	± err	3.1	3.3	5.7	2.9	5.8	2.8		

Since the black colours are strongly absorbent, obtaining diagnostic Raman spectra was challenging by working with laser powers that were also safe for the samples. (Caggiani & Colombari, 2011)

Additionally, intense signals related to k-feldspars were detected also in these areas, resulting in fewer acquired spectra displaying peaks connected to the black pigment.

Two useful Raman spectra are shown in Figure 14.

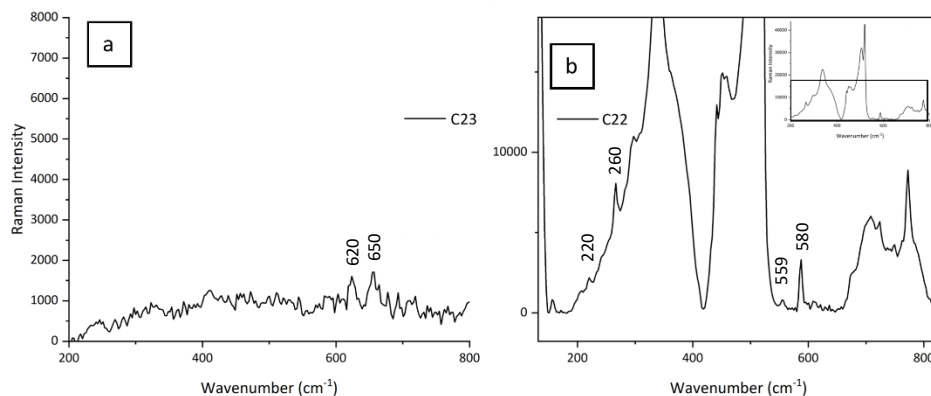


Figure 14 Raman spectra acquired on: a- Black area of sample C23 (1460-1480): Cryptomelane peaks around 620 and 650 cm⁻¹. b-Black/brown area of sample C22 (1600-1630): Manganite peaks around 220, 260, and 559 cm⁻¹ + peak at 580 cm⁻¹ characteristic of a few manganese phases.

Both spectra would report characteristic signals of manganese phases, partially masked in the case of sample C22 by the lead antimonate spectrum (probably due to a mixture of black and yellow pigments to give a brown tone to the colour).

The peaks around 620 and 650 cm⁻¹ revealed by sample C23 can be attributed to Cryptomelane $K(Mn^{4+}, Mn^{2+})_8O_{16}$.

Sample C22 shows signals attributable to Manganite $\gamma-MnO(OH)$ (ca 220, ca 260, 559 cm⁻¹), as well as a clear peak at 580 cm⁻¹ characteristic of various manganese oxides (Hollandite, Bixbyite etc.).(Bernardini et al., 2019)

Based on this evidence and the XRF-IBA data, it is likely that the black colour in Montelupo was created from the mixture of different manganese oxides and hydroxides. Unfortunately, Raman is unable to clarify the role of iron within this colour: no signals attributable to iron phases are detected.(Sparavigna, 2023)

3.2.3 Blue Decorations

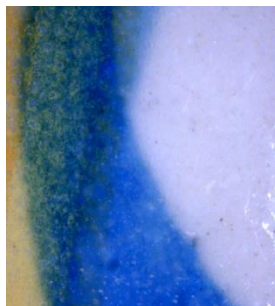


Figure 15 Blue uniforme glaze in sample C20. Optical microscope in reflected light, 180x.

In the case of green, the optical images acquired on the blues suggest the presence of a chromophore (or more) dissolved inside the silicate glaze.

From the preliminary visible-light observations of these areas (Figure 15), it is already possible to distinguish three types of blue: the blue *zaffera* (present in most of the samples), the so-called *zaffera a rilievo* ("in relief" *zaffera*) of samples C17, C18, A13, A14 and A15 and the dark blue tending towards black colour of samples A16, A10, A20, A21, A26 A27 and CR3.

Samples of the same typology showed similar composition in MA-XRF analysis. The set of MA-XRF elemental maps is reported here as an example for each group, in which the presence of Fe and Co is evident in all blue areas. Figure 16: *zaffera*; Figure 18: *zaffera a rilievo*; Figure 17: dark blue.

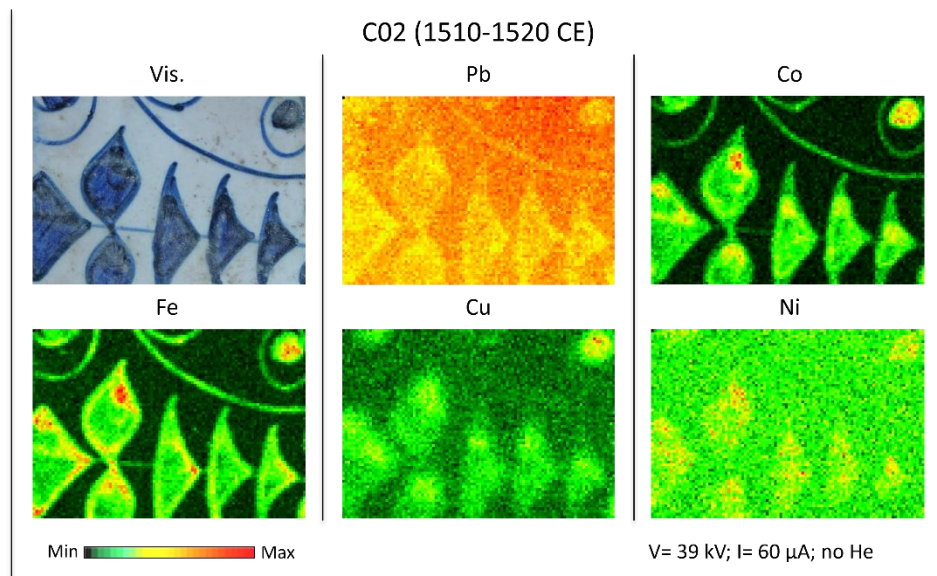


Figure 16 MA-XRF elemental distribution maps of *Zaffera* blue in sample C02.

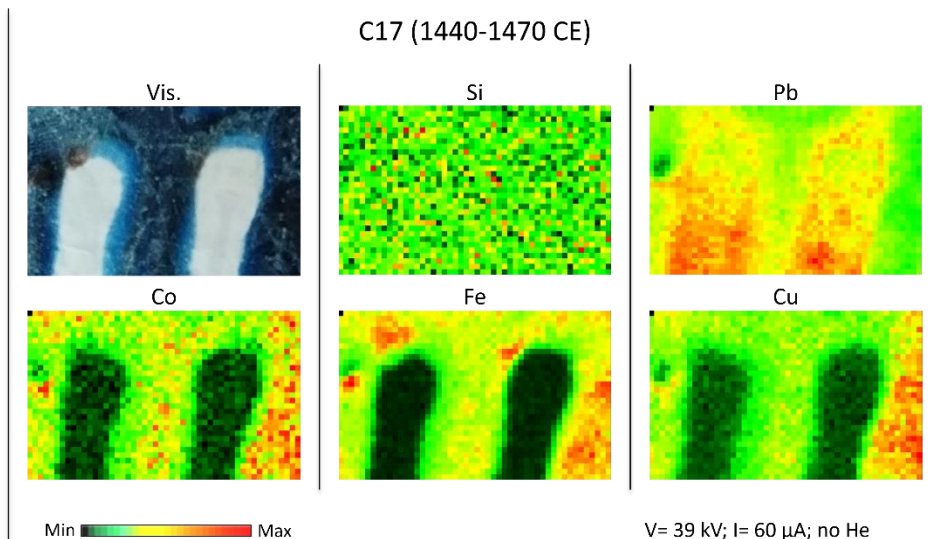


Figure 18 MA-XRF elemental distribution maps of *Zaffera a rilievo* in sample C17.

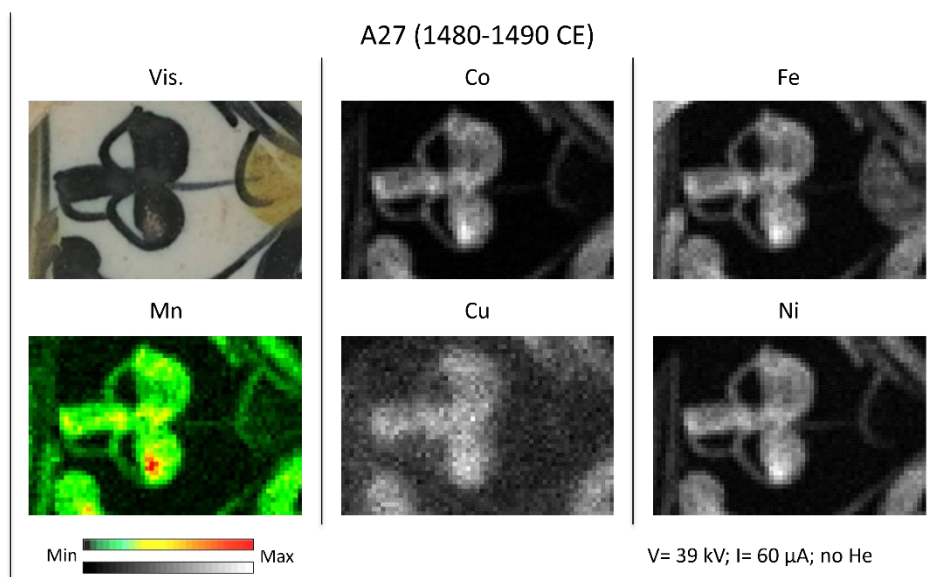


Figure 17 MA-XRF elemental distribution maps of dark/blackish blue in sample A27.

Furthermore, Cu seems to be characteristic of *zaffera a rilievo* and blue *zaffera* before 1500-1520 CE (as well as the 18th century sample). Significant Ni signals are detected in the latter (regardless of dating) and dark blues. The dark blues, specifically, also present the highest counts of manganese characteristic X-rays.

Finally, it is interesting to note that the *zaffera a rilievo* does not present particularly high Pb counts (compared to the related white area). This last

aspect should be underlined, given the mention in various sources of the use of large quantities of *ghetta* (PbO) to create the characteristic three-dimensional effect of this decoration. (Berti, 2008; Mandolesi & Vignozzi Paszkowski, 2019; Marmi & Berti, 2003)

In addition to confirming some of the data emerging from the XRF, the PIXE higher sensitivity and the possibility of obtaining reliable quantitative data proved to be crucial. Semi-quantitative analyses are reported in Table 5.

Table 5 Semi-quantitative IBA analyses on white (Wt.) and blue (Bl.) areas. "-" indicated no detected oxide. In addition to the reported oxides, the following were also detected: Na₂O, MgO, CaO, ZnO, Rb₂O, SrO, BaO in constant concentrations (and <0.1 wt%, in the case of the latter four). Samples C17-C18: Zaffera a rilievo; Sample CR3: dark blue; blue zaffera all the others.

		C17		C18		C09		C13	
wt%		Wt.	Bl.	Wt.	Bl.	Wt.	Bl.	Wt.	Bl.
Al ₂ O ₃	c.	3.6	2.8	5.1	6.8	3.2	3.5	3.6	4.6
	± err	0.2	0.2	0.2	0.3	0.2	0.2	0.2	0.3
SiO ₂	c.	55.6	60.9	63.5	59.9	64.3	59.0	62.1	66.6
	± err	0.6	2.7	0.6	1.6	0.6	0.5	0.5	0.6
K ₂ O	c.	3.7	4.2	2.0	4.5	3.9	3.7	5.2	49.0
	± err	0.1	0.2	0.1	0.1	0.1	0.1	0.1	0.1
MnO	c.	< 0.1	< 0.1	0.27	0.15	< 0.1	0.19	< 0.1	< 0.1
	± err			0.03	0.01		0.01		
Fe ₂ O ₃	c.	0.31	3.3	0.31	2.0	0.29	1.6	0.49	0.8
	± err	0.03	0.2	0.03	0.1	0.04	0.1	0.05	0.1
CoO	c.	-	0.57	-	1.07	-	0.96	-	0.56
	± err		0.03		0.05		0.05		0.06
NiO	c.	< 0.1	-	< 0.1	< 0.1	< 0.1	0.85	< 0.1	0.23
	± err						0.04		0.03
CuO	c.	< 0.1	1.2	< 0.1	0.64	0.16	0.28	< 0.1	0.10
	± err		0.1		0.03	0.02	0.01		0.01
As ₂ O ₅	c.	-	-	-	-	-	-	-	-
	± err								
SnO ₂	c.	10.3	0.2	10.8	1.5	9.1	4.3	0.7	1.1
	± err	1.2	0.1	1.3	0.2	1.5	0.5	0.2	0.6
PbO	c.	19.6	4.8	17.4	12.8	30.3	23.4	31.4	24.8
	± err	2.1	0.2	1.9	0.5	4.4	1.2	3.1	2.7
Bi ₂ O ₃	c.	-	-	-	-	-	-	-	-
	± err								

Chapter 3: Results and Discussion

		C03		C12		C02		C16	
wt%		Wt.	Bl.	Wt.	Bl.	Wt.	Bl.	Wt.	Bl.
Al ₂ O ₃	c.	3.6	4.0	4.4	4.2	3.4	4.1	4.8	5.2
	± err	0.1	0.2	0.2	0.2	0.2	0.2	0.2	0.2
SiO ₂	c.	64.4	63.3	67.5	57.3	65.7	62.4	62.3	62.9
	± err	0.4	0.4	0.5	0.5	0.4	0.4	0.4	0.4
K ₂ O	c.	5.5	5.9	4.7	5.0	5.3	5.9	5.1	4.7
	± err	0.1	0.1	0.1	0.1	0.1	0.1	0.1	0.1
MnO	c.				0.12				
	± err	< 0.1	< 0.1	< 0.1	0.01	< 0.1	< 0.1	< 0.1	< 0.1
Fe ₂ O ₃	c.	0.20	0.41	0.26	2.3	0.26	1.5	0.30	0.39
	± err	0.02	0.04	0.04	0.1	0.03	0.1	0.04	0.04
CoO	c.	-	0.75	-	1.21	-	1.00	-	0.32
	± err	-	0.07	-	0.05	-	0.05	-	0.03
NiO	c.	< 0.1	0.23	< 0.1	0.43	< 0.1	0.17	< 0.1	0.10
	± err	< 0.1	0.02	< 0.1	0.02	< 0.1	0.01	< 0.1	0.01
CuO	c.	< 0.1	< 0.1	< 0.1	0.25	< 0.1	0.46	< 0.1	< 0.1
	± err	< 0.1	< 0.1	< 0.1	0.01	< 0.1	0.02	< 0.1	< 0.1
As ₂ O ₅	c.	-	1.1	-	-	-	-	-	0.60
	± err	-	0.1	-	-	-	-	-	0.07
SnO ₂	c.	0.6	0.8	2.2	1.7	1.6	2.9	2.1	1.1
	± err	0.1	0.2	0.5	0.2	0.3	0.3	0.3	0.2
PbO	c.	19.5	35.8	23.4	24.2	26.5	26.7	23.1	22.4
	± err	2.1	3.2	3.7	1.1	3.5	1.3	2.7	2.3
Bi ₂ O ₃	c.	-	0.6	-	-	-	-	-	0.13
	± err	-	0.1	-	-	-	-	-	0.05

Chapter 3: Results and Discussion

		C20		C22		CR3			C06	
wt%		Wt.	Bl.	Wt.	Bl.	Wt.	lgt. Bl.	dk. Bl.	Wt.	Bl.
Al ₂ O ₃	c.	4.1	3.8	3.6	2.3	5.0	4.4	6.2	4.0	4.1
	± err	0.2	0.2	0.2	0.2	0.2	0.2	0.2	0.2	0.2
SiO ₂	c.	69.7	65.9	59.6	42.0	63.5	60.9	44.8	49.3	50.7
	± err	0.4	0.5	0.5	0.4	0.4	0.4	0.4	0.4	0.4
K ₂ O	c.	5.4	5.3	2.4	2.2	4.8	5.7	2.7	1.4	1.1
	± err	0.1	0.1	0.1	0.1	0.1	0.1	0.1	0.1	0.1
MnO	c.	< 0.1	< 0.1	< 0.1	< 0.1	0.43	< 0.1	18.2	< 0.1	< 0.1
	± err					0.04		0.3		
Fe ₂ O ₃	c.	0.35	0.95	0.29	0.76	0.56	0.84	0.75	0.22	0.35
	± err	0.04	0.06	0.04	0.07	0.05	0.06	0.04	0.03	0.04
CoO	c.	-	0.57	-	0.38	-	0.35	0.10	-	0.19
	± err		0.04		0.04		0.02	0.01		0.02
NiO	c.	< 0.1	0.17	< 0.1	0.11	< 0.1	0.13	< 0.1	< 0.1	0.10
	± err		0.01		0.01		0.01			0.01
CuO	c.	< 0.1	< 0.1	0.32	< 0.1	< 0.1	< 0.1	< 0.1	< 0.1	0.36
	± err			0.05						0.04
As ₂ O ₅	c.	-	0.3	-	0.11	-	0.8	-	-	0.16
	± err		0.1		0.04		0.2			0.04
SnO ₂	c.	1.0	1.0	1.7	2.1	1.1	2.3	1.7	3.3	3.4
	± err	0.2	0.2	0.4	0.4	0.2	0.3	0.3	0.5	0.5
PbO	c.	19.1	24.2	37.6	41.4	24.9	29.2	23.9	41.4	51.8
	± err	1.9	1.6	5.7	3.9	2.3	2.1	0.3	5.8	5.8
Bi ₂ O ₃	c.	-	0.13	-	-	-	0.36	0.12	-	-
	± err		0.06				0.06	0.04		

Oxides' concentrations obtained by GUPIXWin allowed to verify the assumptions based on the XRF maps for the *zaffera a rilievo* and the dark blue areas:

- The firsts do not present higher concentrations of PbO than the white area.
- The seconds are actually characterised by higher MnO amounts, as consistent with the historically documented trend of adding pyrolusite to *zaffera* to darken the colour. The use of this practice has also been confirmed in relation to the nearby Della Robbia production.

Even more interesting are the results obtained for the blue *zaffera*. PIXE's greater sensitivity made it possible to identify the characteristic X-rays of As and Bi (sometimes below MDL), totally missed in XRF analyses.

It is worth noting that these two elements have been associated with Co-Fe-Ni only since the end of the 15th century and in a stable way since 1510-1520 CE, according to a trend inverse to Cu.

There are, therefore, two colourants with different compositions:

- the Co-Fe-Ni-Cu blue in pre-1520 CE samples.
- the Co-Fe-Ni-As(-Bi) blue in post 1510-1520 CE samples.

The production between the two centuries, however, finds itself in an intermediate situation: sample C03 (1490-1500) has a composition aligned with the more modern samples, while samples C08, C12 (1500-1510 CE), C07 (1505-1515 CE) C02 and C04 (1510-1520 CE) present the same element association as the older samples.

The variation in composition observed between the 15th and 16th centuries suggests a significant technological shift, likely accompanied by a change in the origin of the raw materials.

The Fe-Ni-Cu impurities in the earlier *zaffera* blues are most likely attributable to the extraction of cobalt from slag obtained from the purification of metallic silver, according to a process widely used in medieval Europe.

Since these elements are commonly found in silver ores, they do not provide a reliable means for raw materials tracing.

Historical sources indicate the Erzgebirge region as the most exploited for silver and Freiberg mines (rich in Zn and In impurities) as the origin of the most traded cobalt. (Colomban et al., 2021)

The total lack of these impurities in Montelupo would exclude this possibility. However, it should be noted that a similar association of Co with Fe-Ni-Cu is also observed in compositional studies on the contemporary Della Robbia and Aragonese samples. (Pérez-Arantegui et al., 2009), (Zucchiatti et al., 2006)

In addition, the As impurities evident in PIXE analysis in several samples after the 15th and 16th centuries are diagnostic.

Although it is known that in these decades, the widespread diffusion of the new "*forno a riverbero*" (Paragraph 1.3.3) technology enabled the separation of cobalt production from silver ones, allowing Co extraction directly from minerals, the co-presence of As and Bi in Montelupo suggests a different origin. Around the first decades of the 16th century, indeed, the Schneeberg silver mines (also in the Erzgebirge), given the poor yields, were converted to bismuth extraction sites, also leading to the spread of a new extracting strategy of the Co from bismuth slags.

The cobalt thus produced is characterised precisely by that Co-Ni-As-Bi association found in many of the late Montelupo samples.

From the 16th century onwards, it is reasonable to infer that the supply of raw materials for blue glazes changed with the introduction of Co from Schneeberg

in Montelupo. The significant reduction of the copper concentration in the blue glazes strengthens the hypothesis of a supply change rather than just a shift in technological strategy. (Seccaroni & Haldi, 2016)

Regrettably, due to the limited number of eighteenth-century samples available,¹¹ it is not possible to understand whether this strategy persisted in the later periods. The identification in the C06 sample of As solely could suggest that the cobalt was procured by direct mineral extraction. However, detecting Bi in such low concentrations is not straightforward, given the partial overlap between its characteristic lines and those of Pb, and that makes it challenging to gain a clear understanding of the situation.

3.2.4 Yellow and Orange Decorations

From preliminary observations, two different shades of yellow are distinguishable: a proper yellow found in various samples after 1440 CE and an extremely warmer yellow (tending towards orange) used from 1480 CE.

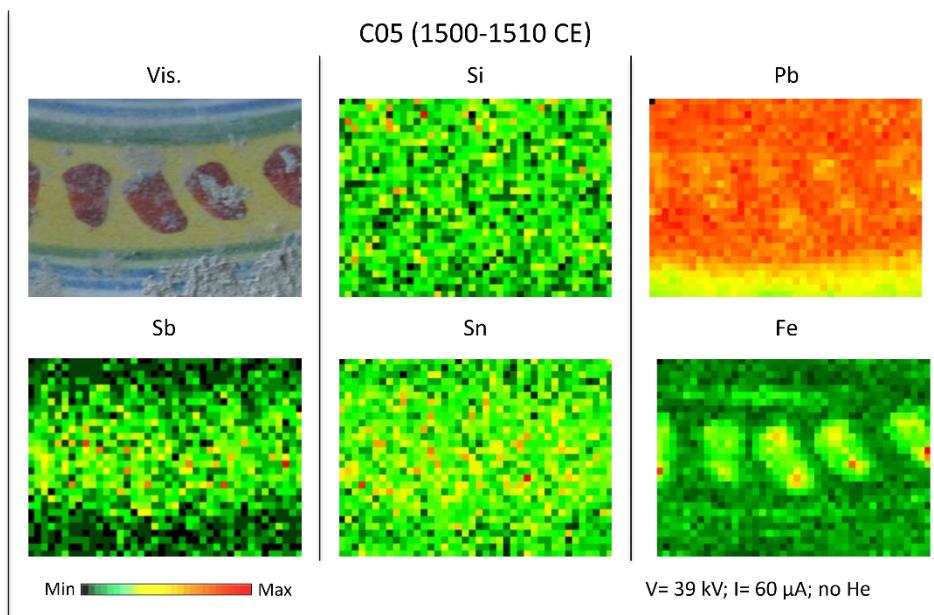


Figure 19 MA-XRF elemental distribution maps of Yellow in sample C05.

¹¹ The use of blue zaffera in the 18th century is poorly represented not only in the samples collected for this research. Referring to Paragraph 1.1.3, eighteenth-century Montelupina production is, in fact, characterised by a technological recession that leads to the almost exclusive use of green and brown for the decorations (and to the white monochrome production).

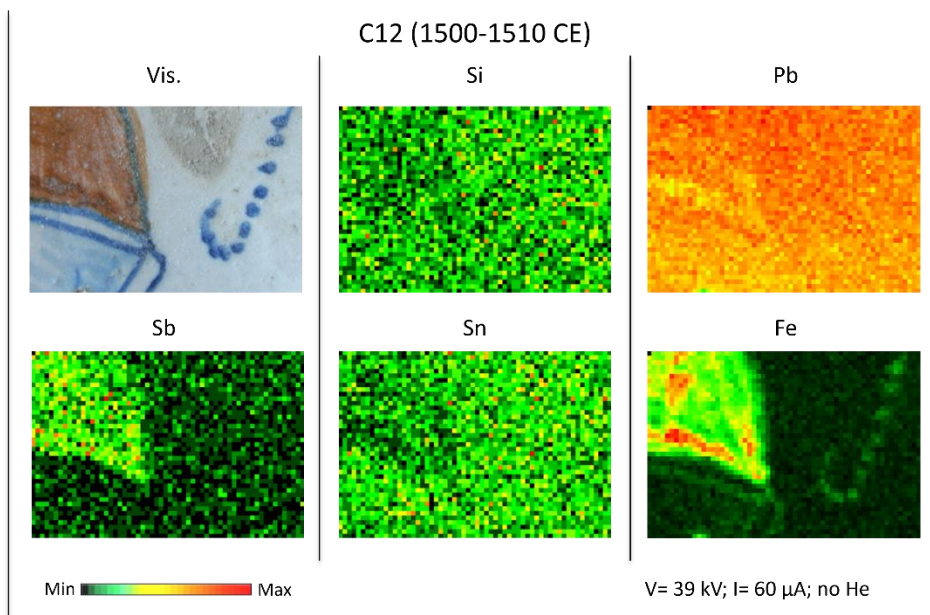


Figure 20 MA-XRF elemental distribution maps of Orange in sample C12.

Analyses conducted with MA-XRF scanner detected significant antimony counts in both shades.

The presence of this element in correspondence with the yellow/orange colour allows us to confidently hypothesise the use of Naples Yellow even if the intense Pb signals deriving from the *vetrina-smalto* system prevent establishing a univocal correspondence between this last element and the antimony.

In the proper yellows, Sb appears to be the predominant element; only in sample C05 (Figure 19) more intense Sn signals are detected, compared to the white areas, probably indicating the use of a modified Naples Yellow. Regrettably, XRF is not the most appropriate method for identifying this particular pigment due to the difficulties in detecting the tin characteristic X-rays (already discussed) and its presence in the white *smalto*.

The orange areas, however, clearly show a co-presence of Fe in correspondence with Sb (Figure 20).

The IBAs provided more information: Table 6.

Chapter 3: Results and Discussion

Table 6 Semi-quantitative IBA analyses on white (Wt.), yellow (Y.) and orange (O.) areas. "-" indicates no detected oxide. In addition to the reported oxides, the following were also detected: MgO, CaO, ZnO, Rb₂O, SrO, BaO in constant concentrations (and <0.1 wt%, in the case of the last four).

		C23		C09		C11		C13		C01	
wt%		Wt.	Y.	Wt.	Y.	Wt.	Y.	Wt.	Y.	Wt.	O.
Na ₂ O	c.	1.0	0.9	1.7	2.9	0.8	0.7	0.6	1.1	0.7	1.3
	± err	0.2	0.1	0.3	0.6	0.1	0.1	0.1	0.3	0.1	0.2
SiO ₂	c.	60.2	41.7	64.3	63.6	58.5	48.3	62.1	60.3	60.9	62.8
	± err	0.5	0.4	0.6	0.7	0.4	0.5	0.5	0.4	0.4	0.4
K ₂ O	c.	1.7	1.5	3.9	3.8	4.0	4.2	5.2	5.2	5.5	5.1
	± err	0.1	0.1	0.1	0.1	0.1	0.1	0.1	0.1	0.1	0.1
CaO	c.	1.0	14.5	2.1	2.1	1.8	2.1	2.2	2.0	2.0	1.9
	± err	0.1	0.2	0.1	0.1	0.1	0.1	0.1	0.1	0.1	0.1
Fe ₂ O ₃	c.	0.26	1.6	0.29	0.28	0.31	2.3	0.49	1.5	0.50	0.42
	± err	0.04	0.1	0.04	0.04	0.04	0.1	0.05	0.1	0.05	0.04
SnO ₂	c.	5.0	2.5	9.1	2.4	8.5	3.8	0.7	1.1	1.4	0.4
	± err	0.9	0.3	1.5	0.4	1.1	0.5	0.2	0.2	0.6	0.1
Sb ₂ O ₅	c.	-	11.3	-	3.8	-	6.0	-	1.2	-	0.7
	± err	-	0.8	-	0.6	-	0.7	-	0.2	-	0.1
PbO	c.	20.0	22.3	30.3	11.0	39.0	34.8	31.4	29.0	36.4	24.3
	± err	3.4	1.1	4.4	1.6	4.8	1.8	3.1	1.3	3.7	2.1

		C03		C14			C05		C10		C12	
wt%		Wt.	O.	Wt.	Y.	O.	Wt.	Y.	Wt.	O.	Wt.	O.
Na ₂ O	c.	0.9	0.7	1.2	1.4	1.6	1.6	1.1	1.3	1.4	0.46	0.65
	± err	0.1	0.1	0.2	0.3	0.4	0.3	0.2	0.2	0.2	0.06	0.07
SiO ₂	c.	64.4	63.9	61.2	46.3	57.3	69.7	59.2	58.8	54.4	67.5	48.5
	± err	0.4	0.4	0.4	0.5	0.5	0.4	0.5	0.5	0.6	0.5	0.5
K ₂ O	c.	5.5	4.5	5.2	3.6	6.7	4.6	5.1	5.1	4.5	4.7	6.2
	± err	0.1	0.1	0.1	0.1	0.1	0.1	0.1	0.1	0.1	0.1	0.2
CaO	c.	1.3	1.4	1.7	1.7	1.6	2.1	1.2	2.6	3.5	2.2	1.9
	± err	0.1	0.1	0.1	0.1	0.1	0.1	0.1	0.1	0.1	0.1	0.1
Fe ₂ O ₃	c.	0.20	0.52	0.25	0.61	4.7	0.24	0.35	0.25	0.73	0.26	7.1
	± err	0.02	0.04	0.01	0.06	0.2	0.03	0.04	0.04	0.06	0.04	0.2
SnO ₂	c.	0.6	0.6	2.5	2.6	0.8	0.5	3.5	0.4	1.6	2.2	1.0
	± err	0.1	0.2	0.4	0.4	0.2	0.2	0.5	0.02	0.5	0.5	0.2
Sb ₂ O ₅	c.	-	0.5	-	4.7	4.5	-	3.7	-	0.4	-	5.7
	± err	-	0.2	-	0.7	0.4	-	0.6	-	0.2	-	0.5
PbO	c.	19.5	33.2	26.8	37.2	27.1	21.5	28.4	30.9	28.3	23.4	30.0
	± err	2.1	2.8	3.5	5.2	0.7	2.2	3.5	4.8	2.3	3.7	0.8

Chapter 3: Results and Discussion

		C07			C02		C04		C16		C21		
		Wt.	Y.	O.	Wt.	Y.	Wt.	Y.	Wt.	Y.	Wt.	Y.	O.
Na ₂ O	c.	1.1	1.3	0.6	0.9	1.1	1.1	1.0	1.1	1.5	0.6	0.9	0.7
	± err	0.2	0.2	0.1	0.1	0.2	0.1	0.1	0.2	0.3	0.1	0.1	0.1
SiO ₂	c.	66.3	59.4	65.3	65.7	61.0	68.8	68.3	62.3	65.7	69.8	53.4	56.0
	± err	0.5	0.4	0.8	0.4	0.4	0.4	0.4	0.4	0.4	0.5	0.5	0.5
K ₂ O	c.	5.6	4.6	5.3	5.3	6.2	5.7	5.1	5.1	6.0	4.4	3.7	5.2
	± err	0.1	0.1	0.1	0.1	0.1	0.1	0.1	0.1	0.1	0.1	0.1	0.2
CaO	c.	1.3	1.5	1.7	1.2	1.3	1.1	1.0	1.0	0.71	1.6	1.4	1.3
	± err	0.1	0.1	0.1	0.1	0.1	0.1	0.1	0.1	0.06	0.1	0.1	0.1
Fe ₂ O ₃	c.	0.45	0.67	1.3	0.26	0.36	0.32	0.35	0.30	0.39	0.38	0.83	3.6
	± err	0.04	0.05	0.1	0.03	0.04	0.03	0.04	0.04	0.04	0.05	0.08	0.1
SnO ₂	c.	1.0	3.2	0.6	1.6	4.9	0.6	1.7	2.1	1.1	2.1	5.8	2.1
	± err	0.2	0.4	0.2	0.3	0.6	0.1	0.3	0.3	0.4	0.4	0.7	0.3
Sb ₂ O ₅	c.	-	4.1	2.8	-	15.5	-	1.2	-	0.6	-	8.8	7.6
	± err	-	0.5	0.4	-	1.7	-	0.3	-	0.2	-	1.1	0.7
PbO	c.	26.6	36.2	23.9	26.5	26.3	19.8	23.5	23.1	23.1	20.0	34.0	29.0
	± err	2.6	2.8	1.6	3.5	2.7	2.2	2.7	2.7	2.2	2.7	3.1	1.1

		C20			C22		CR3			C06	
		Wt.	Y.	O.	Wt.	Y.	Wt.	Y.	O.	Wt.	O.
Na ₂ O	c.	1.1	1.0	1.0	1.0	0.9	1.2	1.0	0.9	1.3	0.9
	± err	0.2	0.1	0.1	0.1	0.1	0.2	0.2	0.1	0.2	0.1
SiO ₂	c.	69.7	60.0	53.0	59.6	52.6	63.5	55.5	58.4	49.3	35.4
	± err	0.4	0.5	0.5	0.5	0.5	0.4	0.4	0.3	0.4	0.4
K ₂ O	c.	5.4	5.2	4.7	2.4	2.2	4.8	5.6	5.1	1.4	0.9
	± err	0.1	0.1	0.1	0.1	0.1	0.1	0.1	0.1	0.1	0.1
CaO	c.	1.1	1.2	1.0	0.4	0.5	2.2	0.5	1.8	0.5	-
	± err	0.1	0.1	0.1	0.1	0.1	0.1	0.1	0.1	0.1	-
Fe ₂ O ₃	c.	0.35	0.57	2.9	0.29	0.38	0.56	0.43	1.3	0.22	3.4
	± err	0.04	0.06	0.1	0.04	0.05	0.05	0.04	0.1	0.03	0.1
SnO ₂	c.	1.0	2.9	1.5	1.7	2.5	1.1	4.7	2.7	3.3	4.3
	± err	0.2	0.4	0.3	0.4	0.5	0.2	0.6	0.3	0.5	0.4
Sb ₂ O ₅	c.	-	2.7	3.6	0.7	2.2	-	8.9	3.3	-	9.9
	± err	-	0.5	0.5	0.3	0.5	-	0.9	0.4	-	0.7
PbO	c.	19.1	27.6	37.5	37.6	37.7	24.9	34.7	34.3	41.4	54.2
	± err	1.9	2.8	1.5	5.7	5.3	2.3	3.3	3.4	5.8	2.1

The quantitative IBA data confirm the Sb-Fe association in the case of the orange colours, along with the higher concentrations of Sn in the C05.

The possibility of measuring, in each sample, the increment of Fe₂O₃ and SnO₂ concentrations in the yellow areas (compared to the white ones) reveal a much more diverse picture than what was initially deduced from the scanning XRF analysis.

Regarding the yellows (in addition to the antimony which is always detected):

- Only samples C09 and C16 actually appear to have a pigment based on pure lead antimoniate (net of the errors affecting the measurements).
- Samples C02, C14, C04, C21, C22 and CR3 likely have a Naples yellow modified with tin.
- Samples C23 and C11 do not show significant contributions of SnO₂ but slight increase of Fe₂O₃.
- Differently from the aforementioned samples, C05 together with C07, see increases in both tin and iron.

Regarding the oranges, however, the C10, C20, C06 and CR3 samples are characterised by the presence of Sn in addition to Fe-Sb.

While, on the one hand, the higher concentrations of Sn are appreciable only in samples from the 16th century onwards (although not in all), the trends in iron do not appear to have a specific pattern over time.

In the case of oranges, it is reasonable to assume a voluntary addition of iron oxide to warm up the colour. Referring to (Marmi & Berti, 2003) and (Piccolpasso, 2007), the use of *ferraccia* (compound based on iron oxides) or *tutia alessandrina* (containing zinc) for this purpose is known; based on the negligible concentrations of ZnO in the samples, it seems reasonable to deduce the use of the first one in Montelupo. In the case of yellows, however, the not appreciable chromatic differences lead towards an involuntary addition, perhaps as an impurity of the raw materials.

The fact that lead oxide concentrations do not appear to increase probably depends on how the signals were treated to obtain the semi-quantitative data. The analyses on GUPIXWin© were performed by forcing the sum of all oxides' concentrations to close to 100%. Where the presence (or increase) of colours-related oxides is detected, there is generally a decrease in the concentrations of glaze's characteristic oxides: SiO₂, Al₂O₃, K₂O, Na₂O and PbO.

Given the widespread (and almost exclusive) use of the Naples Yellow documented in the historical maiolica field and the detection of antimony, it is still reasonable to assume the use of this pigment in Montelupo.

From a chemical point of view, Naples Yellow is a non-stoichiometric phase (A_{2-x}A'B_{2-y}B'O_{7-δ}) belonging to the class of cubic pyrochlore oxides. (Montanari et al., 2020)

The cubic pyrochlore structure is built with two interpenetrating oxygen-sharing networks:

- the $\text{Pb}_2\text{O}'$ units, where oxygen is coordinated by four Pb^{2+} atoms in tetrahedral sites,

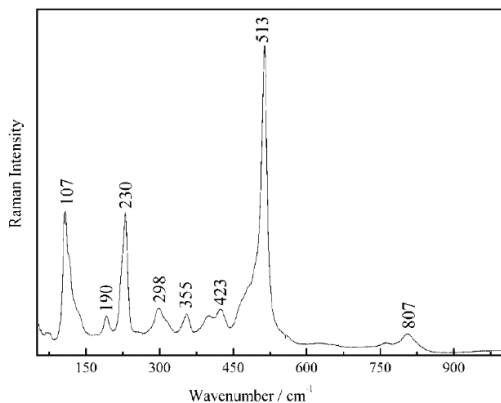


Figure 21 Non-modified Lead antimoniate.

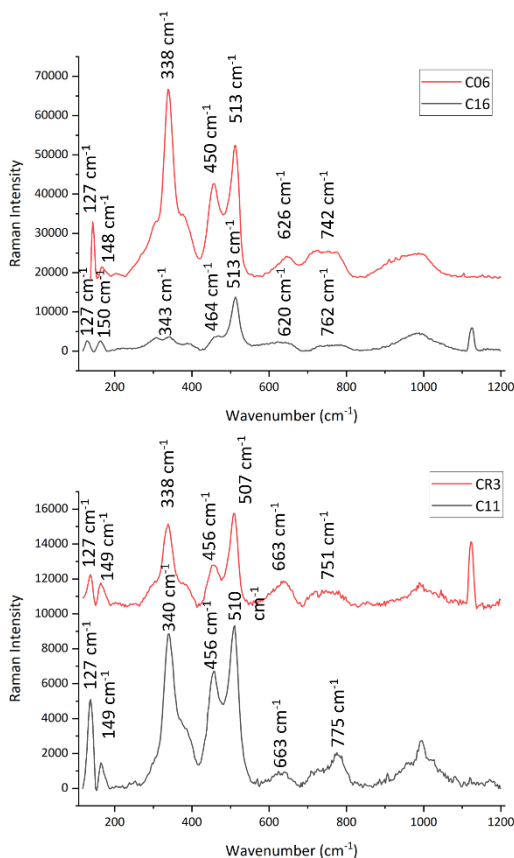


Figure 22 Raman spectra on yellow areas of samples: C06 (possible Sn-Fe-Lead antimoniate), C16 (possible Lead antimoniate), CR3 (possible Sn-Lead antimoniate), C11 (possible Fe-Lead antimoniate).

- and B_2O_6 units formed by smaller covalent bonded cations B (=typically Sb but also Sn, Fe, Zn, Si, etc.) in octahedral coordination.

Theoretical analysis identified 26 normal modes for this type of structure, six of them Raman active: A_{1g} , E_g and $4F_{2g}$ (all dependent solely on oxygen vibration).

Figure 21 reports the spectrum of a non-modified Lead antimoniate.

Based on (Rosi et al., 2009):

- The peak at 510 cm^{-1} (very strong) can be ascribed to A_{1g} mode (totally symmetric elongation of the SbO_6 octahedra).

- The 350 cm^{-1} and 300 cm^{-1} peaks would be related to Sb-O (E_g) and Pb-O (F_{2g}) vibration modes.

- The peaks around $100\text{--}300 \text{ cm}^{-1}$ seem to be due to the vibrations of Pb_4O tetrahedra

- While the band around 800 cm^{-1} , not unequivocally assigned, may be an overtone or combination band or an F_{2g} mode. (Rosi et al., 2009)

In Montelupo samples, no Raman spectra attributable to pure Lead Antimonite are detected. Figure 22

Instead, in most yellows, the characteristic signals of the deformed pyrochlore structure (due to the insertion of a third cation) are observed.

Specifically, are evident:

- The decrease of the peak at 513 cm^{-1} in favour of the resolved band at 450 cm^{-1} .
- The raising of the peak at 330 cm^{-1} , which in many cases becomes the most intense.

Particularly relevant, in our case, is also the region at lower wavenumbers, which would be typically non-diagnostic (several studies proved the extreme variability of the Pb-O vibration mode due to variations in the Pb:Sb ratio and firing temperatures of the pigment).

However, tin-modified lead antimonate exhibits a characteristic doublet around $120\text{-}150\text{ cm}^{-1}$. (Rosi et al., 2011)

It is worth noting that this particular feature is also visible in the spectra acquired on those yellows, which do not contain Sn based on PIXE-PIGE analyses.

Observing the spectrum of sample C16 (as an example of this last category of pigments), it is, in fact, possible to notice how it still presents the doublet peak at low wavenumber (despite being the most similar to that of pure Lead antimonate).

This aspect could probably be explained by hypothesising a partial replacement of Sb in pyrochlore structure with small quantities of Sn (below the sensitivity of the PIXE), which might occur accidentally during the firing phase of the glazing system (we recall in this regard the presence of cassiterite in the inner white opaque glaze).

On the other hand, some type of modification is also evident from the red-shift of the 800 cm^{-1} band.

Focusing on the latter, it is interesting to note how a good part of the samples which, based on the PIXE, present the association Pb-Sb-Sn (no Fe) has the band centred at around 750 cm^{-1} , a value that (Cartechini et al., 2011) report as characteristic of the Pb-Sb-Sn pyroantimonates.

In cases of greater shift, some influence from Fe might be hypothesised.

Finally, the bands at 640 cm^{-1} and 477 cm^{-1} can be attributed to the presence of the $\text{Pb}_{3+x}\text{Sb}_2\text{O}_{8+x}$ phase identified by (Rosi et al., 2011).

3.2.5 Red Decorations

The red colour is undoubtedly the most outstanding feature of Montelupo's chromatic palette, and the technological pinnacle reached by the Tuscany town in maiolica production.

In the historical context of reference (Italian 16th century), it is a unique which finds its equivalent only in the maiolica of Iznik (former Nicaea, current Turkey).

Perhaps for this very reason, many archaeologists believe that the origin of Montelupo red could be traced back to Turkey. According to Berti (Berti, 2008), it is highly probable that the same raw material used by the Iznik potters was also used at Montelupo, imported in Tuscany through the Florentine trading companies.

Several archaeometric studies are available on Nicene production, and practically all agree on the use of the Armenian bole (an intimate mixture of hematite and quartz) for the creation of this colour.

High concentrations of Fe, Al and Si are reported both in the PIXE analysis by Constantinescu (Constantinescu et al., 2014), and in the SEM campaigns conducted by Tite (Tite, 1989) and Amara (Amara et al., 2006). While Raman signals of hematite, quartz and cassiterite are identified by Colombari (Colombari et al., 2004)

Simsek (Simsek et al., 2019) also hypothesise a possible presence of bornite (Cu_5FeS_4 , a common phase in Anatolian mineral deposits of the period) in the starting raw materials to justify the significant copper concentrations found

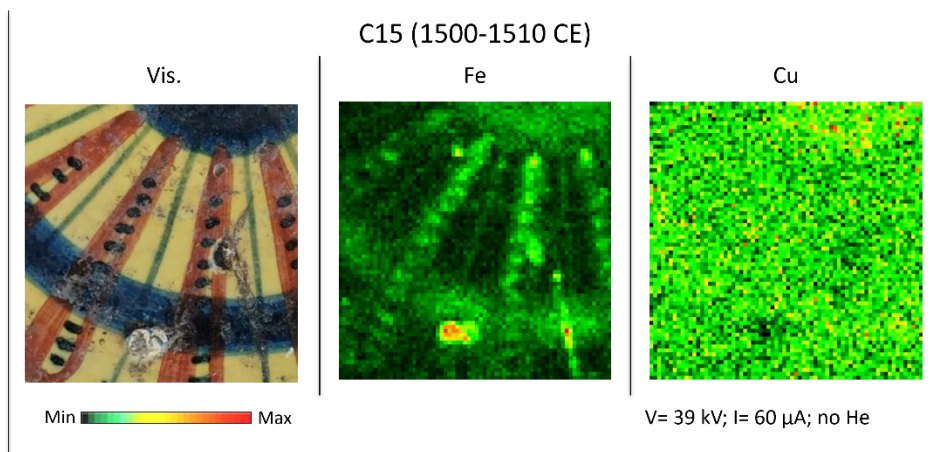


Figure 23 MA-XRF elemental distribution maps of Red in sample C15.

during the XRF analyses.

The MA-XRF campaign conducted on the Montelupo samples identifies a clear correlation between the iron signals detected and the red decorations, but the intrinsic sensitivity limits of the instrument do not allow equally clear distribution maps for Si and Al (Figure 23).

Interestingly, and this is not attributable to the MDL of the technique, the Cu characteristic X-rays have distributions uncorrelated to this colour as well.

Chapter 3: Results and Discussion

Table 7 Semi-quantitative IBA analyses on white (Wt.) and (R.) areas. In addition to the reported oxides, the following were also revealed: MgO, MnO, TiO₂, CuO, ZnO, Rb₂O, SrO, BaO in constant concentrations and <0.1 wt%.

		C01		C03		C14		C05		C08	
wt%		Wt.	R.	Wt.	R.	Wt.	R.	Wt.	R.	Wt.	R.
Na ₂ O	c.	0.68	1.2	0.9	0.8	1.2	2.1	1.6	1.3	1.3	0.7
	± err	0.08	0.2	0.1	0.1	0.2	0.5	0.3	0.2	0.2	0.1
Al ₂ O ₃	c.	3.4	17.3	3.6	3.7	4.1	6.2	5.4	5.0	3.4	4.0
	± err	0.2	0.4	0.1	0.2	0.2	0.2	0.2	0.2	0.2	0.2
SiO ₂	c.	60.9	45.1	64.4	64.4	61.2	51.8	69.7	61.3	61.9	62.4
	± err	0.4	0.6	0.4	0.5	0.4	0.5	0.4	0.5	0.4	0.4
K ₂ O	c.	5.5	7.2	5.5	5.3	5.2	6.9	4.6	6.2	5.2	4.7
	± err	0.1	0.1	0.1	0.1	0.1	0.1	0.1	0.1	0.1	0.1
CaO	c.	2.0	1.8	1.3	1.3	1.7	2.4	2.1	2.1	1.8	2.2
	± err	0.1	0.1	0.1	0.1	0.1	0.1	0.1	0.1	0.1	0.1
Fe ₂ O ₃	c.	0.50	8.7	0.20	0.77	0.25	8.2	0.24	2.7	0.23	1.5
	± err	0.05	0.2	0.02	0.06	0.03	0.2	0.02	0.1	0.03	0.1
SnO ₂	c.	1.4	4.3	0.6	0.4	2.5	5.0	0.5	1.1	0.7	0.4
	± err	0.6	0.5	0.1	0.1	0.4	0.4	0.1	0.2	0.2	0.1
PbO	c.	36.4	15.3	19.5	25.6	26.8	18.4	21.5	28.7	24.9	29.9
	± err	3.7	0.3	2.1	1.9	3.5	0.4	2.2	1.2	3.3	1.3

		C10		C15		C07		C04		C16	
wt%		Wt.	R.	Wt.	R.	Wt.	R.	Wt.	R.	Wt.	R.
Na ₂ O	c.	1.3	1.5	1.1	1.0	1.1	1.3	1.1	2.5	1.2	1.4
	± err	0.2	0.3	0.2	0.2	0.2	0.2	0.1	0.5	0.2	0.3
Al ₂ O ₃	c.	3.8	4.2	3.2	5.2	3.4	4.2	3.2	4.3	4.8	5.2
	± err	0.2	0.2	0.2	0.2	0.2	0.2	0.2	0.2	0.2	0.2
SiO ₂	c.	58.8	57.8	58.1	60.1	66.3	66.5	68.8	69.4	62.3	59.1
	± err	0.5	0.5	0.4	0.5	0.5	0.5	0.4	0.6	0.4	0.4
K ₂ O	c.	5.1	4.8	5.4	4.9	5.6	4.9	5.7	5.1	5.1	6.4
	± err	0.1	0.1	0.1	0.1	0.1	0.1	0.1	0.1	0.1	0.1
CaO	c.	2.6	3.2	2.7	2.9	1.3	1.5	1.1	1.6	1.0	1.3
	± err	0.1	0.1	0.1	0.1	0.1	0.1	0.1	0.1	0.1	0.1
Fe ₂ O ₃	c.	0.25	0.41	0.42	0.58	0.45	0.97	0.32	1.8	0.30	2.9
	± err	0.04	0.04	0.04	0.06	0.04	0.06	0.04	0.1	0.04	0.1
SnO ₂	c.	0.4	0.4	0.6	0.4	1.0	0.3	0.6	-	2.1	0.6
	± err	0.2	0.2	0.2	0.2	0.2	0.1	0.1	-	0.3	0.1
PbO	c.	30.9	36.7	34.4	32.5	26.6	27.4	19.8	16.4	23.1	19.4
	± err	4.8	5.1	3.6	3.5	2.6	1.8	2.2	0.7	2.7	0.6

PIXE's higher sensitivity to low Z elements enabled the identification of a clear increase in aluminium contents (undetected by XRF), while the trend of SiO₂ is more complex to interpret (Table 7).

Furthermore, no appreciable copper concentration growths are visible except for samples C03 and C08 (the first going from 0.026 ± 0.003 wt% in the white to 0.087 ± 0.007 wt% in red, the second from 0.063 ± 0.004 wt% to 0.087 ± 0.007 wt%). However, such mild evidence does not allow the establishment a Cu-red correlation.

Such low copper values are incompatible with the Iznik raw materials hypothesised by (Berti, 2008), and even with the two recipes brought by Marmi for these pigments:

"[40] A fare il vetro rosso: 20 lib di vetro purificato + 1 oncia di "schaglia di anchora cioè schaglia nuova" + 1 oncia di schaglia di rame nuovo + "una chastagnia di tartaro bianco cioè groma di vino bianco": polverizzare e macinare tutto insieme con aceto".

[60] Per fare uno bello rosso di maiolica: Tanto bolo e tanto rame sodo: cottura in fornace".¹² (Marmi & Berti, 2003)

In any case, relying also on Raman spectra acquired, it is possible to confirm hematite as the main chromophore for these coloured areas.

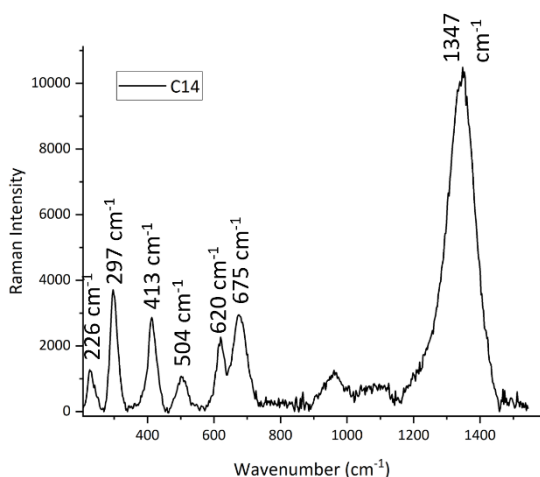


Figure 24 Raman spectra on red area of samples C14. Hematite characteristic peaks.

The spectrum of sample in Figure 24, reported as an example, clearly shows signals attributable to this phase.

Hematite (α -Fe₂O₃) is an antiferromagnetic oxide belonging to the D_{3d}⁶ crystalline space group, characterised by seven Raman active vibrations: two A_{1g} modes (225 and 498 cm⁻¹) and five E_g modes (247, 293, 299, 412 and 613 cm⁻¹, with 293 and 299 cm⁻¹ resolved only at < -170 °C). (De Faria et al., 1997)

All these features are clearly visible in Montelupo spectra

together with two additional bands around 660 and 1300 cm⁻¹.

¹² "[40] To make red glass: 20 lb of purified glass + 1 ounce of "anchor flake, i.e., new anchor" + 1 ounce of new copper flake + 1 chestnut of white tartare, i.e., winey lees": pulverise and shout all together with vinegar.

[60] To make a beautiful red for maiolica: Lots of boles and copper: firing in the kiln".

Pettanayak in the paper (Pattanayak et al., 2022) identify these two quite common, additional Raman modes as the E_u mode ($\sim 650 \text{ cm}^{-1}$) and its higher harmonic $2E_u$ mode ($\sim 1300 \text{ cm}^{-1}$).

The appearance of the E_u mode (it is an infrared active longitudinal optical mode) in the Raman spectrum is interpreted by Pattanayak as a consequence of the internal strain of the hematite lattice due to local disorderedness.

Based on the relatively high concentrations of aluminium detected with IBA and the fact that hematite and corundum are isostructural phases, a partial replacement of Fe^{III} with Al^{III} might be hypothesised.

Zoppi et al. (Zoppi et al., 2008) studying the effects of Al-Fe substitution in hematite point out four effects visible in the Raman spectrum: the red-shift of the peaks/bands, which also became broader and the appearance of the new bands at 670 and 430 cm^{-1} (the latter as a shoulder of the 411 cm^{-1} peak)¹³. All these features are clearly visible in Montelupo spectra.

Overall, though if on one side a good elemental characterisation of red areas is achieved, on the other, the processing conditions are not easy to establish, and further studies will be necessary.

3.3 SEM-EDS

Being able to rely on a rather exhaustive archaeometric analysis of the maiolicas and with the permission of the Montelupo Museum and the Superintendence of Florence, the last phase of the research involved the sampling of a small part of the pieces (Table 8). These samples were strategically chosen to cover all the colours used in Montelupo and all the different production phases under examination.

Table 8 List of samples analysed at SEM-EDS. Gr: green decoration, Bk: black/brown layer, Bl: blue decoration, Y: yellow layer, O: orange layer, R: red layer.

Sample	C23	C01	C14	C04	C21	C22	C06
Date	1460-1480	1490-1500	1490-1510	1510-1520	1520-1530	1600-1630	1750-1780
Colours	Y, Bk, Gr	O, R, Bl	Y, R, Bk, Bl	Y, Bl, Gr	O	Y	O, Gr

A SEM-EDS campaign was conducted to verify:

- The presence/absence of the transparent superficial glaze.
- The thickness of the different layers.
- To obtain the composition of the individual layers.

¹³ Probably due to O–Fe–O bending distortion caused by Al ions.

All this information is exploited to evaluate the validity of our chosen diagnostic approach.

It is essential to keep in mind that the results obtained refer to the single sampled fragment, which may not be representative of the entire sample. However, it is important to underline that the sampling was carried out in trying to avoid the areas of inhomogeneity highlighted by the MA-XRF.

3.3.1 Transparent Glazes and White Glazes

Firstly, the analysis of the polished cross-section revealed the presence of the transparent glaze (T.G.) only on samples C01 (thicknesses around 20-30 μm), C04 (thicknesses quite variable between tens and 100 μm), C14 (tens -100 μm), and C22 (10-70 μm). Samples C06, C21 and C23 do not show any evidence.

The information gain with SEM-EDS aligns with the hypotheses based on XRF and IBA for only five samples.

Based on the Pb/Sn ratio described by (Matin, 2019) for samples C21 and C06, the presence of a T.G. was expected.

Comparing the Pb/Sn ratio calculated from the SEM-EDS data acquired solely on the white glazes (W.G.)¹⁴ with that obtained from the IBA in the white areas (W.A.) (Table 9), an excellent agreement between these two values is actually found, implying that the samples under exam have significantly higher PbO contents compared to Martin's ones.

Table 9 Values of Pb/Sn calculated on samples' white glazes (by SEM-EDS) and samples' white areas (by IBA).

		C23	C21	C06
SEM-EDS	Pb/Sn	3.3	9.9	11.2
	\pm err	0.1	0.1	0.1
IBA	Pb/Sn	3.6	9.5	12.4
	\pm err	0.2	0.2	0.1

Consequently, this method can be deemed reliable only for Pb/Sn values <6.5 ¹⁵ (which would indicate the absence of the T.G.). In the case of higher values, the doubt of having the transparent glaze or of being in the presence of Pb-rich glaze persists.

¹⁴ The ratio was clearly calculated starting from maps and not from individual points in order to avoid any overestimates given by the presence of cassiterite crystals near the probed spot.

¹⁵ or Pb/Sn <3.5 in the case of archaic and early production maiolica.

Table 10 White glaze (W.G.) and transparent glaze (T.G.) quantitative data by SEM-EDS maps.

		W.G.						T.G.				
		C23	C01	C14	C04	C21	C22	C06	C01	C14	C04	C22
Na ₂ O	c.	0.6	0.5	0.8	0.8	0.7	0.7	0.6	0.5	0.9	1.0	0.6
	± err	0.1	0.1	0.2	0.4	0.1	0.2	0.1	0.1	0.1	0.3	0.2
MgO	c.	0.40	0.4	0.4	-	0.51	0.5	0.28	0.4	-	-	-
	± err	0.04	0.1	0.1	-	0.04	0.1	0.04	0.1	-	-	-
Al ₂ O ₃	c.	2.8	2.5	3.0	2.6	4.8	3.9	3.3	3.1	5.3	4.1	4.0
	± err	0.1	0.1	0.3	0.5	0.1	0.3	0.1	0.1	0.1	0.4	0.3
SiO ₂	c.	65.0	49.3	55.3	43.1	59.1	48.9	49.4	54.5	54.9	56.4	50.1
	± err	0.3	0.5	1.2	1.7	0.2	0.9	0.2	0.4	0.4	1.3	0.9
K ₂ O	c.	2.0	6.4	5.5	5.2	7.0	3.6	1.6	6.9	8.0	6.9	3.7
	± err	0.1	0.3	0.4	0.7	0.1	0.3	0.1	0.3	0.1	0.4	0.3
CaO	c.	1.4	1.6	1.9	1.9	1.8	0.5	-	2.3	1.3	1.5	-
	± err	0.1	0.2	0.4	0.6	0.1	0.2	-	0.2	0.1	0.4	-
SnO ₂	c.	6.3	8.7	2.7	2.3	2.4	2.0	3.6	-	-	-	-
	± err	0.4	0.8	1.1	1.8	0.3	0.6	0.2	-	-	-	-
PbO	c.	21.0	29.9	32.6	25.1	23.3	41.0	40.6	29.7	29.1	28.8	41.2
	± err	0.4	0.9	1.1	1.8	0.3	0.8	0.3	0.9	0.3	1.2	0.8

Secondly, focussing on quantitative data obtain by SEM-EDS (Table 10), it is worth noting that, taking into account the presence of cassiterite solely in *smalto* (which nominally reduces the concentration of the other oxides since the analysis closes at 100%), the experimental errors and the natural variability of these objects, the two layers (T.G. and W.G.) basically have the same oxide composition (and concentrations).

In no maiolica there is evidence of the significant increase in PbO contents suggested by historical recipes. Most likely, given the limited number of samples analysed, this data certainly cannot be considered statistically significant for the entire production of Montelupo, but it nevertheless remains an interesting piece of evidence.

The other important aspect, which must be emphasised due to this project's aim, is the excellent agreement between these quantitative data and those obtained from the IBA (as stated in Paragraph 3.1.2), despite the experimental errors.

Finally, thanks to the maps obtained from the backscattered electrons, it is possible to visualise the different crystalline phases in the glazes.

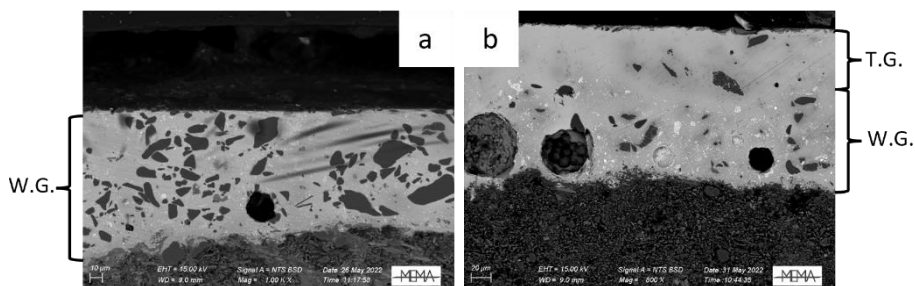


Figure 25 Backscattered electron maps of: a- White Glaze (W.G.) in sample C23. b- White Glaze (W.G.) and Transparent Glaze (T.G.) in sample C14.

From the images of samples C23 and C14 shown in Figure 25, it is clear that not all samples have the same degree of crystallinity: sample C23 exhibits the highest degree of crystallinity, while C06 displays the lowest (the remaining samples fall somewhere in between).

By detecting the characteristic X-rays of these phases,¹⁶ it is also possible to chemically identify them.

The nanometric crystals, probably formed during firing, rendered with the lighter colour (which equals a higher average Z), are confirmed to be SnO₂. Consistent with their mattifying function, they are found in maximum concentration near the interface with the ceramic body. Still, in some samples (and for some colours), however, they are also present in traces in more superficial areas. Clearly, in the case of samples without T.G., the cassiterite is distributed throughout the entire thickness of the coating.

In all samples, there are also two other types of crystals with similar average Z, probably residues of the raw materials.

Those characterised by a more defined habitus are quartzes, while the more anhedral ones (which have been most affected by thermal treatment) are identified as K-feldspars. Ca silicate phases with a composition compatible with plagioclases are also found in sample C06.

¹⁶ In these cases, a series of punctual analyses were performed.

3.3.2 Coloured Glazes

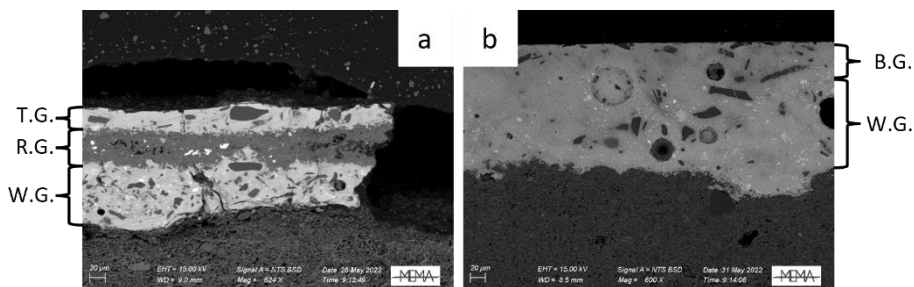


Figure 26 Backscattered electron maps of: a- Sample C01 stratigraphy: Transparent Glaze (T.G.), Red Glaze (R.G.), White Glaze (W.G.). b-Sample C04 stratigraphy: White Glaze (W.G.) and Blue Glaze (B.G.).

Moving on to colours, it is interesting to note, first of all, how the hypothesised three-layer stratigraphy (or two in the case of samples without the transparent glaze) is actually present only in the case of yellow, red and brown/black decorations. Figure 26-a

The green and blue areas (Figure 26-b), indeed, essentially present a homogeneous amorphous appearance without any interface between colour and the transparent glaze (where present), nor a clear separation with the underlying white glaze (often, the cassiterite crystals are also found in more superficial areas). This evidence further strengthens the hypothesis of dissolved chromophores within the glazes.

Given the impossibility of carrying out chromophore analysis on particles/crystals, some punctual analyses were performed with the aim to identify how their concentration varied throughout the entire thickness. In all cases under examination, the maximum concentration is detected at the sample's surface, so maps were acquired in this area.

No further information is added compared to that already obtained with XRF-IBA: Cu^{2+} and Co^{2+} are confirmed as the chromophores of the green and blue decorations, respectively.

In the case of blue (Table 11), the Co-Fe association is always appreciated, while only in one sample Ni's signals are also evident. Cu, As and Bi, otherwise, are never detected, being present probably in concentrations below the Minimum Detection Limit of the technique. Interestingly enough the lower sensitivity of SEM-EDS compared to IBA, does not allow to discriminate the two types of Blue Zaffera present in Montelupo.

In the case of green glazes of samples C22 and C04, a yellow pigment of composition consistent with a Lead Antimoniate is actually identified, confirming the hypothesis made previously.

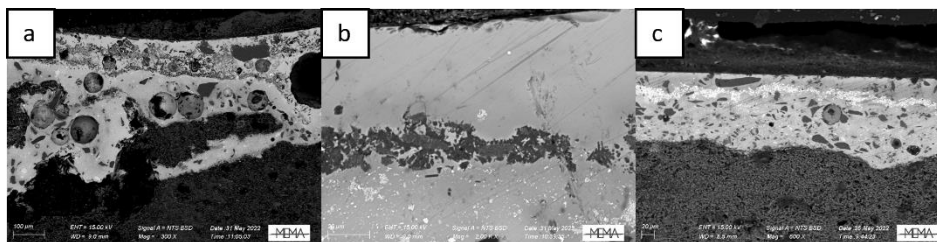


Figure 27 Backscattered electron maps of: a- Black colour in sample C14. B- Red colour in sample C14. C- Yellow colour in sample C01.

Table 11 Blue glaze and Green glaze composition based on SEM-EDS analyses; Na₂O, MgO and CaO are also present in constant concentration (<1 wt%).

		Blue glaze			Green glaze		
		C01	C14	C04	C23	C04	C06
Al ₂ O ₃	c.	1.3	3.6	4.9	4.1	1.4	3.9
	± err	0.1	0.2	0.3	0.1	0.2	0.2
SiO ₂	c.	49.5	54.3	57.6	48.4	44.2	37.9
	± err	0.4	0.7	0.9	0.3	0.5	0.4
K ₂ O	c.	4.1	6.7	7.9	3.0	2.6	1.8
	± err	0.2	0.2	0.3	0.1	0.2	0.2
Fe ₂ O ₃	c.	3.9	1.9	2.6	0.9	-	0.6
	± err	0.4	0.4	0.5	0.2	-	0.2
CoO	c.	3.8	0.8	0.9	-	-	-
	± err	0.5	0.4	0.5	-	-	-
NiO	c.	9.6	-	-	-	-	-
	± err	0.5	-	-	-	-	-
CuO	c.	-	-	-	2.3	1.6	2.8
	± err	-	-	-	0.2	0.3	0.4
SnO ₂	c.	-	-	-	-	-	17.4
	± err	-	-	-	-	-	0.6
PbO	c.	28.0	30.1	23.8	38.6	31.2	33.3
	± err	0.7	0.7	0.9	0.5	0.9	0.8

In the case of yellow, red, and brown/black areas (Figure 27), since the crystals/particles are distinguishable, a series of punctual analyses were performed. However, it should be specified that the small size of the crystals and the fact that they are surrounded by the amorphous matrix did not allow their complete isolation from the glaze.

For the colours (Table 12), though, a satisfactory agreement with the conclusions formulated based on non-invasive analyses is found.

Table 12 SEM-EDS quantitative analyses on pigments: yellow (Y.G.) in C23, C14, C04, C22, C06; orange (O.G.) in C21, C01; red (R.G.) in C01 and black/brown (Bk.G.) in C23.

		Y.G.					O.G.		R.G.	Bk.G.
		C23	C14	C04	C22	C06	C21	C01	C01	C23
Al ₂ O ₃	c.	0.6	0.3	-	-	0.33	-	-	8.5	2.8
	± err	0.1	0.2			0.05			0.1	0.1
SiO ₂	c.	4.4	1.9	3.0	1.8	2.9	-	2.3	52.6	42.5
	± err	0.1	0.2	0.2	0.2	0.1		0.1	0.2	0.3
MnO	c.	4.0	-	-	-	-	-	-	-	19.2
	± err	0.3								0.4
Fe ₂ O ₃	c.	1.1	4.9	-	3.6	2.4	4.5	4.3	15.7	2.7
	± err	0.2	0.6		0.2	0.1	0.2	0.4	0.2	0.3
CuO	c.	-	-	-	-	-	-	-	-	2.8
	± err									0.3
SnO ₂	c.	-	-	18.2	20.2	7.0	-	-	-	-
	± err			0.8	0.7	0.2				
Sb ₂ O ₃	c.	43.2	36.6	21.7	22.5	27.0	34.8	34.1	-	-
	± err	0.6	0.9	0.8	0.7	0.3	0.3	0.7		
PbO	c.	42.8	57.6	55.2	55.2	59.2	59.6	59.1	5.6	24.5
	± err	0.7	1.1	0.8	0.8	0.3	0.3	0.8	0.2	0.6

The SEM-EDS analyses confirm for the black and the red layers the chromophores already hypothesised by the non-invasive approach.

The red pigment, even if not completely isolated from the surrounding glaze, shows compositions consistent with the hematite-rich bolus hypothesised.

The black/brown areas, on the other hand, seem actually to be characterised by the presence of several manganese, iron, and/or Mn-Fe oxides micro and sub-micro crystalline phases. The composition of each crystal although it is not easy to discriminate given the small dimension of the phases; phases which are, however, probably newly formed during the firing, based on the well-developed acicular habitus of the crystals (not appreciable with the only non-invasive approach).

The yellow layers, on the other hands, have a higher degree of uncertainty. Sample C22, for instance, analysed through SEM-EDS, demonstrates iron concentrations not detected using PIXE. Similarly, C23 shows significant contents of manganese, which were not revealed using the non-invasive strategy.

To better clarify the yellow colour compositions and to obtain a more reliable indication of the presence/absence of the transparent glaze, a final differential PIXE campaign was carried out on the samples already analysed at SEM-EDS. Working at different energies of the incident proton beam, different glaze thicknesses are probed, and ideally, a gradient of the concentrations of the different oxides in depth should be obtained. The results achieved by this type of investigation will be reported in a future paper.

3.4 BIBLIOGRAPHY

- Amara, A. B., Schvoerer, M., Cuin, M., & Mami, M. B. B. (2006). An investigation of the ceramic technology of a late Iznik ceramic production (XVIIIth century AD). *34th International Symposium on Archaeometry*, 393–398.
- Bernardini, S., Bellatreccia, F., Casanova Municchia, A., Della Ventura, G., & Sodo, A. (2019). Raman spectra of natural manganese oxides. *Journal of Raman Spectroscopy*, 50(6), 873–888. <https://doi.org/10.1002/jrs.5583>
- Berti, F. (1982). Note sulla maiolica arcaica di Montelupo Fiorentino. *Archeologia Medievale*, 9, 175–192.
- Berti, F. (2003). *Storia della ceramica di Montelupo. Uomini e fornaci in un centro di produzione dal XIV al XVIII secolo. Volume quinto: Le botteghe: tecnologia, produzione, committenze. Indici.: Vol. Quinto* (LCD, Ed.). Aedo srl.
- Berti, Fausto. (2008). *Il Museo della ceramica di Montelupo : storia, tecnologia, collezioni = The Ceramics Museum of Montelupo : history, technology, collections*. Polistampa.
- Caggiani, M. C., & Colomban, P. (2011). Raman identification of strongly absorbing phases: The ceramic black pigments. *Journal of Raman Spectroscopy*, 42(4), 839–843. <https://doi.org/10.1002/jrs.2777>
- Calas, G., Galois, L., & Cormier, L. (2020). The Color of Glass. In P. Richet, R. Conradt, A. Takada, & J. Dyon (Eds.), *Encyclopedia of Glass Science, Technology, History, and Culture* (pp. 671–691). <https://doi.org/https://doi.org/10.1002/9781118801017.ch6.2>
- Cartechini, L., Rosi, F., Miliani, C., D’Acapito, F., Brunetti, B. G., & Sgamellotti, A. (2011). Modified Naples yellow in Renaissance majolica: Study of Pb-Sb-Zn and Pb-Sb-Fe ternary pyroantimonates by X-ray absorption spectroscopy. *Journal of Analytical Atomic Spectrometry*, 26(12), 2500–2507. <https://doi.org/10.1039/c1ja10190k>
- Cesaratto, A., Sichel, P., Bersani, D., Lottici, P. P., Montenero, A., Salvioli-Mariani, E., & Catarsi, M. (2010). Characterization of archeological glasses by micro-Raman spectroscopy. *Journal of Raman Spectroscopy*, 41(12), 1682–1687. <https://doi.org/10.1002/jrs.2613>
- Cherniak, D. J., & Watson, E. B. (2020). Ti diffusion in feldspar. *American Mineralogist*, 105(7), 1040–1050. <https://doi.org/10.2138/am-2020-7272>
- Colomban, P. (2004). Raman spectrometry, a unique tool to analyze and classify ancient ceramics and glasses. *Applied Physics A: Materials Science and Processing*, 79(2), 167–170. <https://doi.org/10.1007/s00339-004-2512-6>
- Colomban, P., Kirmizi, B., & Franci, G. S. (2021). Cobalt and associated impurities in blue (And green) glass, glaze and enamel: Relationships

- between raw materials, processing, composition, phases and international trade. In *Minerals* (Vol. 11, Issue 6). MDPI AG. <https://doi.org/10.3390/min11060633>
- Colomban, P., Milande, V., Le Bihan, L., & Le Bihan On Site Raman, L. (2004). On Site Raman Analysis of Iznik Pottery Glazes and Pigments. *Journal of Raman Spectroscopy*, 35(7), 527–535. <https://doi.org/https://doi.org/10.1002/jrs.1163>
- Colomban, P., Tournie, A., & Bellot-Gurlet, L. (2006). Raman identification of glassy silicates used in ceramics, glass and jewellery: A tentative differentiation guide. *Journal of Raman Spectroscopy*, 37(8), 841–852. <https://doi.org/10.1002/jrs.1515>
- Constantinescu, B., Cristea-Stan, D., Kovács, I., & Szokefalvi-Nagy, Z. (2014). External milli-beam PIXE analysis of the mineral pigments of glazed Iznik (Turkey) ceramics. *Periodico Di Mineralogia*, 83(2), 159–169. <https://doi.org/10.2451/2013PM0009>
- Crupi, V., Majolino, D., Venuti, V., Barone, G., Mazzoleni, P., Pezzino, A., La Russa, M. F., Ruffolo, S. A., & Bardelli, F. (2010). Non-destructive identification of green and yellow pigments: The case of some Sicilian Renaissance glazed pottery. *Applied Physics A: Materials Science and Processing*, 100(3), 845–853. <https://doi.org/10.1007/s00339-010-5660-x>
- De Faria, D. L. A., Venâncio Silva, S., & De Oliveira, M. T. (1997). Raman microspectroscopy of some iron oxides and oxyhydroxides. *Journal of Raman Spectroscopy*, 28(11), 873–878. [https://doi.org/10.1002/\(sici\)1097-4555\(199711\)28:11<873::aid-jrs177>3.0.co;2-b](https://doi.org/10.1002/(sici)1097-4555(199711)28:11<873::aid-jrs177>3.0.co;2-b)
- Kolářová, M., Kloužková, A., Kohoutková, M., Kloužek, J., & Dvořáková, P. (2023). Degradation Processes of Medieval and Renaissance Glazed Ceramics. *Materials*, 16(1). <https://doi.org/10.3390/ma16010375>
- Mandolesi, A., & Vignozzi Paszkowski, M. (2019). *Di tutti i colori : racconti di ceramica a Montelupo, dalla “fabbrica di Firenze” all’industria e al design*. All’Insegna del Giglio s.a.s.
- Mangani, S. M. E., Mazzinghi, A., Mandò, P. A., Legnaioli, S., & Chiari, M. (2021). Characterisation of decoration and glazing materials of late 19th-early 20th century French porcelain and fine earthenware enamels: a preliminary non-invasive study. *European Physical Journal Plus*, 136(10). <https://doi.org/10.1140/epjp/s13360-021-02055-x>
- Marmi, D., & Berti, F. (2003). *Segreti di fornace*. Aedo.
- Matin, M. (2019). Tin-based opacifiers in archaeological glass and ceramic glazes: a review and new perspectives. In *Archaeological and Anthropological Sciences* (Vol. 11, Issue 4, pp. 1155–1167). Springer Verlag. <https://doi.org/10.1007/s12520-018-0735-2>
- Montanari, R., Murakami, N., Colomban, P., Alberghina, M. F., Pelosi, C., & Schiavone, S. (2020). European ceramic technology in the Far East:

- enamels and pigments in Japanese art from the 16th to the 20th century and their reverse influence on China. *Heritage Science*, 8(1). <https://doi.org/10.1186/s40494-020-00391-2>
- Nardecchia, A., Motto-Ros, V., & Duponchel, L. (2021). *Saturated signals in spectroscopic imaging: why and how should we deal with this regularly observed phenomenon?* <https://www.elsevier.com/open-access/userlicense/1.0/>
- Nurdini, N., Ilmi, M. M., Maryanti, E., Setiawan, P., Kadja, G. T. M., & Ismunandar. (2022). Thermally-induced color transformation of hematite: insight into the prehistoric natural pigment preparation. *Heliyon*, 8(8). <https://doi.org/10.1016/j.heliyon.2022.e10377>
- Odelli, E., Tumbiolo, G., Cantini, F., Rousaki, A., Vandenabeele, P., & Raneri, S. (2022). Italian Maiolica and Sgraffito Pottery from Volterra: a Non-Invasive and Non-Destructive Raman and XRF Analytical Investigation. *Archeological Data*, 11, 102–116. <https://doi.org/10.13131/unipi/2785-0668/zmd0-rg20>
- Ollila, A. M., Newsom, H. E., Clark, B., Wiens, R. C., Cousin, A., Blank, J. G., Mangold, N., Sautter, V., Maurice, S., Clegg, S. M., Gasnault, O., Forni, O., Tokar, R., Lewin, E., Dyar, M. D., Lasue, J., Anderson, R., McLennan, S. M., Bridges, J., ... Williams, J. (2014). Trace element geochemistry (Li, Ba, Sr, and Rb) using Curiosity's ChemCam: Early results for Gale crater from Bradbury Landing Site to Rocknest. *Journal of Geophysical Research: Planets*, 119(1), 255–285. <https://doi.org/10.1002/2013JE004517>
- Othman, N., Mustaffar, M. I., Ismail, S. A., & Ibrahim, M. H. (2023). Upgrading silica rock quality by using attrition scrubbing and magnetic separation techniques. *Materials Today: Proceedings*. <https://doi.org/10.1016/j.matpr.2023.04.659>
- Pattanayak, N., Panda, P., & Parida, S. (2022). Al doped hematite nanoplates: Structural and Raman investigation. *Ceramics International*, 48(6), 7636–7642. <https://doi.org/10.1016/j.ceramint.2021.11.308>
- Peng, I., Hills-Kimball, K., Lovelace, I. M., Wang, J., Rios, M., Chen, O., & Wang, L.-Q. (2022). Exploring the Colors of Copper-Containing Pigments, Copper (II) Oxide and Malachite, and Their Origins in Ceramic Glazes. *Colorants*, 1(4), 376–387. <https://doi.org/10.3390/colorants1040023>
- Pérez-Arantegui, J., Montull, B., Resano, M., & Ortega, J. M. (2009). Materials and technological evolution of ancient cobalt-blue-decorated ceramics: Pigments and work patterns in tin-glazed objects from Aragon (Spain) from the 15th to the 18th century AD. *Journal of the European Ceramic Society*, 29(12), 2499–2509. <https://doi.org/10.1016/j.jeurceramsoc.2009.03.004>
- Piccolpasso, C. (2007). *The Three Books of the Potter's Art - Li tre libri dell'arte del vasaio: Vol. single* (A. Fay Halle, A. Bos, T. B. Keeper, & M. Beck Coppola, Eds.; Second). Scolar Press.

- Prinsloo, L. C., Tournié, A., & Colomban, P. (2011). A Raman spectroscopic study of glass trade beads excavated at Mapungubwe hill and K2, two archaeological sites in southern Africa, raises questions about the last occupation date of the hill. *Journal of Archaeological Science*, *38*(12), 3264–3277. <https://doi.org/10.1016/j.jas.2011.07.004>
- Rasmussen, S. C. (2019). A Brief History of Early Silica Glass: Impact on Science and Society. *Substantia*, *3*(2), 125–138. <https://doi.org/10.13128/Substantia-267>
- Ricci, C., Miliani, C., Rosi, F., Brunetti, B. G., & Sgamellotti, A. (2007). Structural characterization of the glassy phase in majolica glazes by Raman spectroscopy: A comparison between Renaissance samples and replica processed at different temperatures. *Journal of Non-Crystalline Solids*, *353*(11–12), 1054–1059. <https://doi.org/10.1016/j.jnoncrysol.2006.12.099>
- Ricciardi, P., Colomban, P., Ricciardi -, P., Amato -, F., & Colomban, P. (2007). *Raman spectroscopy as a tool for the non-destructive characterization of slips and glazes of a Sgraffito Renaissance production* RAMAN SPECTROSCOPY AS A TOOL FOR THE NON-DESTRUCTIVE CHARACTERIZATION OF SLIPS AND GLAZES OF A “SGRAFFITO” RENAISSANCE PRODUCTION. <https://www.researchgate.net/publication/272833120>
- Rosi, F., Manuali, V., Grygar, T., Bezdicka, P., Brunetti, B. G., Sgamellotti, A., Burgio, L., Seccaroni, C., & Miliani, C. (2011). Raman scattering features of lead pyroantimonate compounds: Implication for the non-invasive identification of yellow pigments on ancient ceramics. Part II. in situ characterisation of Renaissance plates by portable micro-Raman and XRF studies. *Journal of Raman Spectroscopy*, *42*(3), 407–414. <https://doi.org/10.1002/jrs.2699>
- Rosi, F., Manuali, V., Miliani, C., Brunetti, B. G., Sgamellotti, A., Grygar, T., & Hradil, D. (2009). Raman scattering features of lead pyroantimonate compounds. Part I: XRD and Raman characterization of Pb₂Sb₂O₇ doped with tin and zinc. *Journal of Raman Spectroscopy*, *40*(1), 107–111. <https://doi.org/10.1002/jrs.2092>
- Seccaroni, Claudio., & Haldi, J.-Pierre. (2016). *Cobalto, zaffera, smalto dall'antichità al XVIII secolo*.
- Simsek, G., Demirsar Arli, B., Kaya, S., & Colomban, P. (2019). On-site pXRF analysis of body, glaze and colouring agents of the tiles at the excavation site of Iznik kilns. *Journal of the European Ceramic Society*, *39*(6), 2199–2209. <https://doi.org/10.1016/j.jeurceramsoc.2019.01.050>
- Sparavigna, A. C. (2023). Raman Spectroscopy of the Iron Oxides in the Form of Minerals, Particles and Nanoparticles Raman Spectroscopy of the Iron Oxides in the Form of Minerals, Particles and Nanoparticles. *ChemRxiv*, 1–47. <https://doi.org/10.26434/chemrxiv-2023-22kh4-v2>

- Tite, M. S. (1989). Iznik Pottery: an Investigation od Methods of Production. *Archaeometry*, 31(2), 115–132. <https://doi.org/10.1111/j.1475-4754.1989.tb01008.x>
- Tite, M. S. (2009a). The production technology of Italian maiolica: a reassessment. In *Journal of Archaeological Science* (Vol. 36, Issue 10, pp. 2065–2080). Academic Press. <https://doi.org/10.1016/j.jas.2009.07.006>
- Tite, M. S. (2009b). The production technology of Italian maiolica: a reassessment. In *Journal of Archaeological Science* (Vol. 36, Issue 10, pp. 2065–2080). Academic Press. <https://doi.org/10.1016/j.jas.2009.07.006>
- Verweij, H., & Konijnendijk, W. L. (1976). Structural Units in K₂O-PbO-SiO₂ Glasses by Raman Spectroscopy. *Journal of the American Ceramic Society*, 517–521. <https://doi.org/https://doi.org/10.1111/j.1151-2916.1976.tb09422.x>
- Wang, C., Liu, K., Chen, X., Shi, W., Li, X., Wang, S., Chang, Q., Wang, Y., & Wang, Q. (2022). Influence of the thickness of the copper glaze layer on the color and its formation mechanism. *Materials Research Express*, 9(8), 1–14. <https://doi.org/10.1088/2053-1591/ac7f10>
- Zoppi, A., Lofrumento, C., Castellucci, E. M., & Sciau, P. (2008). Al-for-Fe substitution in hematite: The effect of low Al concentrations in the Raman spectrum of Fe₂O₃. *Journal of Raman Spectroscopy*, 39(1), 40–46. <https://doi.org/10.1002/jrs.1811>
- Zucchiatti, A., Bouquillon, A., Katona, I., & D’Alessandro, A. (2006). The “della Robbia blue”: A case study for the use of cobalt pigments in ceramics during the Italian Renaissance. *Archaeometry*, 48(1), 131–152. <https://doi.org/10.1111/j.1475-4754.2006.00247.x>

4 CONCLUSIONS

In the field of archaeometric investigations on Cultural Heritage, the choice of a non-invasive and non-destructive approach represents the safest and most universally applicable strategy. This approach allows for the analysis of samples in any state of conservation, from kiln waste to degraded specimens to museum pieces, without the need for sampling or significant damage.

However, the use of this type of instruments, in most cases, has the major disadvantage of providing information limited to samples' surfaces that are, moreover, averaged over the entire probed thickness.

In the case of Montelupo, obtaining information solely on the glazing system does not represent a problem, as a comprehensive archaeometric campaign had previously been conducted on the ceramic bodies.

However, the complex stratification of historical maiolica glazes (comprising white opaque glaze, coloured glaze, and a transparent superficial coating) can constitute a challenge for the analysis.

To address this, a multidisciplinary analytical approach was proposed, primarily based on MA-XRF scanners, micro Raman spectroscopy, and PIXE + PIGE analysis. This approach was then tested in an archaeometric study on forty-two maiolicas from Montelupo, in a diagnostic campaign which allowed to define its limitations and advantages.

Regarding the samples' white areas, the chosen strategy provides information about the system composed by the white opaque glaze (applied in direct contact with the ceramic body) and the (possible) transparent superficial coating.

MA-XRF identified the characteristic elements of the aforementioned two-glaze systems (mainly Si, K, Ca, and Pb) and to trace the detected Sn characteristic X-rays back to the white layer (given the evident absorption effects of this element's L lines in correspondence of the more superficial coloured decorations).

The higher sensitivity of PIXE and PIGE (especially to low-Z elements), combined with the possibility of obtaining reliable semi-quantitative data, provided important insights about the composition of the two glazes.

The identification of Na and Al through the detection of the characteristic gamma- and X-rays, along with Si, K, and Pb (only X-rays), confirms the lead-rich glaze composition typical of the same period Italian maiolica: SiO₂ (45-70 wt%), PbO (20-40 wt%), K₂O (4-5 wt%), and Al₂O₃ (3-5 wt%).

A certain variability in the concentration of the main oxides (especially the fluxes agents) is also evident. The earliest (13th century) and latest samples (17th – 18th century) have higher PbO concentrations, probably deriving from less optimised

production processes (higher concentrations of fluxes may be necessary in the case of firing carried out at lower temperatures or with thermal curves not adequately controlled).

This evidence would reflect not only the lower technological level of the archaic period but also the artistic (and evidently also technological) crisis that has affected Montelupo since the end of the 16th century.

The Archaic products are also characterised by the highest SnO₂ concentrations. The decrease in SnO₂ contents during the Renaissance is consistent with the improvement of the ceramic body's whitening technique with quicklime.

Finally, the micro Raman analyses proved to be fundamental for understanding the nature of the white areas, providing information both on the crystalline and the amorphous phases of the glazes.

Thanks to this technique, it was possible to confirm the use of cassiterite (already hypothesised from the elemental analyses) as opacifier of the white glaze and also to identify the presence of quartz and K-feldspars crystals in all the samples.

Starting from the two characteristic bands of silica amorphous phases (ν_2 banding mode of the SiO₄ tetrahedron at 500 cm⁻¹, and ν_1 and ν_3 stretching modes of Si-O around 1000 cm⁻¹), it is also possible to calculate the polymerisation index of the glazes and obtain an indication about their firing temperature. The IP values obtained place Montelupo maiolica in the so-called First family, which includes lead-rich silicate glazes processed at temperatures lower than 700°C. This data would be consistent with the values reported in the historical bibliography.

Moreover, Raman spectroscopy also distinguishes two different types of coloured areas.

- The blue and (some) green areas appear to be transparent glazes coloured by transition metal ions dissolved within the glass matrix (no resolved peaks in the Raman spectra acquired in these areas).

- The yellow, red, brown/brown (and some Renaissance green) areas instead present signals of crystalline phases dispersed within the silicate matrix.

Two different types of greenery are, therefore, identified.

The first is a bluish-green characteristic of early and later samples. Copper (detected with both XRF and PIXE) appears to be the only chromophore in this case, so a colourant based on Cu²⁺ ions dissolved in the lead-rich glaze could be hypothesised.

The second is the Renaissance green, more tending towards yellow shades. The different nuance might be explained by Naples Yellow dispersed in the green transparent glaze discussed above. Indeed, elemental analyses allowed detecting in this area the copresence of Cu and Sb, while micro-Raman revealed the Naples Yellow characteristic peaks.

Just like the greens, the blue areas also appear to be transparent glazes coloured with one (or more) ions dissolved in the glass matrix.

Three different types of this colour can be identified in the samples at our disposal: the "traditional" blue zaffera, the zaffera a rilievo (characterised by a peculiar three-dimensional appearance) and a significantly darker blue.

All shades reveal the Co-Fe association detected by both XRF and PIXE. The zaffera a rilievo also presents non-negligible concentrations of Cu (but not lead, unlike what historical sources testify), while the darker colour is characterised by manganese.

In the case of zaffera two colourants with different compositions are actually distinguished by PIXE:

- the Co-Fe-Ni-Cu blue in pre-1520 CE samples.

- the Co-Fe-Ni-As(-Bi) blue in post 1510-1520 CE samples.

This variation in composition suggests a significant technological shift, likely accompanied by a change in the origin of the raw materials.

Based on the traces above reported, the pre-1520 cobalt was probably extracted from slag obtained from the purification of metallic silver (a process widely used in medieval Europe).

While the As-Bi impurities of 16th century samples might suggest the use of Co extracted by bismuth slags, probably from the Schneeberg former silver mines. The combination of XRF, IBA and Raman analyses in the case of black/browns did not highlight particularly interesting aspects from a technological point of view. All these shades appear to be made with Mn and Fe crystalline phases (in some cases, traces of Cu have also been identified), probably oxides based on Raman spectra.

On the other hand, the situation for the yellow areas appears to be way more complex. Two shades of this colour are visible: a proper yellow characterised by Sb (based on MA-XRF) and a warmer (almost orange) yellow, appearing post 1480, defined by the Sb-Fe association (Ma-XRF) probably due to the addition of the *ferraccia* (compound based on iron oxides) to the yellow.

The quantitative IBA data and the micro Raman spectroscopy, though, reveal a much more diverse picture.

All the yellows are tin-modified or iron-modified Naples yellows: the firsts are dated from the 16th century onwards, while no pattern over time is highlighted for the seconds.

Only samples C09 and C16 seem to be almost pure lead antimoniate, based on elemental analyses. However, the fact that even in these two samples the Raman spectra show signals of tin-modified lead antimoniate might be an indication of Sn contents below the PIXE Minimum Detection Limit (MDL).

The red colours appear to be mainly characterised by hematite, probably partially modified with aluminium. The high Si concentrations revealed by PIXE in these areas (as well as the Fe and Al already mentioned) could be consistent with the use of the Armenian bolus according to the strategy also used in Iznik. The lack of significant presence of copper, however, seems to be in contrast with some of the analyses carried out on the Turkish samples.

A small set of samples was finally selected to create polished cross-sections to be analysed with the Scanning Electron Microscope (SEM-EDS). The information collected by probing each individual layer/glaze was then compared with those obtained through the chosen non-invasive multi-analytical approach.

Good agreement is found in most cases, but some discrepancies emerge in the case of some Sn-modified Naples yellows (particularly complex to identify due to the presence of cassiterite in all the white glazes).

Summarising, we can conclude that the proposed approach proved to be very effective and allows solving most of the problems about the Montelupo maiolicas. The most significant limitation experienced with the chosen approach is the impossibility of having a direct indication of the presence/absence of the transparent glaze.

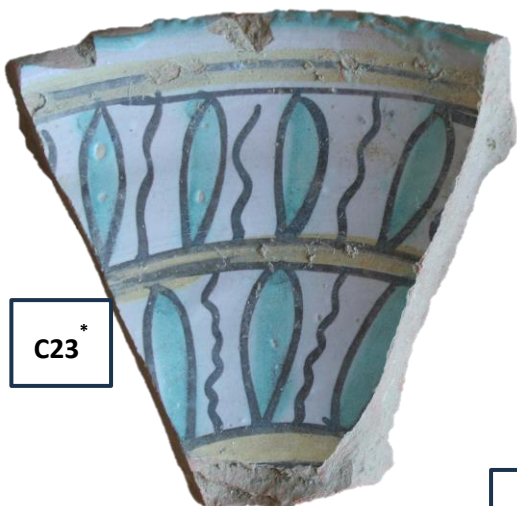
An attempt at indirect identification was made by monitoring the trend of the Pb/Sn ratio. However, it does not seem to be exploitable for every case and, in general, would require further investigation. With this purpose, an additional differential PIXE campaign was planned and conducted. The results will be published in a future paper.

APPENDIX A: SAMPELS









C23*



A16



C21*

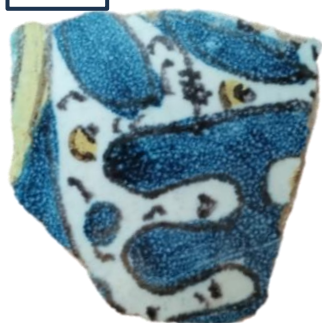
C04*



A20



C09



A15



C14*



5 cm



ACKNOWLEDGMENTS

At the end of this long, and not always easy, journey some acknowledgments are needed.

First of all, I would like to express my gratitude to my two tutors: Prof. Lorenzo Giuntini and Dr Marilena Ricci who made the project possible, following me during these three years.

Secondly, I would like to thank Dr Alessandro Mandolesi (former Scientific Director of the Montelupo Museum System), Dr Lorenza Camin (current Scientific Director of the Montelupo Museum System), Dr Alessio Ferrari (Conservator of the Museum of Montelupo) and Dr Giovanni Baldi (Colorobbia research centre), who kindly provided the samples necessary to start the study. A heartfelt thanks also go to Dr Massimo Chiari, Dr Anna Mazzinghi, Dr Chiara Ruberto and Dr Laura Chiarantini for providing their knowledge and expertise in support of the project allowing me to delve my skills about a vast set of different techniques.

I am very grateful to everybody work behind the Ph.D. in Chemical Sciences: Prof. Anna Maria Papini before everyone, and secondly my internal and external referees, for their invaluable feedback and comments.

- thanks to Prof. Pilario Costagliola and Prof. Franco Lucarelli (internal referees) for providing an exhaustive and well-argued evaluation of my work every year;
- thanks to Prof. Marcos Tascon and Dr Emma Cantisani (external referees) for having read and corrected the final thesis, providing me with very interesting ideas for improvement.

I would also like to manifest my gratitude to Prof. Francesco Arneodo, Prof. Fernando Marte, and Prof. Silvia Nava for being willing to be part of my final evaluation commission.

Lastly, I have to mention my colleagues Dr Sara Calandra, Dr Rosarosa Manca and Dr Diletta Paghi for all the useful feedback and the moral support during these years.

A final special thanks to my family and friends who supports me as always.